Single- and Multi-carrier Quadrature Amplitude Modulation:

Principles and Applications for Personal Communications, WLANs and Broadcasting

by

L. Hanzo, W.T. Webb, T. Keller

Contents

Preface to the Second Edition

Outline

Since its discovery in the early 1960s, quadrature amplitude modulation (QAM) has continued to gain interest and practical application. Particularly in recent years many new ideas and techniques have been proposed, allowing its employment over fading mobile channels. This book attempts to provide an overview of most major QAM techniques, commencing with simple QAM schemes for the uninitiated, while endeavouring to pave the way towards complex, rapidly evolving areas, such as trellis-coded pilot-symbol and transparent-tone-in-band assisted schemes, or arrangements for wide-band mobile channels. The second half of the book is targetted at the more advanced reader, providing a research-oriented outlook using a variety of novel QAM-based single- and multi-carrier arrangements.

The book is structured in five parts. Part I - constituted by Chapters 1-4 - is a rudimentary introduction for those requiring a background in the field of modulation and radio wave propagation. Part II is comprised of Chapters 5-9 and concentrates mainly on classic QAM transmission issues relevant to Gaussian channels. Readers familiar with the fundamentals of QAM and the characteristics of propagation channels, as well as with basic pulse shaping techniques may decide to skip Chapters 1-5. Commencing with Chapter 6, each chapter describes individual aspects of QAM. Readers wishing to familiarize themselves with a particular subsystem, including clock and carrier recovery, equalisation, trellis coded modulation, standardised telephone-line modem features, etc. can turn directly to the relevant chapters, whereas those who desire a more complete treatment might like to read all the remaining chapters.

Parts III-V, including Chapters 10-24, are concerned with QAM-based transmissions over mobile radio channels. These chapters provide a research-based perspective and are dedicated to the more advanced reader. Specifically, Chapter 10 concentrates mainly on coherent QAM schemes, including reference-aided transparent-tone-in-band and pilot-symbol assisted modulation arrangements. In contrast, Chapter 11 focuses on low-complexity differentially encoded QAM schemes and on their performance with and without forward error correction coding and trellis coded modulation. Chapter 12 details various timing recovery schemes.

Part IV of the book commences with Chapter 13, which is concerned with variable rate QAM using one- to six-bits per symbol signal constellations. Chapter 14 is dedicated to high-rate wide-band transmissions and proposes a novel equaliser arrangement. Various QAM-related orthogonal signaling techniques are proposed in Chapter 15, while the spectral efficiency of QAM in cellular frequency re-use structures is detailed in Chapter 16. This is followed by Chapter 17, which concentrates on the employment of QAM in a source-matched speech communications system, including various speech codecs, error correction codecs, a voice activity detector and packet reservation multiple access, providing performance figures in contrast to one and two bits per symbol bench-mark schemes.

Part V first appeared in this new edition of the book, concentrating on multi-carrier modulation. Specifically, following a rudimentary introduction to Orthogonal Frequency Division Multiplexing (OFDM) in Chapter 18, Chapters 19-23 detail a range of implementational and performance aspects of OFDM over both Gaussion and wideband fading channels. Lastly, Chapter 24 concentrates on the performance aspects of various standard-compliant and enhanced OFDM-based Digital Video Broadcasting (DVB) systems designed for transmission to mobile receivers.

To the original text of the first edition dealing with many of the fundamentals of single-carrier QAM and QAM-based systems we have added six new chapters dealing with the complexities of the exciting subject of multi-carrier modulation, which has found wide-ranging applications in a past decade, ranging from Wireless Local Area Network (WLAN) to broadcast systems. Whilst the book aims to portray a rapidly evolving area, where research results are promptly translated into products, it is our hope that you will find this second edition comprehensive, technically challenging and above all, enjoyable.

Lajos Hanzo
William Webb
Thomas Keller

Acknowledgement

The authors would like to express their warmest thanks to Prof. Raymond Steele. Without his shrewd long-term vision the research on single-carrier QAM would not have been performed, and without his earnest exhortations a book on the subject would not have been written. Furthermore, Professor Steele has edited some of the chapters and given advice on the contents and style of this book.

Contributions by Dr. P.M. Fortune, Dr. K.H.H. Wong, Dr. R.A. Salami, D. Greenwood, R. Stedman, R Lucas and Dr. J.C.S. Cheung who were formerly with Southampton University thankfully acknowledged. We thank Multiple Access Communications Ltd. for supporting the work on QAM, particularly in the framework of the DTI LINK Personal Communications Programme, dealing with high data rate QAM transmission over microcellular mobile channels. Special thanks goes to Peter Gould and Philip Evans for the major part they played in the construction of the star QAM test-bed. We are grateful to John Williams of Multiple Access Communications Ltd. for the many simulation results he provided for Chapter 18, the production of many of the figures involving simulated waveforms, and not least, for the cover design. Much of the QAM work at Multiple Access Communications Ltd. derives from the support of BT Labs. Martlesham Heath, the DTI and the Radio Communications Agency. Specifically, we thank the latter for the support of the research on spectral efficiency which facilitated Chapter 17.

Much of the results in Chapters 19-22 are based on our work conducted as a sub-contractor of Motorola ECID, Swindon, UK; as part of our involvement in a collaborative Pan-European Wireless Asyncrhonous Transfer Mode (WATM) project known as Median, which was genereously supported by the European Commission (EC), Brussels, Belgium. We would like to acknowledge all our valued friends and colleagues - too numerous to mention individually - who at some stage were associated with the Median consortium and with whom we have enjoyed a stimulating collaboration under the stirling management of IMST, Germany. Our gratitude is due to Andy Wilton and to Paul Crichton of Motorola, who have whole-heartedly sponsored our research. Further thanks are also due to Dr. Joao Da Silva, Bartolome Aroyo, Bernard Barani, Dr. Jorge Pereira, Demosthenes Ikonomou and to the other equally supportive members of the EC's programme management team in Brussels for their enthusiastic support. Furthermore, we enjoyed the valuable support of EPSRC, Swindon UK, and the Mobile VCE, for which we are equally grateful.

Lastly, we express our gratitude for the creative atmosphere to our colleagues Derek Appleby, Steve Braithwaite, Sheng Chen, David Stewart as well as Stephan Weiss at Southampton University, UK and gratefully acknowledge the stimulating embryonic discussions with Prof. G. Gordos (Technical University of Budapest, Hungary), Prof. H.W. Schüssler (University of Erlangen-Nürnberg, Germany) and Dr.Ing. H.J. Kolb as well as the numerous thought-provoking contributions by many established authorities in the field, who appear also in the Author Index Section of the book.

A number of colleagues have influenced our views concerning various aspects of wireless communications and we thank them for the enlightment gained from our collaborations on various projects, papers and books. We are grateful to J. Brecht, Jon Blogh, Marco Breiling, M. del Buono, Clare Brooks, Peter Cherriman, Stanley Chia, Byoung Jo Choi, Joseph Cheung, Peter Fortune, Lim Dongmin, D. Didascalou, S. Ernst, Eddie Green, David Greenwood, Hee Thong How, Thomas Keller, W.H. Lam, C.C. Lee, M.A. Nofal, Xiao Lin, Chee Siong Lee, Tong-Hooi Liew, Matthias Muenster, V. Roger-Marchart, Redwan Salami, David Stewart, Juergen Streit, Jeff Torrance, Spyros Vlahoyiannatos, William Webb, John Williams, Jason Woodard, Choong Hin Wong, Henry Wong, James Wong, Lie-Liang Yang, Bee-Leong Yeap, Mong-Suan Yee, Kai Yen, Andy Yuen and many others with whom we enjoyed an association. Special thanks are due to Dr. Lie-Liang Yang for his insightful contributions on the theory of the coding schemes used in Chapter 23, to Tong-Hooi Liew for his kind assistance in the preparation of Chapter 23, which resulted in a joint journal submission. Furthermore, the contributions of Chee-Siong Lee and Spyros Vlahoyiannatos to Chapter 24 are also gratefully acknowledged. We are also grateful to our editors, Mark Hammond and Juliet Booker at Wiley. Finally, the authors warmly thank Rita Hanzo, Denise Harvey and Dr. Peter Cherriman for their dedicated and skilful assistance in typesetting the manuscript in Latex, scanning the missing figures and amalgamating the new material of the second edition with the first edition.

Lajos Hanzo
William Webb
Thomas Keller

Single- and Multi-Carrier Quadrature Amplitude Modulation: by L. Hanzo, W.T. Webb and T. Keller

This book attempts to provide an overview of most major QAM techniques, commencing with simple QAM schemes for the uninitiated, while endeavouring to pave the way towards complex, rapidly evolving areas, such as trellis-coded pilot symbol and transparent tone in band assisted orthogonal multiplex schemes, or arrangements for wide-band mobile channels. The second half of the book is targeted at the more advanced reader, providing a research-oriented outlook using a variety of novel QAM-based arrangements.

The book is structured in five parts. Part I is a rudimentary introduction for readers requiring a background in the field of modulation and communications channels. Part II concentrates mainly on classic QAM transmission issues relevant to Gaussian channels, including clock and carrier recovery, equalisation, trellis coded modulation, standardised CCITT V-series modem features, etc. Parts III-V are concerned with QAM for mobile radio channels, including more complex coherent reference-aided transparent-tone-in-band, pilot symbol assisted and trellis coded modulation schemes. These are contrasted with various differentially coded low-complexity non-coherent arrangements. Then the reader is guided through an adaptive modem optimising its phasor constellation for various conditions, before high-rate wide-band transmissions and a novel channel equaliser are considered. Part IV incorporates QAM-related orthogonal techniques and considers the spectral efficiency of QAM in cellular frequency re-use structures, before concluding with a QAM-based speech communications system design study, including various speech codecs, error correction codecs, a voice activity detector and packet reservation multiple access, providing performance figures in contrast to one and two bits per symbol bench-mark schemes. Lastly, Part V provides an in-depth study of Orthogonal Frequency Division Multiplex systems, which are applicable to Wireless Local Area Networks (WLAN) and Digital Video Broadcasting (DVB).

Chapter 22

Adaptive OFDM Techniques

22.1 Introduction

Steele and Webb [48] proposed adaptive modulation for exploiting the time-variant Shannonian channel capacity of fading narrowband channels, which stimulated further research at Osaka University by Sampei et al [315], at the University of Stanford by Goldsmith et al [316], by Pearce, Burr and Tozer at the University of York [317], Lau and McLeod at the University of Cambridge [318], and at Southampton University [319,320]. The associated principles can also be invoked in the context of parallel modems, as it has been demonstrated by Kalet [78], Czylwik et al [321] as well as by Chow, Cioffi and Bingham [322].

22.1.1 Motivation

We have seen in Figure 20.12 of Chapter 20 that the bit error probability of different OFDM subcarriers transmitted in time dispersive channels depends on the frequency domain channel transfer function. The occurrence of bit errors is normally concentrated in a set of severely faded subcarriers, while in the rest of the OFDM spectrum often no bit errors are observed. If the subcarriers that will exhibit high bit error probabilities in the OFDM symbol to be transmitted can be identified and excluded from data transmission, the overall BER can be improved in exchange for a slight loss of system throughput. As the frequency domain fading deteriorates the SNR of certain subcarriers, but improves others' above the average SNR value, the potential loss of throughput due to the exclusion of faded subcarriers can be mitigated by employing higher order modulation modes on the subcarriers exhibiting high SNR values.

In addition to excluding sets of faded subcarriers and varying the modulation modes employed, other parameters such as the coding rate of error correction coding schemes can be adapted at the transmitter according to the perceived channel transfer function. This issue will be addressed in Chapter 23.

Adaptation of the transmission parameters is based on the transmitter's perception of the channel conditions in the forthcoming timeslot. Clearly, this estimation of future channel parameters can only be obtained by extrapolation of previous channel estimations, which are acquired upon detecting each received OFDM symbol. The channel characteristics therefore have to be varying sufficiently slowly compared to the estimation interval.

Adapting the transmission technique to the channel conditions on a timeslot–by–timeslot basis for serial modems in narrowband fading channels has been shown to considerably improve the BER performance [323] for Time Division Duplex (TDD) systems assuming duplex reciprocal channels. However, the Doppler fading rate of the narrow–band channel has a strong effect on the achievable system performance: if the fading is rapid, then the prediction of the channel conditions for the next transmit timeslot is inaccurate, and therefore the wrong set of transmission parameters may be chosen. If however the channel varies slowly, then the data throughput of the system is varying dramatically over time, and large data buffers are required at the transmitters in order to smoothen the bitrate fluctuation. For time–critical applications, such as interactive speech transmission, the potential delays can become problematic. A given single–carrier adaptive system in narrowband channels will therefore operate efficiently only in a limited range of channel conditions.

Adaptive OFDM modems channels can ease the problem of slowly time–varying channels, since the variation of the signal quality can be exploited in both the time– and the frequency–domain. The channel conditions still have to be monitored based on the received OFDM symbols, and relatively slowly varying channels have to be assumed, since we have seen in Section 20.2.2 that OFDM transmissions are not well suited to rapidly varying channel conditions.

22.1.2 Adaptive techniques

Adaptive modulation is only suitable for duplex communication between two stations, since the transmission parameters have to be adapted using some form of two–way transmission in order to allow channel measurements and signalling to take place. These issues are studied below.

Transmission parameter adaptation is a response of the transmitter to time–varying channel conditions. In order to efficiently react to the changes in channel quality, the following steps have to be taken:

- *Channel quality estimation:* In order to appropriately select the transmission parameters to be employed for the next transmission, a reliable estimation of the channel transfer function during the next active transmit timeslot is necessary.

- *Choice of the appropriate parameters for the next transmission:* Based on the prediction of the channel conditions for the next timeslot, the transmitter has to select the appropriate modulation modes for the subcarriers.

- *Signalling or blind detection of the employed parameters:* The receiver has to be informed, as to which demodulator parameters to employ for the received packet. This information can either be conveyed within the OFDM symbol itself, at the cost of loss of effective data throughput, or the receiver can attempt to estimate the parameters employed by the remote transmitter by means of blind detection mechanisms.

22.1.2.1 Channel quality estimation

The transmitter requires an estimate of the expected channel conditions for the time when the next OFDM symbol is to be transmitted. Since this knowledge can only be gained by prediction from past channel quality estimations, the adaptive system can only operate efficiently in an environment exhibiting relatively slowly varying channel conditions.

The channel quality estimation can be acquired from a range of different sources. If the communication between the two stations is bidirectional and the channel can be considered reciprocal, then each station can estimate the channel quality on the basis of the received OFDM symbols, and adapt the parameters of the local transmitter to this estimation. We will refer to such a regime as *open–loop adaptation*, since there is no feedback between the receiver of a given OFDM symbol and the choice of the modulation parameters. A Time Division Duplex (TDD) system in absence of interference is an example of such a system, and hence a TDD regime is assumed for generating the performance results below. Channel reciprocity issues were addressed for example in [324, 325].

If the channel is not reciprocal, as in a Frequency Division Duplex (FDD) system, then the stations cannot determine the parameters for the next OFDM symbol's transmission from the received symbols. In this case, the receiver has to estimate the channel quality and explicitly signal this perceived channel quality information to the transmitter in the reverse link. Since in this case the receiver explicitly instructs the remote transmitter as to which modem modes to invoke, this regime is referred to as *closed–loop adaptation*. The adaptation algorithms can — which the aid of this technique — take into account effects such as interference as well as non–reciprocal channels. If the communication between the stations is essentially unidirectional, then a low–rate signalling channel must be implemented from the receiver to the transmitter. If such a channel exists, then the same technique as for non-reciprocal channels can be employed.

Different techniques can be employed to estimate the channel quality. For OFDM modems, the bit error probability in each subcarrier is determined by the fluctuations of the channel's instantaneous frequency domain channel transfer function H_n, if no interference is present. The estimate of the channel transfer function $\hat{H}_n$ can be acquired by means of pilot–tone based channel estimation, as it was demonstrated in Section 20.3.1.1. More accurate measures of the channel transfer function can be gained by means of decision–directed or time–domain training sequence based techniques. The estimate of the channel transfer function $\hat{H}_n$ does not take into account effects, such as co–channel or inter–subcarrier interference. Alternative channel quality measures including interference effects can be devised on the basis of the error correction decoder's soft output information or by means of decision-feedback local SNR estimations.

The delay between the channel quality estimation and the actual transmission of the OFDM symbol in relation to the maximal Doppler frequency of the channel is crucial as regards to the adaptive system's performance. If the channel estimate is obsolete at the time of transmission, then poor system performance will result. For a closed–loop adaptive system the delays between channel estimation and transmission of the packet are generally longer than for an open–loop adaptive system, and therefore the Doppler frequency of the channel is a more critical parameter for the system's performance than in the context of open–loop adaptive systems.

22.1.2.2 Parameter adaptation

Different transmission parameters can be adapted to the anticipated channel conditions, such as the modulation and coding modes. Adapting the number of modulation levels in response to the anticipated local SNR encountered in each subcarrier can be employed, in order to achieve a wide range of different trade–offs between the received data integrity and throughput. Corrupted subcarriers can be excluded from data transmission and left blank or used for example for Crest–factor reduction. A range of different algorithms for selecting the appropriate modulation modes are investigated below.

The adaptive channel coding parameters entail code rate, adaptive interleaving and puncturing for convolutional and turbo codes, or varying block lengths for block codes [297]. These techniques can be combined with adaptive modulation mode selection an dwill be discussed in Chapter 23.

Based on the estimated frequency–domain channel transfer function, spectral pre–distortion at the transmitter of one or both communicating stations can be invoked, in order to partially of fully counteract the frequency–selective fading of the time–dispersive channel. Unlike frequency–domain equalisation at the receiver — which corrects for the amplitude– and phase–errors inflicted upon the subcarriers by the channel but cannot improve the signal–to–noise ratio in poor quality channels — spectral pre–distortion at the OFDM transmitter can deliver near–constant signal–to–noise levels for all subcarriers and can be thought of as power control on a subcarrier–by–subcarrier basis.

In addition to improving the system's BER performance in time–dispersive channels, spectral pre–distortion can be employed in order to perform all channel estimation and equalisation functions at only one of the two communicating duplex stations. Low–cost, low power consumption mobile stations can communicate with a base station that performs the channel estimation and frequency–domain equalisation of the uplink, and uses the estimated channel transfer function for pre–distorting the down–link OFDM symbol. This setup would lead to different overall channel quality on the up– and downlink, and the superior downlink channel quality could be exploited by using a computationally less complex channel decoder having weaker error correction capabilities in the mobile station than in the base station.

If the channel's frequency–domain transfer function is to be fully counteracted by the spectral pre-distortion upon adapting the subcarrier power to the inverse of the channel transfer function, then the output power of the transmitter can become excessive, if heavily faded subcarriers are present in the system's frequency range. In order to limit the transmitter's maximal output power, hybrid channel pre–distortion and adaptive modulation schemes can be devised, which would de–activate transmis-

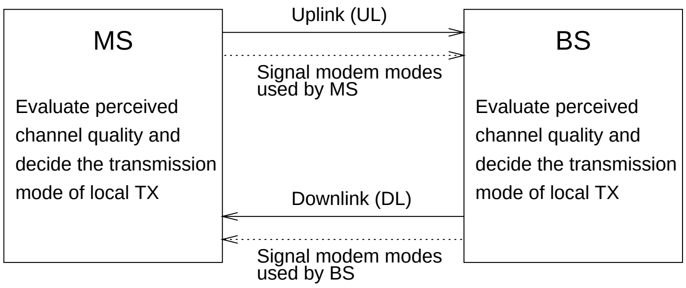

(a) Reciprocal channel, open–loop control

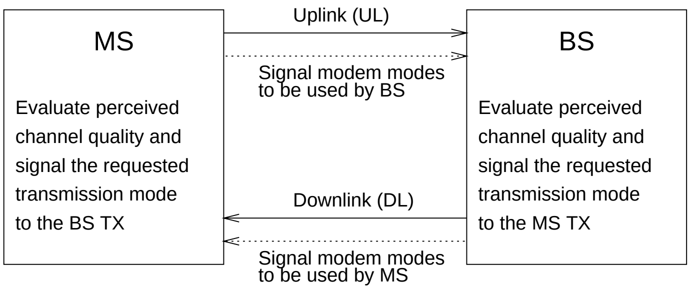

(b) Non–reciprocal channel, closed–loop signalling

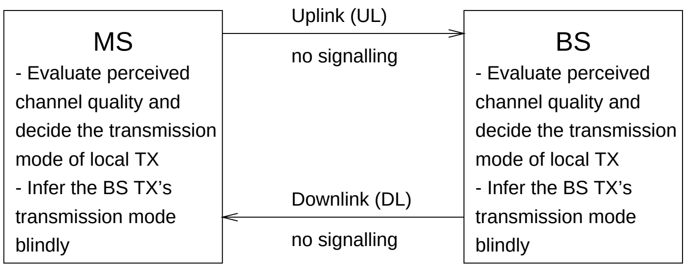

(c) Reciprocal channel, blind modem–mode detection

Figure 22.1: Signalling scenarios in adaptive modems

sion in deeply faded subchannels, while retaining the benefits of pre–distortion in the remaining subcarriers.

22.1.2.3 Signalling the parameters

Signalling plays an important role in adaptive systems and the range of signalling options is summarised in Figure 22.1 for both open–loop and closed–loop signalling, as well as for blind detection. If the channel quality estimation and parameter adaptation have been performed at the transmitter of a particular link, based on open–loop adaptation, then the resulting set of parameters has to be communicated to the receiver in order to successfully demodulate and decode the OFDM symbol. If the receiver itself determines the requested parameter set to be used by the remote transmitter — the closed–loop scenario — then the same amount of information has to be transported to the remote transmitter in the reverse link. If this signalling information is corrupted, then the receiver is generally unable to correctly decode the OFDM symbol corresponding to the incorrect signalling information.

Unlike adaptive serial systems, which employ the same set of parameters for all data symbols in a transmission packet [319, 320], adaptive OFDM systems have to react to the frequency selective nature of the channel, by adapting the modem parameters across the subcarriers. The resulting signalling overhead may become significantly higher than that for serial modems, and can be prohibitive for example for subcarrier–by–subcarrier modulation mode adaptation. In order to overcome these limitations, efficient and reliable signalling techniques have to be employed for practical implementation of adaptive OFDM modems.

If some flexibility in choosing the transmission parameters is sacrificed in an adaptation scheme, like in the sub–band adaptive OFDM schemes described below, then the amount of signalling can be reduced. Alternatively, blind parameter detection schemes can be devised, which require little or no signalling information, respectively. Two simple blind modulation scheme detection algorithms are investigated in Section 22.2.6.2 [326].

22.1.3 System aspects

The effects of transmission parameter adaptation for OFDM systems on the overall communication system have to be investigated in at least the following areas: data buffering and latency due to varying data throughput, the effects of co–channel interference and bandwidth efficiency.

22.2 Adaptive modulation for OFDM

22.2.1 System model

The system model of the N–subcarrier Orthogonal Frequency Division Multiplexing (OFDM) modem is shown in Figure 22.2 [66]. At the transmitter, the modulator generates N data symbols S_n, $0 \leq n \leq N-1$, which are multiplexed to the N subcarriers. The time–domain samples s_n transmitted during one OFDM symbol are generated by the Inverse Fast Fourier Transform (IFFT) and transmitted over the channel after the cyclic extension (C. Ext.) has been inserted. The channel is modelled by its time–variant impulse response $h(\tau, t)$ and AWGN. At the receiver,

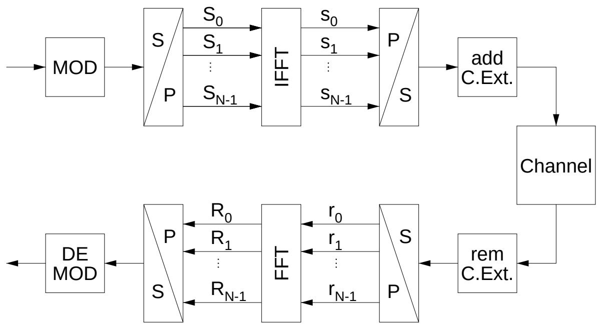

Figure 22.2: Schematic model of the OFDM system

the cyclic extension is removed from the received time–domain samples, and the data samples r_n are Fast Fourier Transformed, in order to yield the received frequency–domain data symbols R_n.

The channel's impulse response is assumed to be time–invariant for the duration of one OFDM symbol, therefore it can be characterised for each OFDM symbol period by the N-point Fourier transform of the impulse response, which is referred to as the frequency domain channel transfer function H_n. The received data symbols R_n can be expressed as:

$$R_n = S_n \cdot H_n + n_n,$$

where n_n is an AWGN sample. Coherent detection is assumed for the system, therefore the received data symbols R_n have to be de–faded in the frequency–domain with the aid of an estimate of the channel transfer function H_n. This estimate $\hat{H}_n$ can be obtained by the use of pilot subcarriers in the OFDM symbol, or by employing time–domain channel sounding training sequences embedded in the transmitted signal. Since the noise energy in each subcarrier is independent of the channel's frequency domain transfer function H_n, the 'local' Signal–to–Noise Ratio SNR in subcarrier n can be expressed as

$$\gamma_n = |H_n|^2 \cdot \gamma,$$

where γ is the overall SNR. If no signal degradation due to Inter–Subcarrier Interference (ISI) or interference from other sources appears, then the value of γ_n determines the bit error probability for the transmission of data symbols over the subcarrier n.

The goal of adaptive modulation is to choose the appropriate modulation mode for transmission in each subcarrier, given the local SNR γ_n, in order to achieve a good trade–off between throughput and overall BER. The acceptable overall BER varies depending on other systems parameters, such as the correction capability of the error correction coding and the nature of the service supported by this particular link.

As discussed before, the adaptive system has to employ appropriate techniques in order to fulfill the following requirements:

- Channel quality estimation,
- Choice of the appropriate modulation modes, and

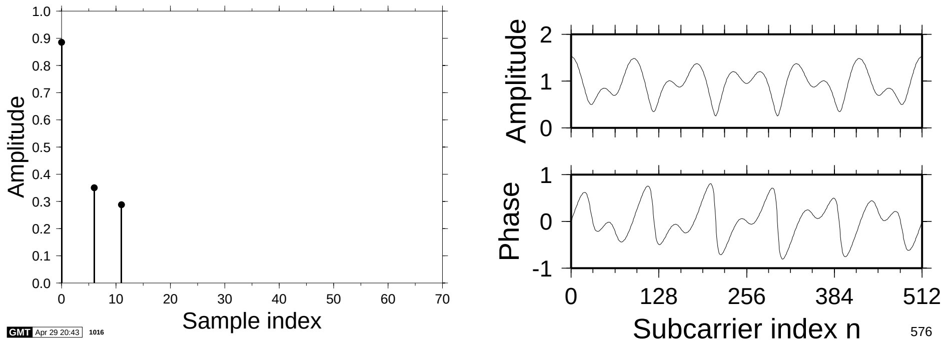

(a) $h(n)$ **(b)** H_n

Figure 22.3: WATM Wideband channel (a) – unfaded symbol spaced impulse response (b) – corresponding frequency domain channel transfer function

- Signalling or blind detection of the modulation modes.

We will examine these three points with reference to Figure 22.1 in the following sections for the example of a 512–subcarrier OFDM modem in the shortened WATM channel of Section 20.1.1.2.

22.2.2 Channel model

The impulse response $h(\tau, t)$ used in our experiments was generated on the basis of the symbol–spaced impulse response shown in Figure 22.3(a) by fading each of the impulses obeying a Rayleigh distribution of a normalised maximal Doppler frequency of $f'_d = 1.235 \cdot 10^{-5}$, which corresponds to the WLAN channel experienced by a modem transmitting at a carrier frequency of 60 GHz with a sample rate of 225 MHz and a vehicular velocity of 50 km/h. The complex frequency domain channel transfer function H_n corresponding to the unfaded impulse response is shown in Figure 22.3(b).

22.2.3 Channel estimation

The most convenient setting for an adaptive OFDM (AOFDM) system is a Time Division Duplex (TDD) system in a slowly varying reciprocal channel, allowing open–loop adaptation. Both stations transmit an OFDM symbol in turn, and at each station, the most recent received symbol is used for the channel estimation employed for the modulation mode adaptation for the next transmitted OFDM symbol. The channel estimation on the basis of the received symbol can be performed by PSAM (see Section 20.3.1.1), or upon invoking more sophisticated methods, such as decision–directed channel estimation. Initially, we will assume perfect knowledge of the channel transfer function during the received timeslot.

22.2.4 Choice of the modulation modes

The two communicating stations use the open–loop predicted channel transfer function acquired from the most recent received OFDM symbol, in order to allocate the appropriate modulation modes to the subcarriers. The modulation modes were chosen from the set of Binary Phase Shift Keying (BPSK), Quadrature Phase Shift Keying (QPSK), 16-Quadrature Amplitude Modulation (16-QAM), as well as "No Transmission", for which no signal was transmitted. These modulation modes are denoted by M_m, where $m \in (0, 1, 2, 4)$ is the number of data bits associated with one data symbol of each mode.

In order to keep the system complexity low, the modulation mode is not varied on a subcarrier–by–subcarrier basis, but instead the total OFDM bandwidth of 512 subcarriers is split into blocks of adjacent subcarriers, referred to as sub–bands, and the same modulation scheme is employed for all subcarriers of the same sub–band. This substantially simplifies the task of signalling the modem mode and renders the employment of alternative blind detection mechanisms feasible, which will be discussed in Section 22.2.6.

Three modulation mode allocation algorithms were investigated in the sub–bands: a fixed threshold controlled algorithm, an upper–bound BER estimator and a fixed–throughput adaptation algorithm.

22.2.4.1 Fixed threshold adaptation algorithm

The fixed threshold algorithm was derived from the adaptation algorithm proposed by Torrance for serial modems [323]. In the case of a serial modem, the channel quality is assumed to be constant for all symbols in the time slot, and hence the channel has to be slowly varying, in order to allow accurate channel quality prediction. Under these circumstances, all data symbols in the transmit time slot employ the same modulation mode, chosen according to the predicted SNR. The SNR thresholds for a given long–term target BER were determined by Powell–optimisation [327]. Torrance assumed two uncoded target bit error rates: 1% for a high data rate "speech" system, and 10^{-4} for a higher integrity, lower data rate "data" system. The resulting SNR thresholds l_n for activating a given modulation mode M_n in a slowly Rayleigh fading narrow–band channel for both systems are given in Table 22.1. Specifically, the modulation mode

	l_0	l_1	l_2	l_4
speech system	$-\infty$	3.31	6.48	11.61
data system	$-\infty$	7.98	10.42	16.76

Table 22.1: Optimised switching levels for adaptive modulation over Rayleigh fading channels for the "speech" and "data" system, shown in instantaneous channel SNR [dB] (from [327]).

M_n is selected if the instantaneous channel SNR exceeds the switching level l_n.

This adaptation algorithm originally assumed a constant instantaneous SNR over all of the block's symbols, but in the case of an OFDM system in a frequency selective channel the channel quality varies across the different subcarriers. For sub–band

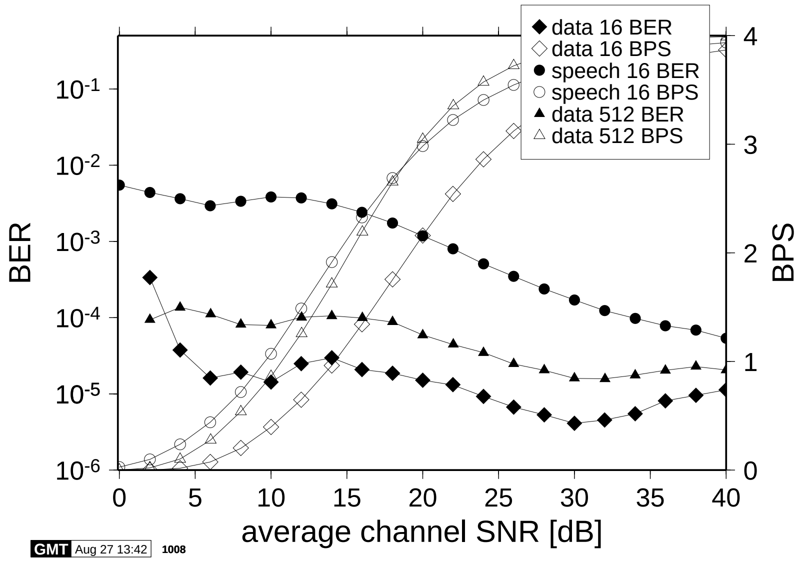

Figure 22.4: BER and BPS throughput performance of the 16–sub–band 512–subcarrier switching level adaptive OFDM modem employing BPSK, QPSK, 16-QAM and "no transmission" over the Rayleigh fading time dispersive channel of Figure 20.3 using the switching thresholds of Table 22.1

adaptive OFDM transmission, this implies that if the the sub–band width is wider than the channel's coherence bandwidth [297], then the original switching algorithm cannot be employed. For our investigations, we have therefore employed the lowest quality subcarrier in the sub–band for the adaptation algorithm based on the thresholds given in Table 22.1. The performance of the 16 sub–band adaptive system over the shortened WATM Rayleigh fading channel of Figure 20.3 is shown in Figure 22.4.

Adjacent or consecutive timeslots have been used for the up– and downlink slots in these simulations, so that the delay between channel estimation and transmission was rendered as short as possible. Figure 22.4 shows the long–term average BER and throughput of the studied modem for the "speech" and "data" switching levels of Table 22.1 as well as for a subcarrier–by–subcarrier adaptive modem employing the "data" switching levels. The results show the typical behaviour of a variable–throughput AOFDM system, which constitutes a tradeoff between the best BER and best throughput performance. For low SNR values, the system achieves a low BER by transmitting very few bits and only when the channel conditions allow. With increasing long–term SNR, the throughput increases, without significant change in the BER. For high SNR values the BER drops as the throughput approaches its maximum of 4 bits per symbol, since the highest–order constellation was 16QAM.

It can be seen from the figure that the adaptive system performs better than its target bit error rates of 10^{-2} and 10^{-4} for the "speech" and "data" system, respectively, resulting in measured bit error rates lower than the targets. This can be

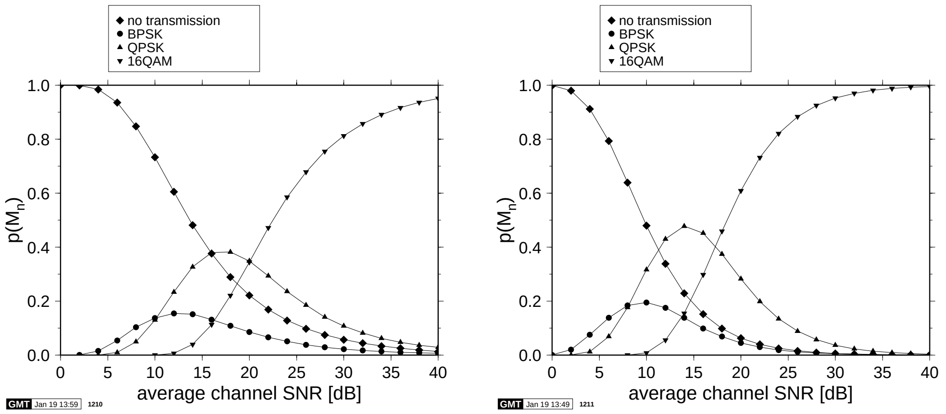

(a) 16 sub–bands

(b) subcarrier-by-subcarrier

Figure 22.5: Histograms of modulation modes versus channel SNR for the "data" switching level adaptive 512–subcarrier 16–sub–band OFDM modem over the Rayleigh fading time dispersive channel of Figure 20.3 using the switching thresholds of Table 22.1.

explained by the adaptation regime, which was based on the conservative principle of using the lowest quality subcarrier in each sub–band for channel quality estimation, leading to a pessimistic channel quality estimate for the entire sub–band. For low values of SNR, the throughput in bits per data symbol is low and exceeds the fixed BPSK throughput of 1 bit/symbol only for SNR values in excess of 9.5 dB and 14 dB for the "speech" and "data" systems, respectively.

The upper–bound performance of the system with subcarrier–by–subcarrier adaptation is also portrayed in the figure, shown as 512 independent sub–bands, for the "data" optimised set of threshold values. It can be seen that in this case the target BER of 10^{-4} is closely met over a wide range of SNR values from about 2dB to 20dB, and that the throughput is considerably higher than in the case of the 16–sub–band modem. This is the result of more accurate subcarrier-by-subcarrier channel quality estimation and fine–grained adaptation, leading to better exploitation of the available channel capacity.

Figure 22.5 shows the long–term modulation mode histograms for a range of channel SNR values for the "data" switching levels in both the 16–sub–band and the subcarrier-by-subcarrier adaptive modems using the switching thresholds of Table 22.1. Comparison of the graphs shows that higher order modulation modes are used more frequently by the subcarrier–by–subcarrier adaptation algorithm, which is in accordance to the overall throughput performance of the two modems in Figure 22.4.

The throughput penalty of employing sub–band adaptation depends on the frequency–domain variation of the channel transfer function. If the sub–band band-

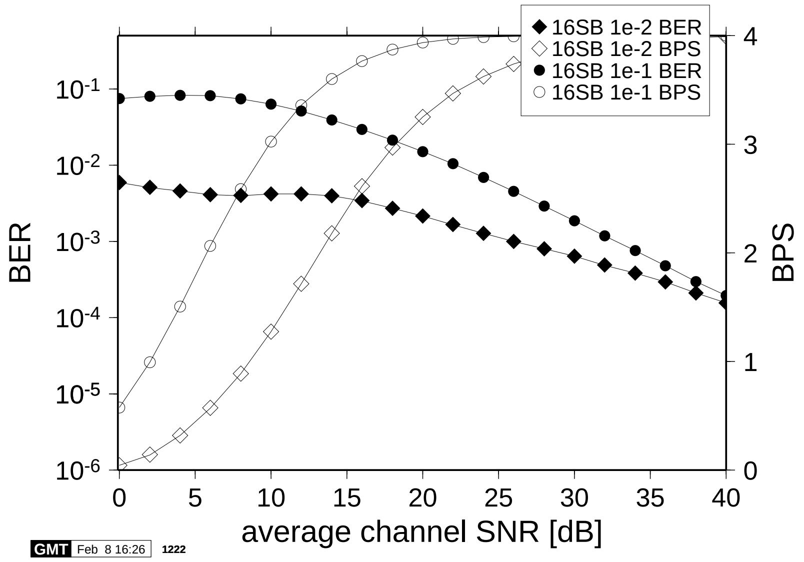

Figure 22.6: BER and BPS throughput performance of the 16–sub–band 512–subcarrier **BER estimator** adaptive OFDM modem employing BPSK, QPSK, 16-QAM and "no transmission" over the Rayleigh fading time dispersive channel of Figure 20.3

width is lower than the channel's coherence bandwidth, then the assumption of constant channel quality per sub–band is closely met, and the system performance is equivalent to that of a subcarrier–by–subcarrier adaptive scheme.

22.2.4.2 Sub–band BER estimator adaptation algorithm

We have seen above that the fixed switching level based algorithm leads to a throughput performance penalty, if used in a sub–band adaptive OFDM modem, when the channel quality is not constant throughout each sub–band. This is due to the conservative adaptation based on the subcarrier experiencing the most hostile channel in each sub–band.

An alternative scheme taking into account the non–constant SNR values γ_j across the N_s subcarriers in the j-th sub–band can be devised by calculating the expected overall bit error probability for all available modulation modes M_n in each sub–band, which is denoted by $\bar{p}_e(n) = 1/N_s \sum_j p_e(\gamma_j, M_n)$. For each sub–band, the mode having the highest throughput, whose estimated BER is lower than a given threshold, is then chosen. While the adaptation granularity is still limited to the sub–band width, the channel quality estimation includes not only the lowest–quality subcarrier, which leads to an improved throughput.

Figure 22.6 shows the BER and throughput performance for the 16–sub–band adaptive OFDM modem employing the BER estimator adaptation algorithm in the Rayleigh fading time dispersive channel of Figure 20.3. The two sets of curves in the

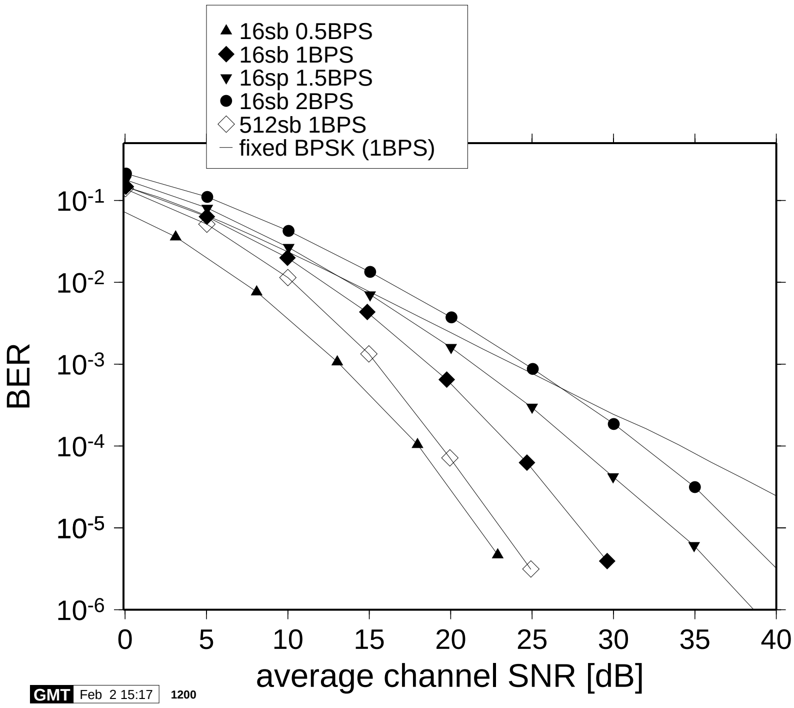

Figure 22.7: BER performance versus SNR for the 512–subcarrier 16–sub–band **constant throughput** adaptive OFDM modem employing BPSK, QPSK, 16-QAM and "no transmission" in Rayleigh fading time dispersive channel of Figure 20.3 for 0.5, 1, 1.5 and 2 Bits Per Symbol (BPS) target throughput.

figure correspond to target bit error rates of 10^{-2} and 10^{-1}, respectively. Comparing the modem's performance for a target BER of 10^{-2} with that of the "speech" modem in Figure 22.4 it can be seen that the BER estimator algorithm results in significantly higher throughput, while meeting the BER requirements. The BER estimator algorithm is readily adjustable to different target bit error rates, which is demonstrated in the figure for a target BER of 10^{-1}. Such adjustability is beneficial, when combining adaptive modulation with channel coding, as it will be discussed in Section 22.2.7.

22.2.5 Constant throughput adaptive OFDM

The time–varying data throughput of an adaptive OFDM modem operating with either of the two adaptation algorithms discussed above makes it difficult to employ such a scheme in a variety of constant–rate applications. Torrance [323] studied the system implications of variable–throughput adaptive modems in the context of narrow–band channels, stressing the importance of data buffering at the transmitter, in order to accommodate the variable data rate. The required length of the buffer is related to the Doppler frequency of the channel, and a slowly varying channel — as required for adaptive modulation — results in slowly varying data throughput and therefore the need for a high buffer capacity. Real–time interactive audio or video transmission is sensitive to delays, and therefore different modem mode adaptation algorithms are needed for such applications.

The constant throughput AOFDM scheme proposed here exploits the frequency selectivity of the channel, while offering a constant bit rate. Again, sub–band adaptivity is assumed, in order to simplify the signalling or the associated blind detection of the modem schemes.

The modulation mode allocation of the sub–bands is performed on the basis of a cost function to be introduced below, based on the expected number of bit errors in each sub–band. The expected number of bit errors, $e_{n,s}$,for each sub–band n and for each possible modulation mode index s, is calculated on the basis of the estimated channel transfer function $\hat{H}$, taking into account also the number of bits transmitted per sub–band and per modulation mode, $b_{n,s}$.

Each sub–band is assigned a state variable s_n holding the index of a modulation mode. Each state variable is initialised to the lowest order modulation mode, which in our case is 0 for "no transmission". A set of cost values $c_{n,s}$ is calculated for each sub–band n and state s as follows:

$$c_{n,s} = \frac{e_{n,s+1} - e_{n,s}}{b_{n,s+1} - b_{n,s}} \tag{22.1}$$

for all but the highest modulation mode index s. This cost value is related to the expected increase in the number of bit errors, divided by the increase of throughput, if the modulation mode having the next higher index is used instead of index s in sub–band n. In other words, Equation 22.1 quantifies the expected incremental bit error rate of the state transition $s \rightarrow s+1$ in sub–band n.

The modulation mode adaptation is performed by repeatedly searching for the block n having the lowest value of c_{n,s_n}, and incrementing its state s_n. This is repeated until the total number of bits in the OFDM symbol reaches the target number of bits. Because of the granularity in bit numbers introduced by the sub-bands, the total number of bits may exceed the target. In this case, the data is padded with dummy bits for transmission.

Figure 22.7 gives an overview of the BER performance of the fixed–throughput 512–subcarrier OFDM modem over the time dispersive channel of Figure 20.3 for a range of target bit numbers. The graph without markers represents the performance of a fixed BPSK OFDM modem over the same channel, which transmits 1 bit over each data subcarrier per OFDM symbol. The diamond–shaped markers give the performance of the equivalent–throughput adaptive scheme, both for the 16–sub–band arrangement in black, as well as for the subcarrier-by-subcarrier adaptive scheme in white. It can be seen that the 16–sub–band adaptive scheme yields a significant improvement in BER terms for SNR values above 10 dB. The SNR gain for a bit error rate of 10^{-4} is 8 dB compared to the non–adaptive case. Subcarrier-by-subcarrier adaptivity increases this gain by a further 4 dB. The modem can readily be adapted to the system requirements by adjusting the target bit rate, as it is shown in Figure 22.7. Halving the throughput to 0.5 BPS, the required SNR is reduced by 6 dB for a BER of 10^{-4}, while increasing the throughput to 2 BPS deteriorates the noise resilience by 8 dB at the same BER.

22.2.6 Signalling and blind detection

The adaptive OFDM receiver has to be informed of the modulation modes used for the different sub–bands. This information can either be conveyed using signalling subcarriers in the OFDM symbol itself, or the receiver can employ blind detection techniques in order to estimate the transmitted symbols' modulation modes, as seen in Figure 22.1.

22.2.6.1 Signalling

The simplest way of signalling the modulation mode employed in a sub–band is to replace one data symbol by an M-PSK symbol, where M is the number of possible modulation modes. In this case, reception of each of the constellation points directly signals a particular modulation mode in the current sub–band. In our case, for four modulation modes, and assuming perfect phase recovery, the probability of a signalling error $p_s(\gamma)$, when employing one signalling symbol is the symbol error probability of QPSK. Then the correct sub–band mode signalling probability is:

$$(1 - p_s(\gamma)) = (1 - p_{b,QPSK}(\gamma))^2 ,$$

where $p_{b,QPSK}$ is the bit error probability for QPSK:

$$p_{b,QPSK}(\gamma) = Q(\sqrt{\gamma}) = \frac{1}{2} \cdot \mathrm{erfc}\left(\sqrt{\frac{\gamma}{2}}\right),$$

which leads to the expression for the modulation mode signalling error probability of

$$p_s(\gamma) = 1 - \left(1 - \frac{1}{2} \cdot \mathrm{erfc}\left(\sqrt{\frac{\gamma}{2}}\right)\right)^2 .$$

The modem mode signalling error probability can be reduced by employing multiple signalling symbols and maximum ratio combining of the received signalling symbols $R_{s,n}$, in order to generate the decision variable R'_s prior to decision:

$$R'_s = \sum_{n=1}^{N_s} R_{s,n} \cdot \hat{H}^*_{s,n},$$

where N_s is the number of signalling symbols per sub–band, the quantities $R_{s,n}$ are the received symbols in the signalling subcarriers, and $\hat{H}_{s,n}$ represents the estimated values of the frequency domain channel transfer function at the signalling subcarriers. Assuming perfect channel estimation and constant values of the channel transfer function across the group of signalling subcarriers, the signalling error probability for

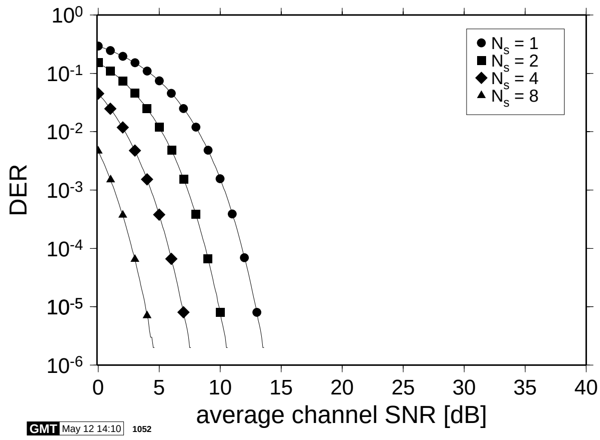

Figure 22.8: Modulation mode detection error ratio (DER), if signalling with maximum ratio combining is employed for QPSK symbols in an AWGN channel for 1, 2, 4 and 8 signalling symbols per sub–band, evaluated from Equation 22.2.

N_s signalling symbols can be expressed as:

$$p'_s(\gamma, N_s) = 1 - \left(1 - \frac{1}{2} \cdot \mathrm{erfc}\left(\sqrt{\frac{N_s\gamma}{2}}\right)\right)^2. \qquad (22.2)$$

Figure 22.8 shows the signalling error rate in an AWGN channel for 1, 2, 4 and 8 signalling symbols per sub–band, respectively. It can be seen that doubling the number of signalling subcarriers improves the performance by 3dB. Modem mode detection error ratios (DER) below 10^{-5} can be achieved at 10dB SNR over AWGN channels if two signalling symbols are used. The signalling symbols for a given sub–band can be interleaved across the entire OFDM symbol bandwidth, in order benefit from frequency diversity in fading wideband channels.

As seen in Figure 22.1, blind detection algorithms aim to estimate the employed modulation mode directly from the received data symbols, therefore avoiding the loss of data capacity due to signalling subcarriers. Two algorithms have been investigated, one based on geometrical SNR estimation, and another one incorporating error correction coding.

22.2.6.2 Blind detection by SNR estimation

The receiver has no a–priory knowledge of the modulation mode employed in a particular received sub–band and estimates this parameter by quantising the de–faded received data symbols $R_n/\hat{H}_n$ in the sub–band to the closest symbol $\hat{R}_{n,m}$ for all possible modulation modes M_m for each subcarrier index n in the current sub–band. The decision–directed error energy e_m for each modulation mode is calculated according

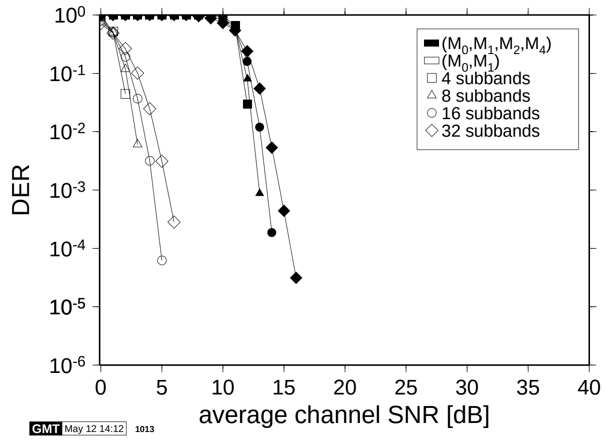

Figure 22.9: Blind modulation mode detection error ratio (DER) for 512–subcarrier OFDM systems employing (M_0, M_1) as well as for (M_0, M_1, M_2, M_4) for different numbers of subbands in an AWGN channel

to:

$$e_m = \sum_n \left(R_n/\hat{H}_n - \hat{R}_{n,m} \right)^2$$

and the modulation mode M_m which minimises e_m is chosen for the demodulation of the sub–band.

The DER of the blind modulation mode detection algorithm described in this section for a 512–subcarrier OFDM modem in an AWGN channel is depicted in Figure 22.9. It can be seen that the detection performance depends on the number of symbols per sub–band, with fewer sub–bands and therefore longer symbol sequences per sub–band leading to a better detection performance. It is apparent, however, that the number of available modulation modes has a more significant effect on the detection reliability than the block length. If all four legitimate modem modes are employed, then reliable detection of the modulation mode is only guaranteed for AWGN SNR values of more than 15–18 dB, depending on the number of sub–bands per OFDM symbol. If only M_0 and M_1 are employed, however, the estimation accuracy is dramatically improved. In this case, AWGN SNR values above 5–7 dB are sufficient to ensure reliable detection.

Figure 22.10 shows the BER performance of the fixed–threshold "data"–type 16–subband adaptive system in the fading wideband channel of Figure 20.3 for both sets of modulation modes, namely for (M_0, M_1) and (M_0, M_1, M_2, M_4) with blind modulation mode detection. Erroneous modulation mode decisions were assumed to yield a BER of 50% in the received block. This is optimistic, since in a realistic scenario the receiver would have no knowledge of the number of bits actually transmitted, leading to loss of synchronisation in the data stream. This problem is faced by all systems having a variable throughput and not employing an ideal reliable signalling channel. This impediment must be mitigated by data synchronisation measures.

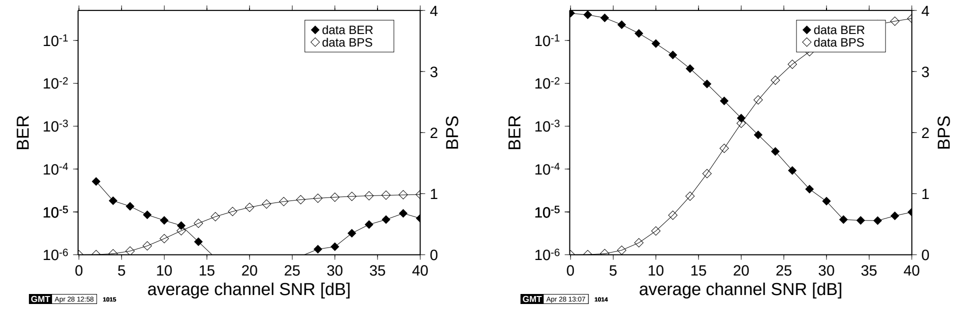

(a) (M_0, M_1) **(b)** (M_0, M_1, M_2, M_4)

Figure 22.10: BER and BPS throughput performance of a 16–subband 512–subcarrier adaptive OFDM modem employing (a) — No Transmission (M_0) and BPSK (M_1) or (b) — (M_0, M_1, M_2, M_4), both using the data–type switching levels of Table 22.1 and the SNR–based blind modulation mode detection of Section 22.2.6.2 over the Rayleigh fading time–dispersive channel of Figure 20.3

It can be seen from Figure 22.10 that while blind modulation mode detection yields poor performance for the quadruple–mode adaptive scheme, the twin–mode scheme exhibits BER results consistently better than 10^{-4}.

22.2.6.3 Blind detection by multi–mode trellis decoder

If error correction coding is invoked in the system, then the channel decoder can be employed to estimate the most likely modulation mode per sub–band. Since the number of bits per OFDM symbol is varying in this adaptive scheme, and the channel encoder's block length therefore is not constant, for the sake of implementational convenience we have chosen a convolutional encoder at the transmitter. Once the modulation modes to be used are decided upon at the transmitter, the convolutional encoder is employed to generate a zero–terminated code–word having the length of the OFDM symbol's capacity. This codeword is modulated on the subcarriers according to the different modulation modes for the different sub–bands, and the OFDM symbol is transmitted over the channel.

At the receiver, each received data subcarrier is demodulated by all possible demodulators, and the resulting hard decision bits are fed into parallel trellises for Viterbi decoding. Figure 22.11 shows a schematic sketch of the resulting parallel trellis if 16QAM (M_4), QPSK (M_2), BPSK (M_1), and "no transmission" (M_0) are employed, for a convolutional code having four states. Each sub–band in the adaptive scheme corresponds to a set of four parallel trellises, whose inputs are generated independently by the four demodulators of the legitimate modulation modes. The number of transitions in each of the trellises depends on the number of output bits received from the different demodulators, so that the 16QAM (M_4) trellis contains

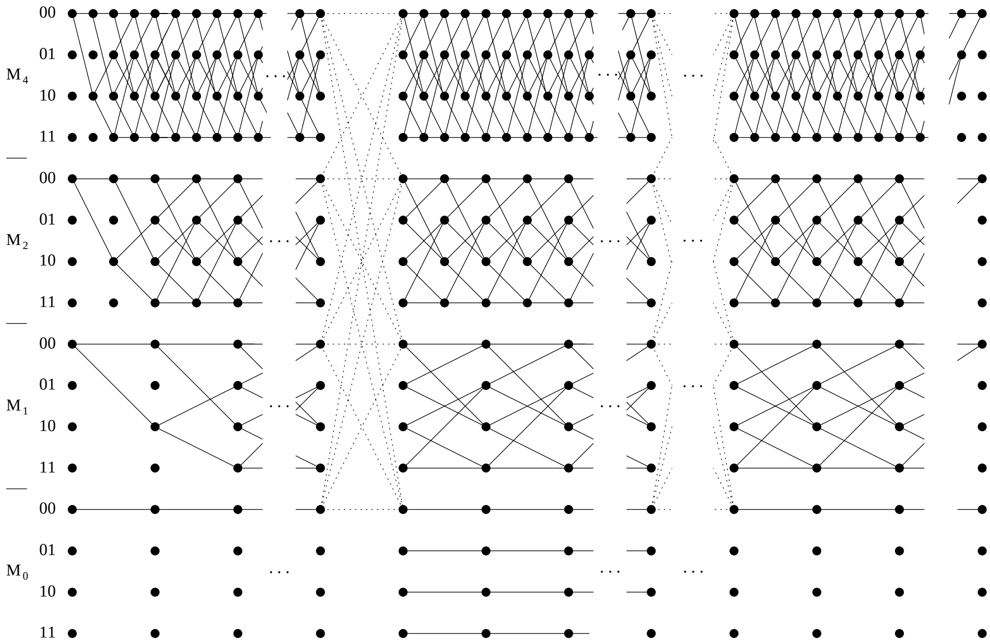

Figure 22.11: Schematic plot of the parallel trellises for blind modulation mode detection employing convolutional coding. In this example, a four–state 00–terminated convolutional encoder was assumed. The dotted lines indicate the inter–sub–band transitions for the 00 state, and are omitted for the other three states.

four times as many transitions as the BPSK and "no transmission" trellises. Since in the case of "no transmission" no coded bits are transmitted, the state of the encoder does not change. Therefore, legitimate transitions for this case are only horizontal ones.

At sub–band boundaries, transitions are allowed between the same state of all the parallel trellises associated with the different modulation modes. This is not a transition due to a received bit, and therefore preserves the metric of the originating state. Note that in the figure only the possible allowed transitions for the state 00 are drawn; all other states originate the equivalent set of transitions. The initial state of the first sub–band is 00 for all modulation modes, and, since the code is 00–terminated, the last sub–band's final states are 00.

The receiver's viterbi decoder calculates the metrics for the transitions in the parallel trellises, and once all data symbol have been processed, it traces back through the parallel trellis on the surviving path. This back–tracing commences at the most likely 00 state at the end of the last sub–band. If no termination was used at the decoder, then the back–tracing would start at the most likely of all the final states of the last block.

Figure 22.12 shows the modulation mode detection error ratio (DER) for the parallel trellis decoder in an AWGN channel for 16 and 8 sub–bands, if a convolutional

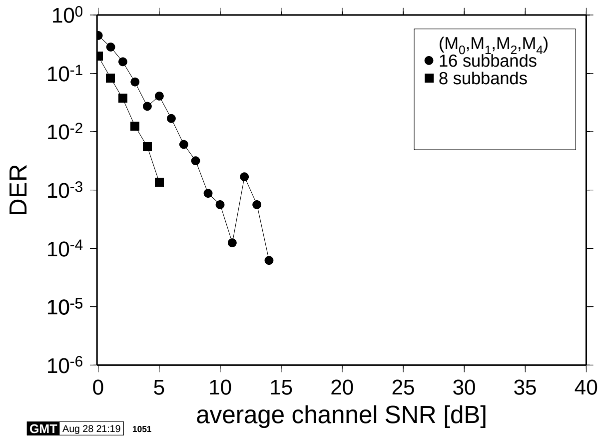

Figure 22.12: Blind modulation mode detection error ratio (DER) using the parallel trellis algorithm of Section 22.2.6.3 with a $K = 7$ convolutional code in an AWGN channel for a 512 subcarrier OFDM modem.

code of constraint length 7 is used. Comparison with Figure 22.9 shows considerable improvements relative to the BER–estimation based blind detection scheme of Section 22.2.6.2, both for 16 as well as for 8 sub–bands. Higher sub–band lengths improve the estimation accuracy by a greater degree, than what has been observed for the BER estimation algorithm of Figure 22.9. A DER of less than 10^{-5} was observed for an AWGN SNR value of 6 and 15dB in the 8– and 16–sub–band scenarios, respectively. The use of stronger codes could further improve the estimation accuracy, at the cost of higher complexity.

22.2.7 Sub–band adaptive OFDM and channel coding

Adaptive modulation can reduce the BER to a level, where channel decoders can perform well. Figure 22.13 shows both the uncoded and coded BER performance of a 512–subcarrier OFDM modem in the fading wideband channel of Figure 20.3, assuming perfect channel estimation. The channel coding employed in this set of experiments was a turbo coder [328] with a data block length of 1000 bits, employing a random interleaver and 8 decoder iterations. The log–MAP decoding algorithm was used [329]. The constituent half–rate convolutional encoders were of constraint length 3, with octally represented generator polynomials of $(7, 5)$ [297]. It can be seen that the turbo decoder provides a considerable coding gain for the different fixed modulation schemes, with a BER of 10^{-4} for SNR values of 13.8dB, 17.3dB and 23.2dB for BPSK, QPSK and 16QAM transmission, respectively.

Figure 22.14 depicts the BER and throughput performance of the same decoder employed in conjunction with the adaptive OFDM modem for different adaptation algorithms. Figure 22.14(a) shows the performance for the “speech” system employing the switching levels listed in Table 22.1. As expected, the half–rate channel coding results in a halved throughput compared to the uncoded case, but offers low–BER

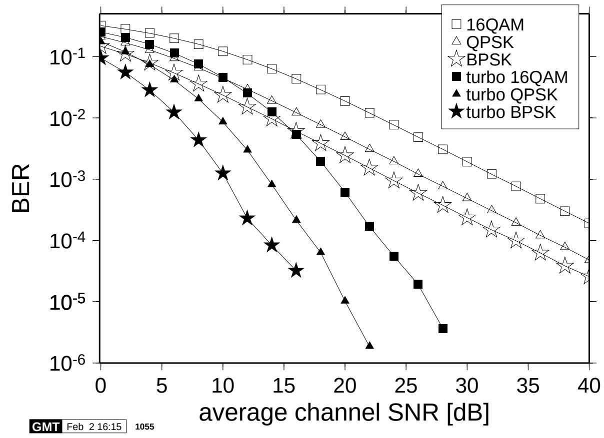

Figure 22.13: BER performance of the 512–subcarrier OFDM modem in the fading time–dispersive channel of Figure 20.3 for both uncoded and half–rate turbo–coded transmission, using 8–iteration log–MAP turbo decoding, 1000–bit random interleaver, and a constraint length of 3.

transmission over the channel of Figure 20.3 for SNR values of down to 0dB, maintaining a BER below 10^{-6}.

Further tuning of the adaptation parameters can ensure a better average throughput, while retaining error–free data transmission. The switching level based adaptation algorithm of Table 22.1 is difficult to control for arbitrary bit error rates, since the set of switching levels was determined by an optimisation process for uncoded transmission. Since the turbo–codec has a non–linear BER versus SNR characteristic, direct switching–level optimisation is an arduous task. The sub–band BER predictor of Section 22.2.4.2 is easier to adapt to a channel codec, and Figure 22.14(b) shows the performance for the same decoder, with the adaptation algorithm employing the BER–prediction method having an upper BER–bound of 1%. It can be seen that the less stringent uncoded BER constraints when compared to Figure 22.14(a) lead to a significantly higher throughput for low SNR values. The turbo–decoded data bits are error–free, hence a further increase in throughput is possible while maintaining a high degree of coded data integrity.

The second set of curves in Figure 22.14(b) show the system's performance, if an uncoded target BER of 10% is assumed. In this case, the turbo decoder's output BER is below 10^{-5} for all the SNR values plotted, and shows a slow decrease for increasing values of SNR. The throughput of the system, however, exceeds 0.5 data bits per symbol for SNR values of more than 2dB.

22.2.8 The effect of channel Doppler frequency

Since the adaptive OFDM modem employs the most recently received OFDM symbol in order to predict the frequency domain transfer function of the reverse channel for

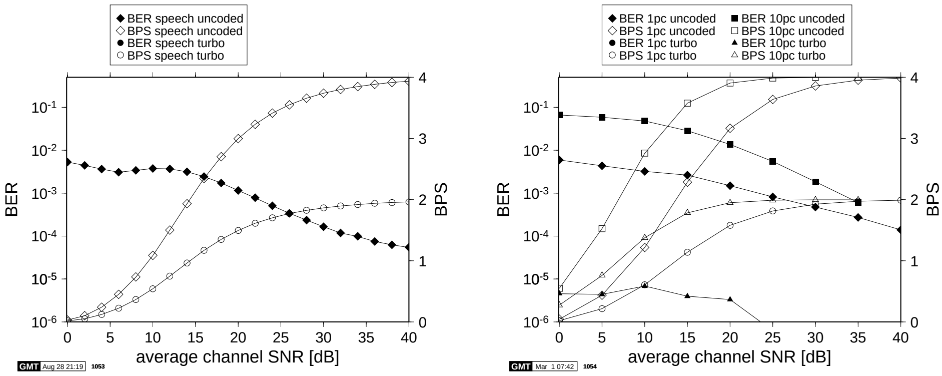

(a) speech system   **(b)** maximal BER 1% and 10%

Figure 22.14: BER and BPS throughput performance of 16-subband 512–subcarrier adaptive turbo coded and uncoded OFDM modem employing (M_0, M_1, M_2, M_4) for (a) — speech type switching levels of Table 22.1 and (b) — a maximal estimated sub–band BER of 1% and 10% over the channel of Figure 20.3. The turbo coded transmission over the speech system and the 1% maximal BER system are error free for all examined SNR values and therefore the corresponding BER curves are omitted from the graphs.

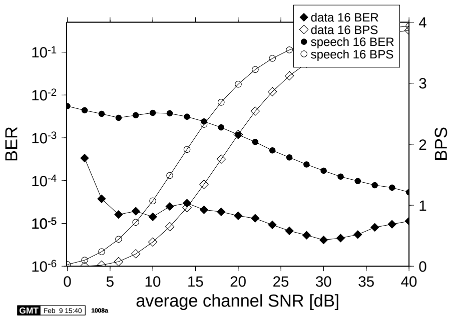

(a) $F'_d = 7.41 \cdot 10^{-3}$

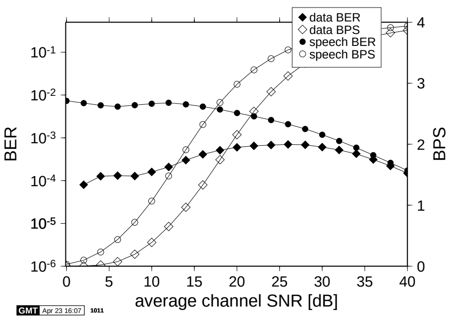

(b) $F'_d = 5.928 \cdot 10^{-2}$

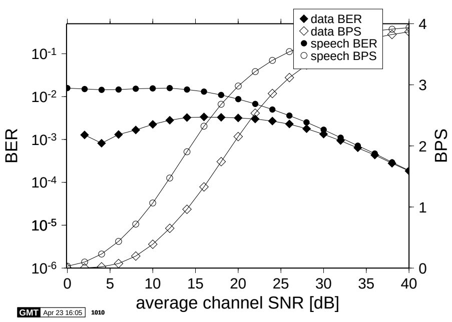

(c) $F'_d = 1.1856 \cdot 10^{-1}$

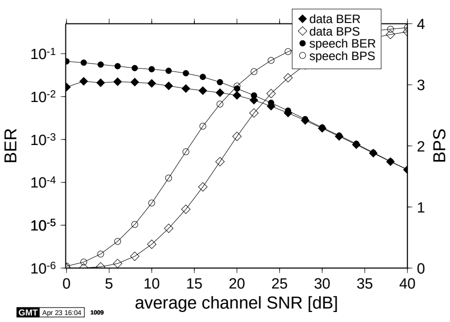

(d) $F'_d = 2.3712 \cdot 10^{-1}$

Figure 22.15: BER and BPS throughput performance of 16–subband 512–subcarrier adaptive OFDM modem employing (M_0, M_1, M_2, M_4) for both data–type and speech–type switching levels with perfect modulation mode detection and different frame normalised Doppler frequencies F'_d over the channel of Figure 20.3. The triangular markers in (a) show the performance of a subcarrier–by–subcarrier adaptive modem using the data–type switching levels of Table 22.1 for comparison.

the next transmission, the quality of this prediction suffers from the time–variance of the channel transfer function between the uplink and downlink timeslots. We assume that the time delay between the up– and downlink slots is the same as the delay between the down– and uplink slots, and we refer to this time as the frame duration T_f. We normalise the maximal Doppler frequency f_d of the channel to the frame duration T_f, and define the *frame–normalised Doppler frequency* F'_d as $F'_d = f_d \cdot T_f$. Figure 22.15 depicts the fixed switching level (see Table 22.1) modem's BER and throughput performance in bits–per–symbol (BPS) for values of F'_d between $7.41 \cdot 10^{-3}$ and $2.3712 \cdot 10^{-1}$. These values stem from the studied WATM system with a time slot duration of 2.67μs and up–/downlink delays of 1, 8, 16, and 32 timeslots at a channel Doppler frequency of 2.78 kHz. As mentioned in Section 20.1.1.1, this corresponds to a system employing a carrier frequency of 60 GHz, a sampling rate of 225 MSamples/s and a vehicular velocity of 50 km/h or $13.\bar{8}$ m/s.

Figure 22.15(a) shows the BER and BPS throughput of the studied modems in a framework with consecutive up– and downlink timeslots. This corresponds to $F_d' = 7.41 \cdot 10^{-3}$, while the target bit error rates for the speech and data system are met for all SNR values above 4 dB, and the BER performance is generally better than the target error rates. This was explained above with the conservative choice of modulation modes based on the most corrupted subcarrier in each sub–band, resulting in lower throughput and lower bit error rates for the switching–level based sub–band adaptive modem.

Comparing Figure 22.15(a) with the other performance curves, it can be seen that the bit error rate performance for both the speech and the data system suffer from increasing decorrelation of the predicted and actual channel transfer function for increasing values of F_d'. In Figure 22.15(b) an 8–timeslot delay was assumed between up– and downlink timeslots, which corresponds to $F_d' = 5.928 \cdot 10^{-2}$, and — as a consequence — the BER performance of the modem was significantly deteriorated. The "speech" system still maintains its target BER, but the "data" system delivers a BER of up to 10^{-3} for SNR values between 25 and 30dB. It is interesting to observe that the delayed channel prediction mainly affects the higher order modulation modes, which are employed more frequently at high SNR values. This explains the shape of the BER curve for the "data" system, which is rising from below 10^{-4} at 2dB SNR up to 10^{-3} at 26dB SNR. The average throughput of the modem is mainly determined by the statistics of the estimated channel transfer function at the receiver, and this is therefore not affected by the delay between the channel estimation and the packet transmission.

22.2.9 Channel estimation

All the adaptive modems above rely on the estimate of the frequency–domain channel transfer function, both for equalisation of the received symbols at the receiver, as well as for the modem mode adaptation of the next transmitted OFDM symbol. Figure 22.16 shows the BER versus SNR curves for the 1% target–BER modem, as it was presented above, if pilot symbol assisted channel estimation [7] is employed instead of the previously used delayed, but otherwise perfect, channel estimation.

Comparing the curves for perfect channel estimation and for the 64–pilot based lowpass interpolation algorithm, it can be seen that the modem falls short of the target bit error rate of 1% for channel SNR values of up to 20dB. More noise–resilient channel estimation algorithms can improve the modem's performance. If the pass–band width of the interpolation lowpass filter (see Section 20.3.1.1) is halved, which is indicated in Figure 22.16 as the reduced bandwidth (red. bw.) scenario, then the BER gap between the perfect and the pilot symbol assisted channel estimation narrows, and a BER of 1% is achieved at an SNR of 15dB. Additionally, employing pairs of pilots with the above bandwidth–limited interpolation scheme further improves the modem's performance, which results in BER values below 1% for SNR values above 5dB. The averaging of the pilot pairs improves the noise resilience of the channel estimation,

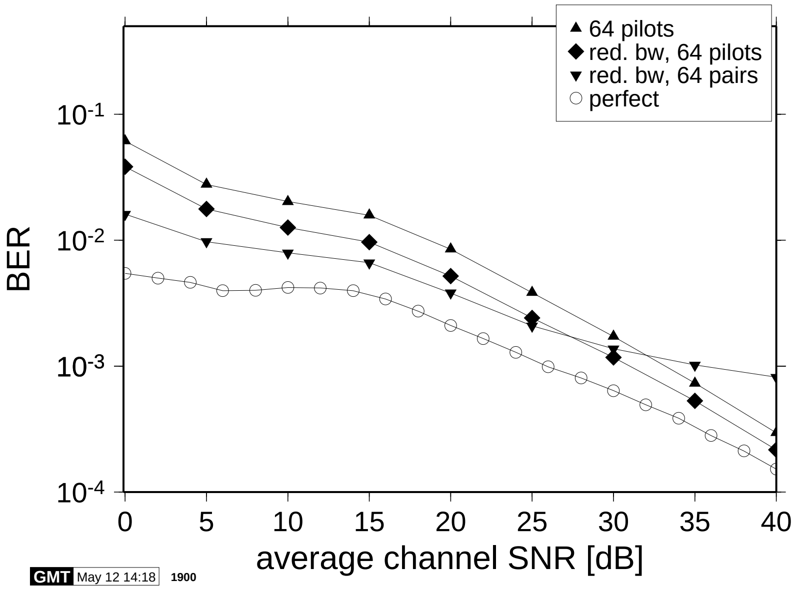

Figure 22.16: BER versus channel SNR performance for the 1% target–BER adaptive 16–sub–band 512–subcarrier OFDM modem employing pilot symbol assisted channel transfer function estimation over the channel of Figure 20.3.

but introduces estimation errors for high SNR values. This can be observed in the residual BER in the figure.

Having studied a range of different AOFDM modems, let us now embark on a system–design study in the context of an adaptive interactive speech system.

22.3 Adaptive speech transmission system

The proposed speech transmission system discussed here has been developed in co–operation with the co–authors of [330]. Details about the source codec and its performance are discussed in the above publication.

22.3.1 Introduction

In this section we introduce a bi–directional high quality audio communications system, which will be used to highlight the systems aspects of adaptive OFDM transmissions over time dispersive channels. Specifically, the channel coded adaptive transmission characteristics and a potential application for joint adaptation of modulation, channel coding and source coding is studied.

The basic principle of adaptive modulation is to react to the anticipated channel capacity for the next OFDM symbol transmission burst, by employing modulation modes of different robustness to channel impairments and of different data throughput. The trade–off between data throughput and integrity can be adapted to different system environments. For data transmission systems, which are not dependent on a fixed data rate and do not require low transmission delays, variable–throughput adaptive schemes can be devised that operate efficiently with powerful error correction coders, such as long block length turbo codes [331]. Real–time audio or video communications employing source codecs, which allow variable bit rates, can also be used in conjunction with variable rate adaptive schemes, but in this case block–based error correction coders cannot be readily employed.

Fixed rate adaptive OFDM systems — which sacrifice a guaranteed BER performance for the sake of a fixed data throughput — are more readily integrated into interactive communications systems, and can co–exist with long block–based channel coders in real–time applications.

For these investigations, we propose a hybrid adaptive OFDM scheme, based on a multi–mode constant throughput algorithm, consisting of two adaptation loops: an inner constant throughput algorithm, having a bit rate consistent with the source and channel coders, and an outer mode switching control loop, which selects the target bit rate of the whole system from a set of distinct operating modes. These issues will become more explicit during our further discourse.

22.3.2 System overview

The structure of the studied adaptive OFDM modem is depicted schematically in Figure 22.17. The top half of the diagram is the transmitter chain, which consists of the source- and channel coders, a channel interleaver de–correlating the channel's frequency–domain fading, an adaptive OFDM modulator, a multiplexer adding signalling information to the transmit data, and an IFFT/RF OFDM block. The receiver, at the lower half of the schematic, consists of a RF/FFT OFDM receiver, a demultiplexer extracting the signalling information, an adaptive demodulator, a de–interleaver/channel decoder and the source decoder. The parameter adaptation linking the receiver- and transmitter chain consists of a channel estimator, and the

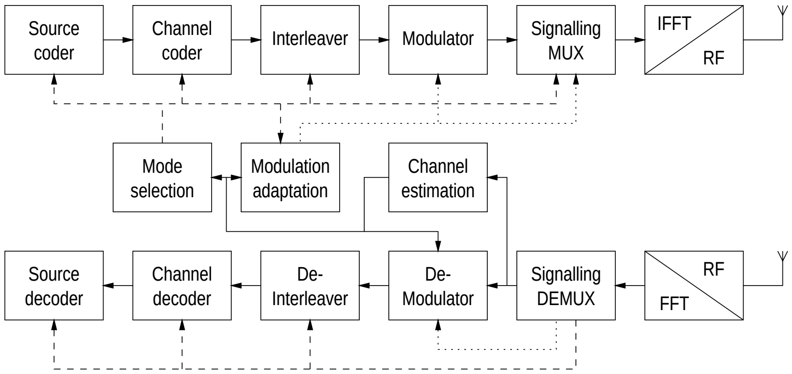

Figure 22.17: Schematic model of the multi–mode adaptive OFDM system

throughput mode selection as well as the modulation adaptation blocks.

The open–loop control structure of the adaptation algorithms can be seen in the figure: the receiver's operation is controlled by the signalling information that is contained in the received OFDM symbol, while the channel quality information generated by the receiver is employed to determine the remote transmitter's matching parameter set by the modulation adaptation algorithms. The two distinct adaptation loops distinguished by the dotted and dashed lines are the inner and outer adaptation loops, respectively. The outer adaptation loop controls the overall throughput of the system, which is chosen from a finite set of pre–defined modes, so that a fixed–delay decoding of the received OFDM data packets becomes possible. This outer loop controls the block length of the channel encoder and interleaver, and the target throughput of the inner adaptation loop. The operation of the adaptive modulator, controlled by the inner loop, is transparent to the rest of the system. The operation of the adaptation loops is described in more detail below.

22.3.2.1 System parameters

The transmission parameters have been adopted from the TDD–mode of the UMTS system of Section 20.1.3, with a carrier frequency of 1.9GHz, a time–frame and time–slot duration of 4.615ms and 122μs, respectively. The sampling rate is assumed to be 3.78MHz, leading to a 1024–subcarrier OFDM symbol with a cyclic extension of 64 samples in each time slot. For spectral shaping of the OFDM signal, there are a total of 206 virtual subcarriers at the bandwidth boundaries.

The 7 kHz bandwidth PictureTel audio codec[1] has been chosen for this system because of its good audio quality, robustness to packet dropping and adjustable bit rate. The channel encoder/interleaver combination is constituted by a convolutional turbo codec [328] employing block turbo interleavers with in conjunction with a subsequent pseudo–random channel interleaver. The constituent half–rate recursive systematic convolutional (RSC) encoders are of constraint length 3, with octal generator

[1] see http://www.picturetel.com

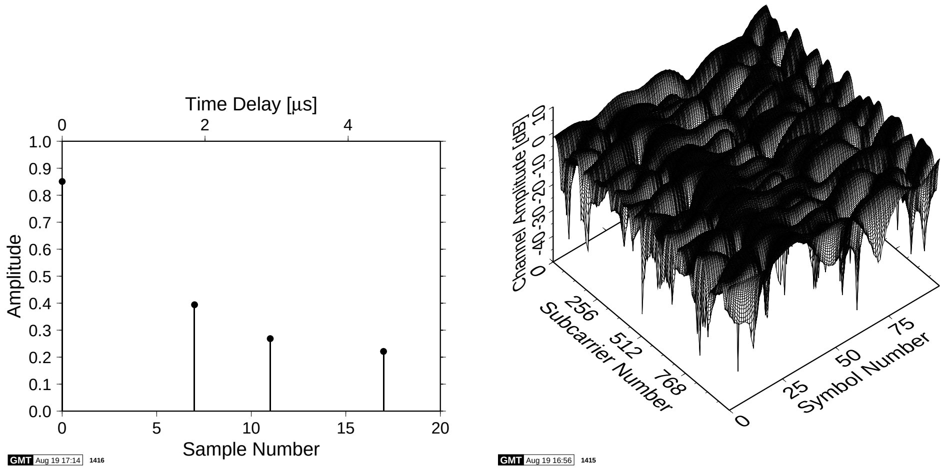

(a) unfaded impulse response **(b)** time varying amplitude

Figure 22.18: Channel for PictureTel experiments: (a) – unfaded channel impulse response (b) – time varying channel amplitude for 100 OFDM symbols.

polynomials of $(7, 5)$ [297]. At the decoder, 8 iterations are performed, utilising the so–called Maximum Aposteriory (MAP) [329] algorithm and log-likelihood ratio soft inputs from the demodulator.

The channel model consists of a four path COST 207 Typical Urban impulse response [305], where each impulse is subjected to independent Rayleigh fading with a normalised Doppler frequency of $2.25 \cdot 10^{-6}$, corresponding to a pedestrian scenario with a walking speed of 3mph.

The unfaded impulse response and the time– and frequency–varying amplitude of the channel transfer function is depicted in Figure 22.18.

22.3.3 Constant throughput adaptive modulation

The constant throughput adaptive algorithm attempts to allocate a given number of bits for transmission in subcarriers exhibiting a low BER, while the use of high BER subcarriers is minimised. We employ the open–loop adaptive regime of Figure 22.1, basing the decision concerning the next transmitted OFDM symbol's modulation scheme allocation on the channel estimation gained at the reception of the most recently received OFDM symbol by the local station. Sub–band adaptive modulation [332] — where the modulation scheme is adapted not on a subcarrier–by–subcarrier basis, but for sub–bands of adjacent subcarriers — is employed in order to simplify the signalling requirements. The adaptation algorithm was highlighted in Section 22.2.5. For these investigations we employed 32 subbands of 32 subcarriers in each OFDM symbol. Perfect channel estimation and signalling were used.

22.3.3.1 Constant–rate BER performance

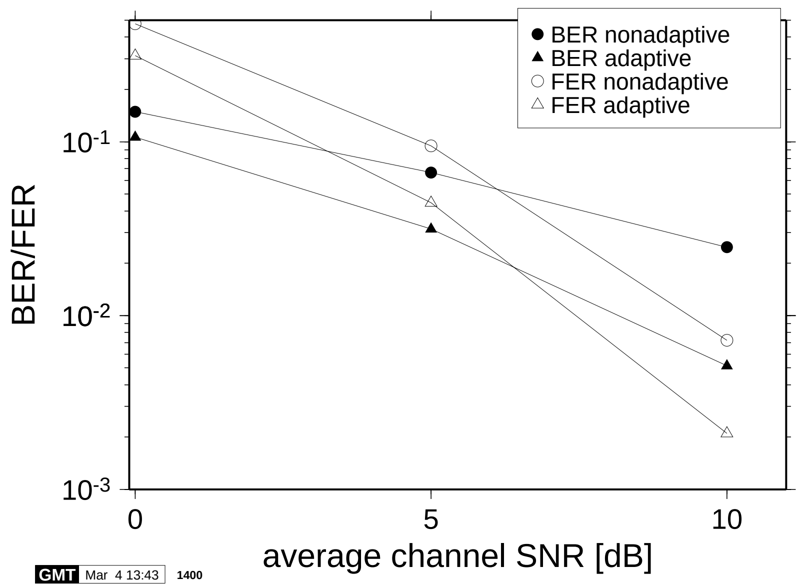

Figure 22.19: BER and FER performance for the fixed throughput adaptive and non–adaptive OFDM modems in the fading time dispersive channel of Section 20.1.3 for a block length of 578 coded bits.

Figure 22.19 characterises the fixed–throughput adaptive modulation scheme's performance under the channel conditions characterised above, for a block length of 578 coded bits. As a comparison, the BER curve of a fixed BPSK modem transmitting the same number of bits in the same channel, employing 578 out of 1024 subcarriers, is also depicted. The number of useful audio bits per OFDM symbol was based on a 200–bit target data throughput, which corresponds to a 10 kbps data rate, padded with 89 bits, which can contain a check–sum for error detection and high–level signalling information. Furthermore, half–rate channel coding was used.

The BER plotted in the figure is the hard–decision based bit error rate at the receiver before channel decoding. It can be seen that the adaptive modulation scheme yields a significantly improved performance, which is reflected also in the Frame Error Rate (FER). This FER approximates the probability of a decoded block containing errors, in which case it is unusable for the audio source decoder and hence it is dropped. This error event can be detected by using the check–sum in the OFDM data symbol.

As an example, the modulation mode allocation for the 578–data–bit adaptive modem at an average channel SNR of 5dB is given in Figure 22.20(a) for 100 consecutive OFDM symbols. The unused sub–bands with indexes 15 and 16 contain the virtual carriers, and therefore do not transmit any data. It can be seen that the constant throughput adaptation algorithm of Section 22.2.5 allocates data to the higher

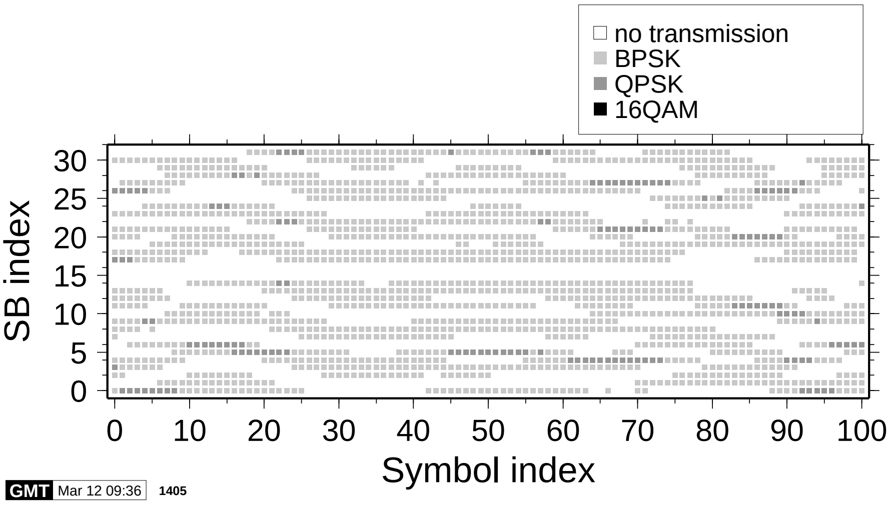

(a) 578 data bits per OFDM symbol

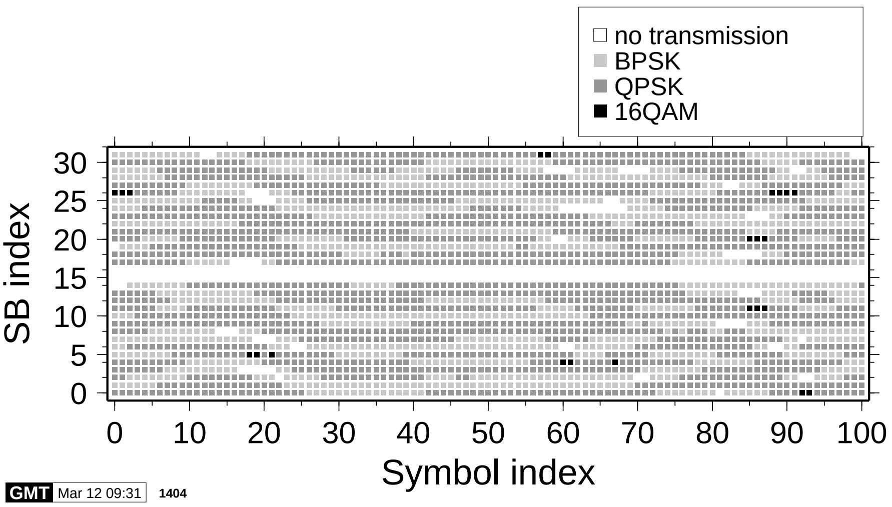

(b) 1458 data bits per OFDM symbol

Figure 22.20: Overview of modulation mode allocation for fixed throughput adaptive modems over the fading time–dispersive channel of Figure 22.18(b) at 5dB average channel SNR.

quality subcarriers on a symbol–by–symbol basis, while keeping the total number of bits per OFDM symbol constant. As a comparison, Figure 22.20(b) shows the equivalent overview of the modulation modes employed for a fixed bit rate of 1458 bits per OFDM symbol. It can be seen that in order to meet this increased throughput target, hardly any sub–bands are in "no transmission" mode, and overall higher order modulation schemes have to be employed.

22.3.4 Multi–mode adaptation

While the fixed–throughput adaptive algorithm described above copes with the frequency–domain fading of the channel, there is a medium-term variation of the overall channel capacity due to time–domain channel quality fluctuations as indicated in Figure 22.18(b). While it is not straightforward to employ powerful block–based channel coding schemes — such as turbo coding — in variable throughput adaptive OFDM schemes for real–time applications like voice or video telephony, a multi–mode adaptive system can be designed that allows us to switch between a set of different source– and channel codecs as well as transmission parameters, depending on the overall channel quality. We have investigated the use of the estimated overall BER at the output of the receiver, which is the sum of all the $e(j, s_j)$ quantities of Equation 22.1 after adaptation. On the basis of this expected bit error rate at the input of the channel decoder, the probability of a frame error (FER) must be estimated and compared with the estimated FER of the other modem modes. Then, the mode having the highest throughput exhibiting an estimated FER of less than 10^{-6} — or alternatively the mode exhibiting the lowest FER — is selected and the source encoder, the channel encoder and the adaptive modem are set up accordingly.

We have defined four different operating modes, which correspond to unprotected audio data rates of 10, 16, 24, and 32 kbps at the source codec's interface. With half–rate channel coding and allowing for check–sum and signalling overhead, the number of transmitted coded bits per OFDM symbol was 578, 722, 1058, and 1458 for the four modes, respectively.

22.3.4.1 Mode switching

Figure 22.21 shows the *observed* FER for all four modes versus the unprotected BER that was *predicted* at the transmitter. The predicted unprotected BER was discretised into intervals of 1%, and the channel coded FER was evaluated over these BER intervals. It can be seen from the figure that for estimated protected BER values below 5% no frame errors were observed for any of the modes. For higher estimated unprotected BER values, the higher throughput modes exhibited a lower FER than the lower throughput modes, which was consistent with the turbo coder's performance increase for longer block lengths. A FER of 1% was observed for a 7% predicted unprotected error rate for the 10kbps mode, while BER values of 8% to 9% were allowed for the longer blocks, whilst still maintaining a FER of less than 1%

For this experiment, we assumed the best–case scenario of using the actual measured FER statistics of Figure 22.21 for the mode switching algorithm rather than estimating the FER on the basis of the estimated uncoded BER. In this case, the

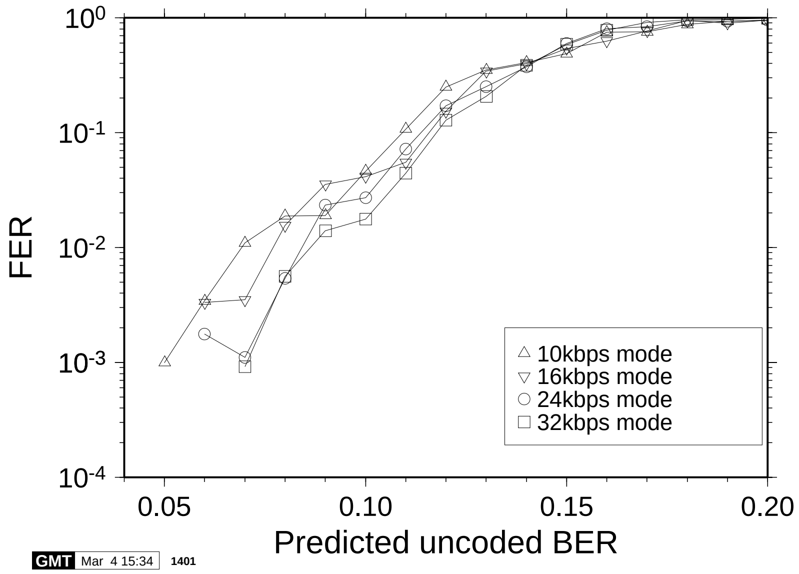

Figure 22.21: Frame error rate versus the predicted unprotected BER for 10kbps, 16kbps, 24kbps and 32kbps modes.

previously observed FER corresponding to the predicted overall BER values for the different modes were compared, and the mode having the lowest FER was chosen for transmission. The mode switching sequence for the first 500 OFDM symbols at 5dB channel SNR over the channel of Figure 22.18(b) is depicted in Figure 22.22. It can be seen that in this segment of the sequence 32kbps transmission is the most frequently employed mode, followed by the 10kbps mode. The intermediate modes are mostly transitory, as the improving or deteriorating channel conditions render switching between the 10kbps and 32kbps modes necessary. This behaviour is consistent with Table 22.2, for the "Switch-I" scheme.

22.3.5 Simulation results

The comparison between the different adaptive schemes will be based on a channel SNR of 5 dB over the channel of Figure 22.18(b), since the audio codec's performance is unacceptable for SNR values around 0 dB, and as the adaptive modulation is most effective for channel SNR values below 10 dB (see [330]).

22.3.5.1 Frame error results

The audio experiments [330] have shown that the audio quality is acceptable for frame dropping rates of about 5%, and that the perceived audio quality increases with increasing throughput. Table 22.2 gives an overview of the frame error rates and mode switching statistics of the system for a channel SNR of 5dB over the channel of Figure 22.18(b). It can be seen that for the fixed modes the FER increases with the

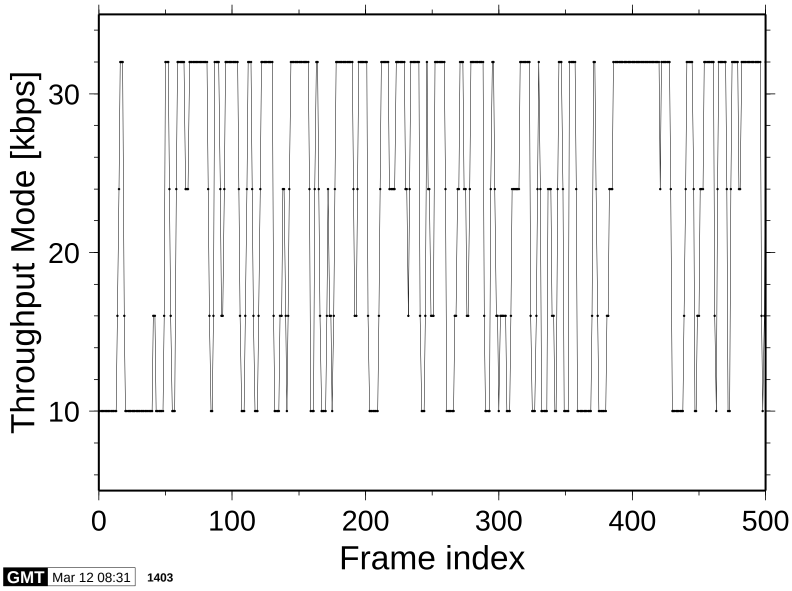

Figure 22.22: Mode switching pattern at 5dB channel SNR over the channel of Figure 22.18(b).

Scheme	FER [%]	Rate-10kbps [%]	Rate-16kbps [%]	Rate-24kbps [%]	Rate-32kbps [%]
Fixed-10kbps	4.45	95.55	0.0	0.0	0.0
Fixed-16kbps	5.58	0.0	94.42	0.0	0.0
Fixed-24kbps	10.28	0.0	0.0	89.72	0.0
Fixed-32kbps	18.65	0.0	0.0	0.0	81.35
Switch-I	4.44	21.87	13.90	11.59	48.20
Switch-II	5.58	0.0	34.63	11.59	48.20

Table 22.2: FER and relative usage of different bitrates in the fixed bit rate and the variable–rate schemes Switch I and II (successfully transmitted frames) for a channel SNR of 5dB over the channel of Figure 22.18(b)

throughput, from 4.45% in the 10kbps mode up to 18.65% for the 32kbps mode. This is because, the turbo–codecs performance improves for longer interleavers, the OFDM symbol had to be loaded with more bits, resulting in a higher unprotected BER. The time–variant bitrate mode–switching schemes, referred to as *Switch I* and *Switch II* for the four– and three–mode switching regimes used, deliver frame dropping rates of 4.44% and 5.58%, respectively. Both these FER values are acceptable for the audio transmission. It can be seen that upon incorporating the 10kbps mode in the switching regime *Switch I* of Table 22.2 the overall FER is lowered only by an insignificant amount, while the associated average throughput was reduced considerably, as it can be seen from the rate statistics of Table 22.2.

22.3.5.2 Audio segmental SNR

Figure 22.23 displays the cumulative density function (CDF) of the segmental SNR (SEGSNR) [297] obtained from the reconstructed signal of an audio test sound for all the modes of Table 22.2 discussed above at a channel SNR of 5 dB over the channel of Figure 22.18(b).

Focusing our attention on the figure, a whole range of interesting conclusions accrue. As expected, for any given SEGSNR it is desirable to maintain as low a proportion of the audio frames' SEGSNRs below a given abscissa value as possible. Hence we conclude that the best SEGSNR CDF was attributable to the *Switch II* scheme, while the worst performance was observed for the fixed–10kbps scheme. Above a SEGSNR of 15dB the CDFs of the fixed 16, 24 and 32kbps modes follow our expectations. Viewing matters from a different perspective, the *Switch II* scheme exhibits a SEGSNR of less than 20dB with a probability of 0.8, compared to 0.95 for the fixed–10kbps scheme.

Before concluding we also note that the CDFs do not have a smoothly tapered tail, since for the erroneous audio frames a SEGSNR of 0dB was registered. This results in the step–function like behaviour associated with the discontinuities corresponding to the FER values in the FER column of Table 22.2.

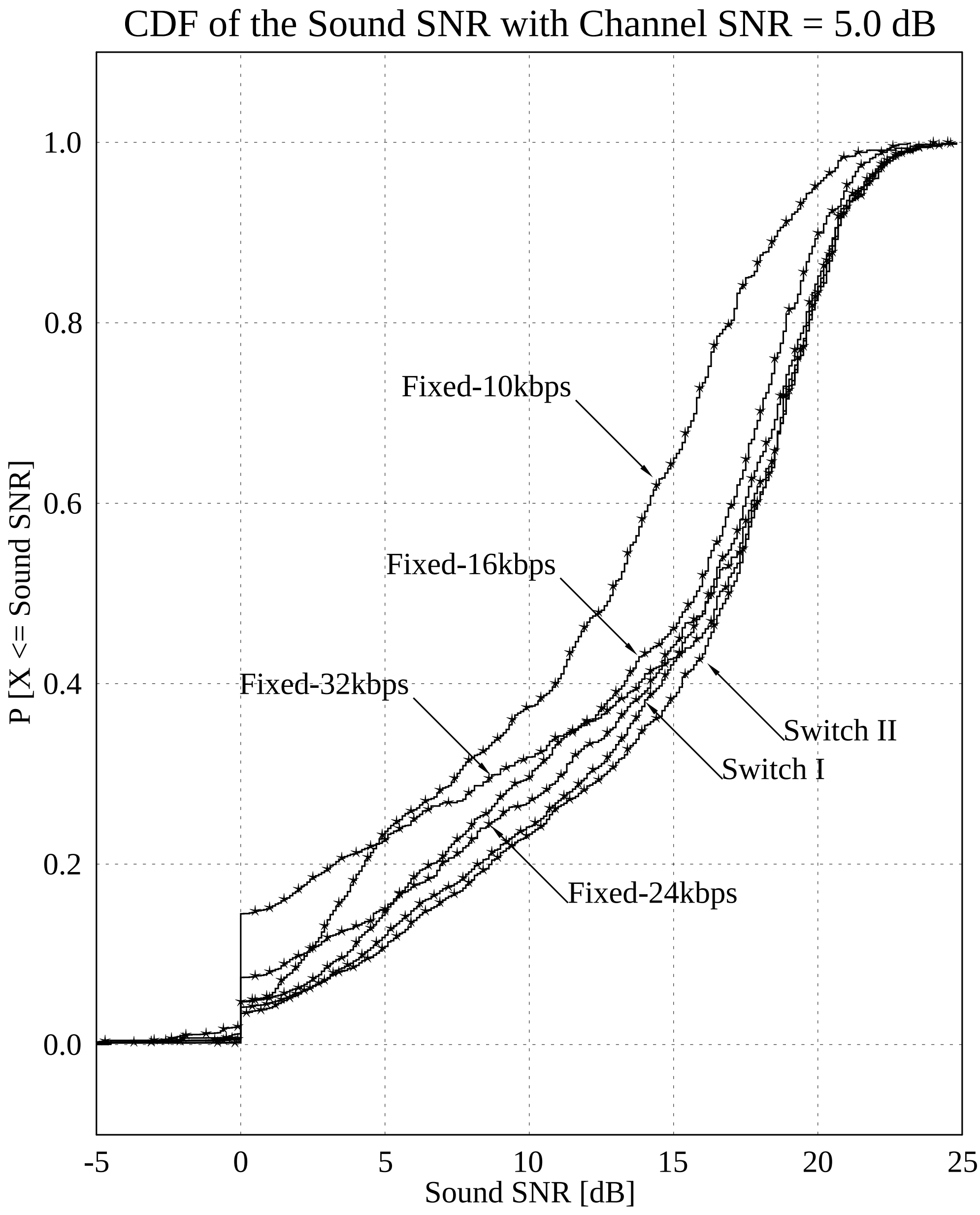

Figure 22.23: Typical CDF of the Segmental SNR of a reconstructed audio signal transmitted over the fading time dispersive channel of Section 20.1.3 at a channel SNR of 5dB. (from [330])

22.4 Pre–Equalisation

We have seen above how the receiver's estimate of the channel transfer function can be employed by the transmitter in order to dramatically improve the performance of an OFDM system by adapting the subcarrier modulation modes to the channel conditions. For subchannels exhibiting a low signal–to–noise ratio, robust modulation modes were used, while for subcarriers having a high SNR, high throughput multi–level modulation modes can be employed. An alternative approach to combating the frequency selective channel behaviour is to apply pre–equalisation to the OFDM symbol prior to transmission on the basis of the anticipated channel transfer function. We will investigate a range of related topics in this section.

22.4.1 Motivation

As discussed above, the received data symbol R_n of subcarrier n over a stationary time–dispersive channel can be characterised by:

$$R_n = S_n \cdot H_n + n_n,$$

where S_n is the transmitted data symbol, H_n is the channel transfer function of subcarrier n, and n_n is a noise sample.

The frequency–domain equalisation at the receiver — which is necessary for non–differential detection of the data symbols — corrects the phase and amplitude of the received data symbols using the estimate of the channel transfer function $\hat{H}_n$ as follows:

$$R'_n = R_n/\hat{H}_n = S_n \cdot H_n/\hat{H}_n + n_n/\hat{H}_n.$$

If the estimate $\hat{H}_n$ is accurate, this operation de–fades the constellation points before decision. However, upon de–fading the noise sample n_n is amplified by the same amount as the signal, therefore preserving the SNR of the received sample.

Pre–equalisation for the OFDM modem operates by scaling the data symbol of subcarrier n, S_n, by a pre–distortion function E_n, computed from the inverse of the anticipated channel transfer function, prior to transmission. At the receiver, no equalisation is performed, hence the received symbols can be expressed as:

$$R_n = S_n \cdot E_n \cdot H_n + n_n.$$

Since no equalisation is performed, there is no noise amplification at the receiver. Similarly to the adaptive modulation techniques illustrated above, pre–equalisation is only applicable to a duplex link, since the transmitted signal is adapted to the specific channel conditions perceived by the receiver. Like for other adaptive schemes, the transmitter needs an estimate of the current frequency–domain channel transfer function, which can be obtained from the received signal in the reverse link, as seen in Figure 22.1.

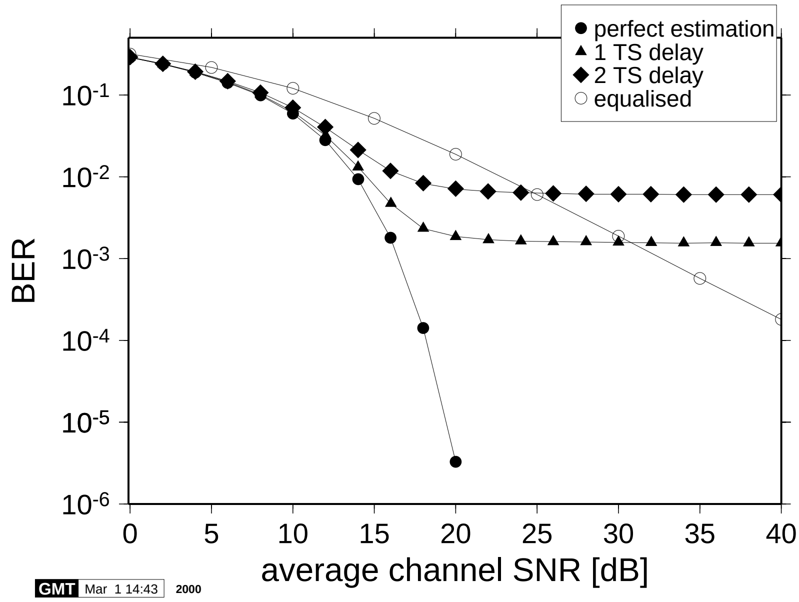

Figure 22.24: BER performance of the 512–subcarrier 16–QAM OFDM modem over the fading short WATM channel of Figure 20.3 employing full channel inversion and delays of 0, 1, and 2 timeslots (TS) between the instant of perfect channel estimation and reception. Also depicted is the performance of a perfectly equalised modem under the same channel conditions.

22.4.2 Perfect channel inversion

The simplest choice of the pre–equalisation transfer function E_n is the inverse of the estimated frequency domain channel transfer function, $E_n = 1/\hat{H}_n$. If the estimation of the channel transfer function is accurate, then channel inversion will result in an AWGN–like channel perceived at the receiver, since all time- and frequency-dependent behaviour of the channel is pre–compensated at the transmitter. The BER performance of such a system, accordingly, is identical to that of the equivalent modem in an AWGN channel. Figure 22.24 shows the BER performance of the 512-subcarrier OFDM modem in the short WATM channel of Figure 20.3, with adjacent up– and downlink time slots (TS). The average channel SNR on the ordinate is the average SNR at the receiver, provided that the pre–equalisation algorithm compensates only for the effects of frequency–domain fading. The different SNR values can be viewed as a result of additional constant path loss variation, and are not corrected by the pre–equalisation algorithm. The channel estimation is assumed to be perfect at the time of receiving an OFDM symbol in the timeslot, and this estimation is used for the next reverse link transmission. It can be seen that the performance for 1 timeslot delay between up– and downlink is fairly close to the Gaussian performance for SNR values of up to 10dB, but that there is a BER floor of about $1.5 \cdot 10^{-3}$. This is due to the delay between the instant of channel estimation and the reception. The curve

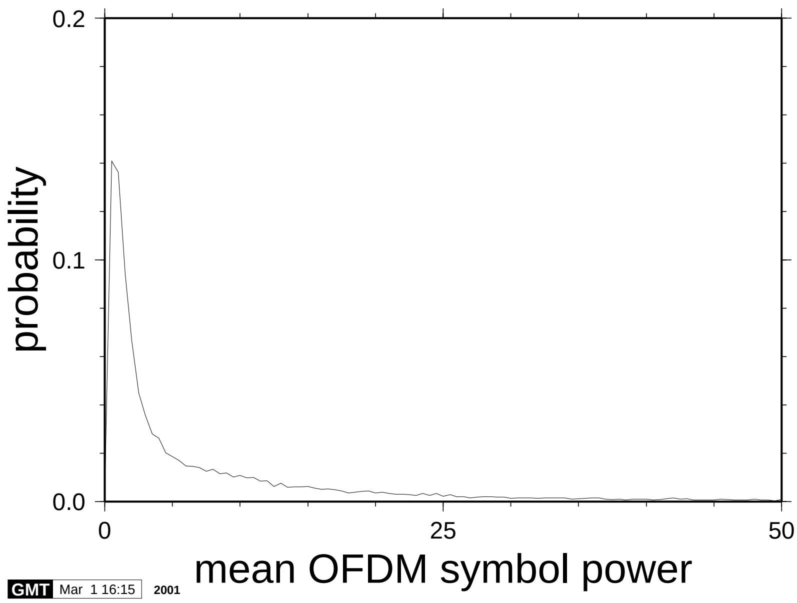

Figure 22.25: OFDM symbol energy histogram for 512–subcarrier 16–QAM with full channel inversion over the short WATM channel of Figure 20.3. The corresponding BER curves are given in Figure22.24.

referred to as "perfect estimation" in the figure represents the case of no delay between channel estimation and reception, which has been implemented by invoking a lookahead in the channel, so that the transmitter exactly knows the channel transfer function in the future transmit timeslot. In this case, there is no error floor and the system's performance follows closely the theoretical Gaussian curve for 16QAM transmission. A further curve on the graph indicates the measured performance of the modem for a delay of 2 timeslots between channel estimation and reception. It can be observed that the BER performance deteriorates further, with a BER floor of 0.7%.

Since the pre–equalisation algorithm amplifies the power in each subcarrier by the corresponding estimate of the channel transfer function, the transmitter's output power fluctuates in an inverse fashion with respect to time–variant channel. The fades in the frequency domain channel transfer function can be deep, hence the transmit power in the corresponding subcarriers may be high. Figure 22.25 shows the histogram of the total OFDM symbol energy at the transmitter's output for the short WLAN channel of Figure 20.3 with 'full channel inversion', normalised to the fixed average output energy. It can be seen that the OFDM symbol energy fluctuates widely, with observed peak values in excess of 55. The long–term mean symbol energy was measured to be 22.9, which corresponds to an average output power increase of 13.6dB. Since this imposes unacceptable constraints on the power amplifier, in the next section we considered a range of limited–dynamic scenarios.

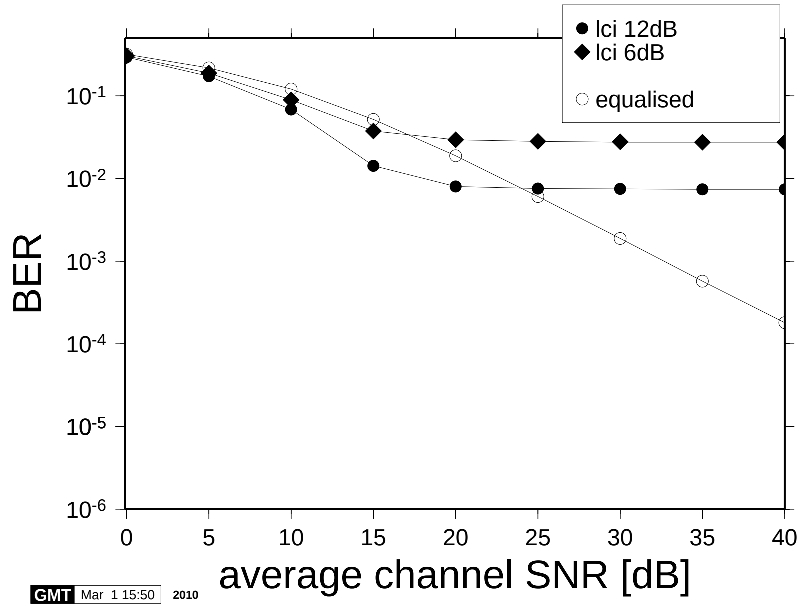

Figure 22.26: BER performance of the 512–subcarrier 16–QAM OFDM modem over the fading short WATM channel of Figure 20.3 employing limited channel inversion (lci) and a delay of 1 timeslot between the instants of perfect channel estimation and reception.

22.4.3 Limited dynamic range pre–equalisation

We have seen in Figure 22.24 that although the full channel inversion algorithm produces the best BER performance at the receiver, the output power fluctuations at the transmitter are prohibitive, as was evidenced in Figure 22.25. In order to limit the signal power fluctuations, the dynamic range of the pre–equalisation algorithm can be limited to a value l, so that the following relations apply:

$$E_n = a_n \cdot e^{-j\phi_n}, \text{with} \tag{22.3}$$

$$\phi_n = \angle \hat{H}_n \quad \text{and} \tag{22.4}$$

$$a_n = \begin{cases} \left|\hat{H}_n\right| & \text{for} \left|\hat{H}_n\right| \leq l \\ l & \text{otherwise.} \end{cases} \tag{22.5}$$

Limiting the values of E_n to the value of l does not affect the phase of the channel pre–equalisation. Depending on the modulation mode employed for the transmission, reception of the symbols affected by the amplitude limitation is still possible, for example for phase shift keying. Multi–level modulation modes exploiting the received symbol's amplitude will be affected by the imperfect pre–equalisation. This effect is shown in Figure 22.26 for 16QAM transmissions with $l = 2$ and $l = 4$, which corresponds to a maximal frequency-domain amplitude amplification of 6dB and 12dB,

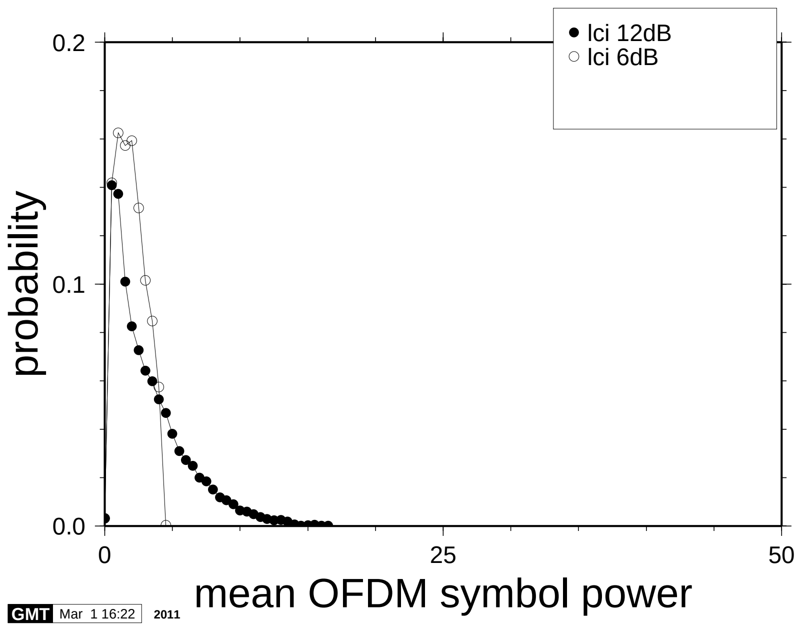

Figure 22.27: OFDM symbol energy histogram for 512–subcarrier 16–QAM transmission with limited dynamic range channel inversion (lci) over the WATM channel of Figure 20.3. The corresponding BER curves are given in Figure 22.26. . The corresponding results for unlimited amplitude pre–equalisation are given in Figure 22.29.

respectively. It can be seen that for 16QAM transmission, BER floors of 2% and 0.8% are experienced for the 6dB and 12dB limits, respectively. In addition to the time–delay effects highlighted for the full channel inversion algorithm in Figure 22.24, this is due to the inability of the system to correct for the channel's deep frequency domain fades, which makes it impossible to demodulate multi–level symbols correctly. It can be observed that for the higher permissible dynamic range of the pre–equalisation algorithm the BER floor is lower than for the more limited scenario of 6dB clipping, but it is still considerably worse than that for the full channel inversion. The associated mean OFDM symbol power histogram is shown in Figure 22.27. Given the maximum allowed amplification factors of 6 and 12dB, the normalised OFDM symbol power in the figure should be limited to 4 and 16, respectively. However, higher values are observed, which is due to the OFDM symbol's energy fluctuating as a function of the specific data sequence, if multi–level modulation schemes are used.

22.4.4 Pre–equalisation with sub–band blocking

We have demonstrated in Figures 22.24 and 22.26 that while limiting the pre–equalisation function's amplitude can help to mitigate the problem of transmitter power fluctuation, the incorrect pre–equalisation of the amplitude leads to a BER performance degradation of the system. This BER degradation can be mitigated by identifying the subcarriers that cannot be fully pre–equalised and disabling subsequent transmission in these subcarriers. This "blocking" of the transmission in certain subcarriers can be seen as adaptive modulation with two modulation modes, and introduces the problem of modulation mode signalling. As it has been discussed in the context of Figure 22.1 for the adaptive modulation modems above, this signalling task can be solved in different ways, namely by blind detection of blocked subcarriers, or by transmitting explicit signalling information contained in the data block. We have seen above that employing sub–band adaptivity rather than subcarrier–by–subcarrier adaptivity simplifies both detection as well as signalling, at the expense of a lower system throughput. In order to keep the system's complexity low and to allow for simple signalling or blind detection, we will assume a 16–subband adaptive scheme here.

Analogously to the adaptive modulation schemes above, the transmitter decides for all subcarriers in each sub–band, whether to transmit data or not. If pre–equalisation is possible under the power constraints, then the subcarriers are modulated with the pre–equalised data symbols. The information whether a sub–band is used for transmission or not is signalled to the receiver.

Since no attempt is made to transmit in the sub–bands that cannot be pre–equalised, the power not employed in the blank subcarriers can be used for 'boosting' the data–bearing sub–bands. This scheme allows for a more flexible pre–equalisation algorithm than the fixed threshold based method described above, which is summarised as follows:

- Calculate the necessary transmit power p_n for each sub–band n, assuming perfect pre–equalisation.
- Sort sub–bands according to their required transmit power p_n.
- Select sub–band n with the lowest power p_n, and add p_n to the total transmit power. Repeat this procedure with the next–lowest power, until no further sub–bands can be added without the total power $\sum p_j$ exceeding the power limit l.

Figure 22.28 depicts the 16–QAM BER performance over the short WATM channel of Figure 20.3. It can be seen that the modem performance is improved considerably, when compared to the limited dynamic range algorithm of Figure 22.26, which can be explained by invoking blocking in the unuseable subcarriers. The BER floor stems from the channel variability, as it has been observed for the full channel inversion algorithm in Figure 22.24. The average throughput figures for the 6dB and 12dB symbol energy limits are 3.54 and 3.92 bits per data symbol, respectively. It can be noted that the BER floor is lower for $l = 6$dB than for $l = 12$dB. This is because the effects of the channel variation due to the delay between the instants of channel estimation and reception in the faded subcarriers on the equalisation function is much greater than in the higher–quality subcarriers. The lower the total symbol energy limit l, the fewer the number of low–quality subcarriers used for transmission. For both $l = 6$dB and $l = 12$dB, the BER performance of the blocking modem is better than that of the modem employing full channel inversion in Figure 22.24, provided that 1

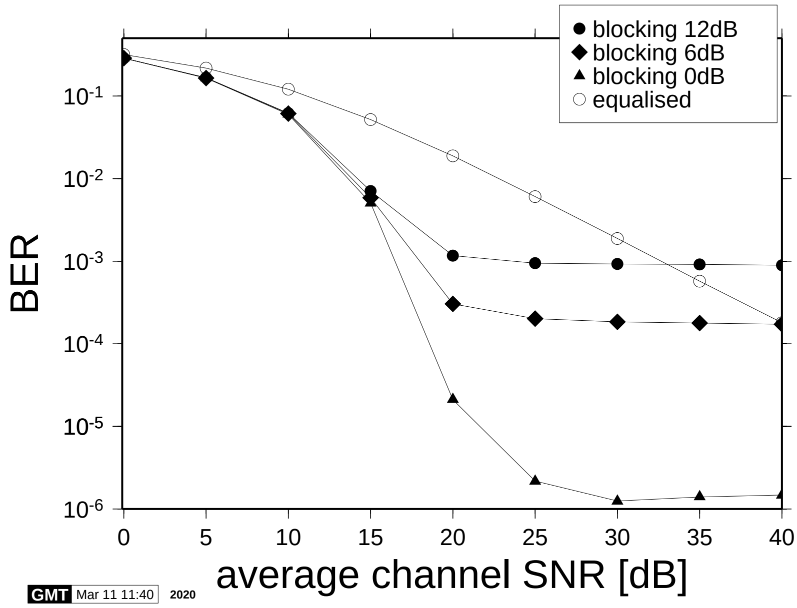

Figure 22.28: BER performance of the 512–subcarrier 16–QAM OFDM modem over the fading short WATM channel of Figure 20.3 employing 16 sub–band pre–equalisation with blocking and a delay of 1 timeslot between the instants of perfect channel estimation and reception.

time slot delay is assumed. Again, the reason for this is the exclusion of the deeply faded corrupted subcarriers. If the symbol energy is limited to 0dB, then the BER floor drops to $1.5 \cdot 10^{-6}$ at the expense of the throughput, which attains 2.5 BPS. Figure 22.29 depicts the mean OFDM symbol energy histogram for this scenario. It can be seen that, compared with the limited channel inversion scheme of Figure 22.27, the allowable symbol energy is more efficiently allocated, with a higher probability of high–energy OFDM symbols. This is the result of the flexible reallocation of energy from blocked sub–bands, instead of limiting the output power on a subcarrier–by–subcarrier basis.

22.4.5 Adaptive modulation with spectral pre–distortion

The pre–equalisation algorithms discussed above invert the channel's anticipated transfer function, in order to transform the resulting channel into a Gaussian–like non–fading channel, whose SNR is dependent only on the path–loss. Sub–band blocking has been introduced above, in order to limit the transmitter's output power, while maintaining the near–constant–SNR across the used subcarriers. The pre–equalisation algorithms discussed above do not cancel out the channel's path loss, but rely on the receiver's gain control algorithm to automatically account for the channel's average path–loss.

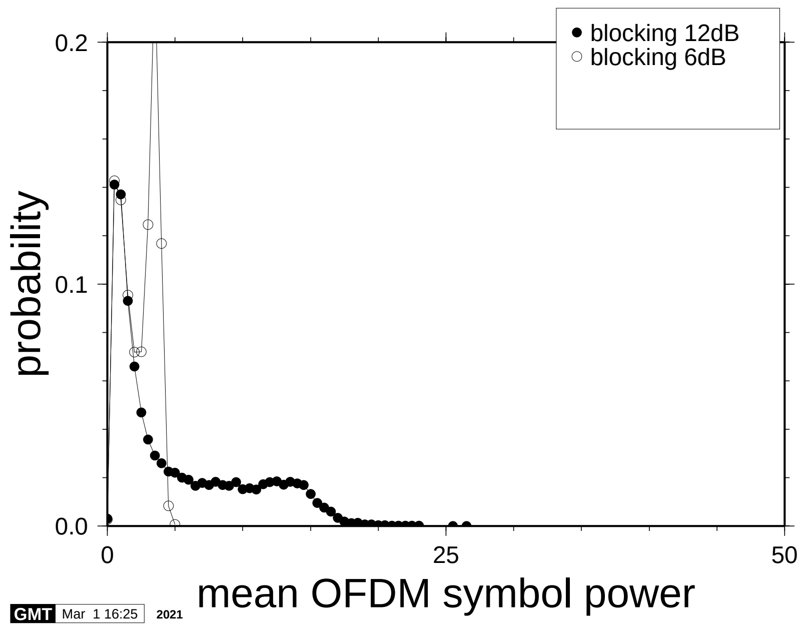

Figure 22.29: OFDM symbol energy histogram for 512–subcarrier 16–subband pre–equalisation with blocking over the short WATM channel of Figure 20.3 using 16-QAM. The corresponding BER curves are given in Figure 22.28

We have seen in Chapter 22 on adaptive modulation algorithms that maintaining Gaussian channel characteristics is not the most efficient way of exploiting the channel's time–variant capacity. If maintaining a constant data throughput is not required by the rest of the communications system, then a fixed BER scheme in conjunction with error correction coding can assist in maximising the system's throughput. The results presented for the target–BER adaptive modulation scheme in Figure 22.14(b) showed that for the particular turbo coding scheme used an uncoded BER of 1% resulted in error–free channel coded data transmission, and that for an uncoded target BER of 10% the turbo decoded data BER was below 10^{-5}. We have seen that it is impossible to exactly reach the anticipated uncoded target BER with the adaptive modulation algorithm, since the adaptation algorithm operates in discrete steps between modulation modes.

Combining the target–BER adaptive modulation scheme and spectral pre–distortion allows the transmitter to react to the channel's time– and frequency–variant nature, in order to fine–tune the behaviour of the adaptive modem in fading channels. It also allows the transmitter to invest the energy that is not used in "no transmission" sub–bands into the other sub–bands without affecting the equalisation at the receiver.

The combined algorithm for adaptive modulation with spectral pre–distortion described here does not intend to invert the channel's transfer function across the OFDM

target BER	10^{-4}	1%	10%
SNR(BPSK)[dB]	8.4	4.33	−0.85
SNR(QPSK)[dB]	11.42	7.34	2.16
SNR(16QAM)[dB]	18.23	13.91	7.91

Table 22.3: Required target SNR levels for 1% and 10% target BER for the different modulation schemes over an AWGN channel.

symbol's range of subcarriers, it is therefore not a pure pre–equalisation algorithm. Instead, the aim is to transmit a sub–band's data symbols at a power level which ensures a given target SNR at the receiver, that is constant for all subcarriers in the sub–band, which in turn results in the required BER. Clearly, the receiver has to anticipate the different relative power levels for the different modulation modes, so that error–free demodulation of the multi–level modulation modes employed can be ensured.

The joint adaptation algorithm requires the estimates of the noise floor level at the receiver as well as the channel transfer function, which includes the path–loss. On the basis of these values, the necessary amplitude of E_n required to transmit a data symbol over the subcarrier n for a given received SNR of γ_n can be calculated as follows:

$$|E_n| = \frac{\sqrt{N_0 \cdot \gamma_n}}{\left|\hat{H}_n\right|},$$

where N_0 is the noise floor at the receiver. The phase of E_n is used for the pre–equalisation, and hence:

$$\angle E_n = -\angle \hat{H}_n.$$

The target SNR of subcarrier n, γ_n, is dependent on the modulation mode that is signalled over the subcarrier, and determines the system's target BER. We have identified three sets of target SNR values for the modulation modes, with uncoded target BER values of 1% and 10% for use in conjunction with channel coders, as well as 10^{-4} for transmission without channel coding. Table 22.3 gives an overview of these levels, which have been read from the BER performance curves of the different modulation modes in a Gaussian channel.

Figure 22.30 shows the performance of the joint pre–distortion and adaptive modulation algorithm over the fading time–dispersive short WATM channel of Figure 20.3 for the set of different target BER values of Table 22.3, as well as the comparison curves of the perfectly equalised 16-QAM modem under the same channel conditions. It can be seen that the BER achieved by the system is close to the BER targets. Specifically, for a target BER of 10%, no perceptible deviation from the target has been recorded, while for the lower BER targets the deviations increase for higher channel SNRs. For a target BER of 1%, the highest measured deviation is at the SNR of 40dB, where the recorded BER is 1.36%. For the target BER of 10^{-4}, the BER deviation is small at 0dB SNR, but at an SNR of 40dB the experimental BER is $2.2 \cdot 10^{-3}$. This increase of the BER with increasing SNR is due to the rapid channel

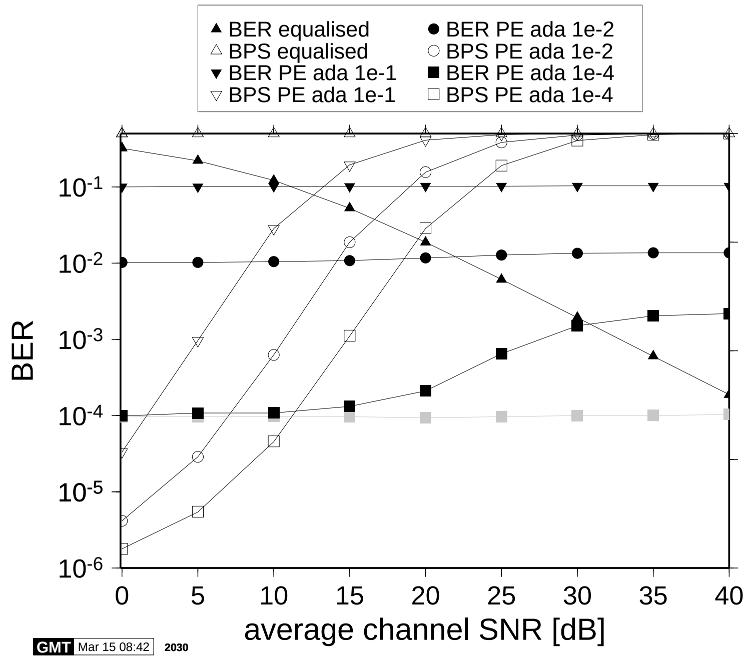

Figure 22.30: BER performance and BPS throughput of the 512–subcarrier 16–subband adaptive OFDM modem with spectral pre–distortion over the Rayleigh fading time dispersive short WATM channel of Figure 20.3, and that of the perfectly equalised 16-QAM modem. The half–tone BER curve gives the performance of the adaptive modem for a target BER of 10^{-4} with no delay between channel estimation and transmission, while the other results assume 1 timeslot delay between up– and downlink.

variations in the deeply faded subcarriers, which are increasingly used at higher SNR values. The half–tone curve in the figure denotes the system's performance, if no delay is present between the channel estimation and the transmission. In this case, the simulated BER shows only very little deviation from the target BER value. This is consistent with the behaviour of the full channel inversion pre–equalising modem.

22.5 Comparison of the adaptive techniques

Figure 22.31 compares the different adaptive modulation schemes discussed in this chapter. The comparison graph is split into two sets of curves, depicting the achievable data throughput for a data BER of 10^{-4} highlighted for the fixed throughput systems in Figure 22.31(a), and for the time–variant–throughput systems in Figure 22.31(b).

The fixed throughput systems — highlighted in black in Figure 22.31(a) — comprise the non–adaptive BPSK, QPSK and 16QAM modems, as well as the fixed–throughput adaptive scheme, both for coded and uncoded applications. The non–

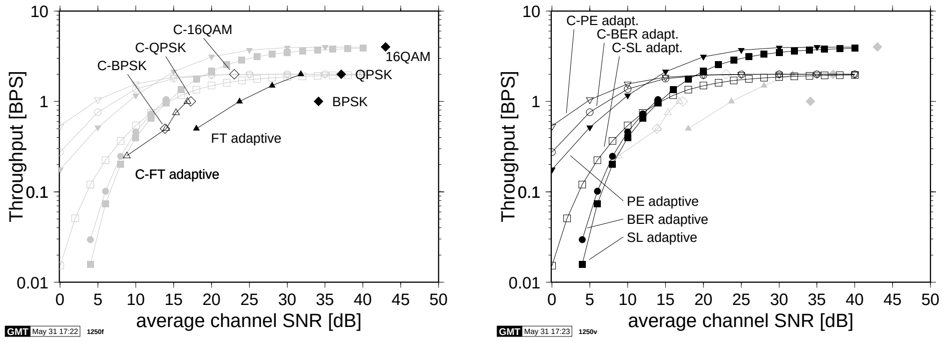

(a) fixed throughput schemes **(b)** variable throughput schemes

Figure 22.31: BPS throughput versus average channel SNR for non–adaptive and adaptive modulation as well as for pre–equalised adaptive techniques, for a data bit error rate of 10^{-4}. Note that for the coded schemes the achieved BER values are lower than 10^{-4}. (a) – fixed throughput systems: coded (C-) and uncoded BPSK, QPSK, 16QAM, and fixed throughput (FT) adaptive modulation. (b) – variable throughput systems: coded (C-) and uncoded switching level adaptive (SL), target–BER adaptive (BER) and pre–equalised adaptive (PE) systems. Note that the separately plotted variable–throughput graph also shows the lightly shaded benchmarker curves of the complementary fixed–rate schemes and vice versa.

adaptive modems' performance is marked on the graph as diamonds, and it can be seen that the uncoded fixed schemes require the highest channel SNR of all examined transmission methods to achieve a data BER of 10^{-4}. Channel coding employing the advocated turbo coding schemes dramatically improves the SNR requirements, at the expense of half the data throughput. The uncoded fixed–throughput (FT) adaptive scheme, marked by filled triangles, yields consistently worse data throughput than the coded (C-) fixed modulation schemes C-BPSK, C-QPSK and C-16QAM, with its throughput being about half the coded fixed scheme's at the same SNR values. The coded FT–adaptive (C-FT) system, however, delivers very similar throughput to the C-BPSK and C-QPSK transmission, and can deliver a BER of 10^{-4} for SNR values down to about 9dB.

The variable throughput schemes, highlighted in Figure 22.31(b), outperform the comparable fixed throughput algorithms. For high SNR values, all uncoded schemes' performance curves converge to a throughput of 4bits/symbol, which is equivalent to 16QAM transmission. The coded schemes reach a maximal throughput of 2bits/symbol. Of the uncoded schemes, the "data" switching–level (SL) and target–BER adaptive modems deliver a very similar BPS performance, with the target–BER scheme exhibiting slightly better throughput than the SL adaptive modem. The adaptive modem employing pre–equalisation (PE) significantly outperforms the other uncoded adaptive schemes and offers a throughput of 0.18 BPS at an SNR of 0dB.

The coded transmission schemes suffer from limited throughput at high SNR values, since the half–rate channel coding limits the data throughput to 2 BPS. For low SNR values, however, the coded schemes offer better performance than the uncoded schemes, with the exception of the "speech" SL–adaptive coded scheme, which is outperformed by the uncoded PE-adaptive modem. The poor performance of the coded SL–scheme can be explained by the lower uncoded target BER of the "speech" scenario, which was 1%, in contrast to the 10% uncoded target BER for the coded BER– and PE–adaptive schemes. The coded PE–adaptive modem outperforms the target–BER adaptive scheme, thanks to its more accurate control of the uncoded BER, leading to a higher throughput for low SNR values.

It is interesting to observe that for the given set of four modulation modes the uncoded PE–adaptive scheme is close in performance to the coded adaptive schemes, and that for SNR values of more than 14dB it outperforms all other studied schemes. It is clear, however, that the coded schemes would benefit from higher order modulation modes, which would allow these modems to increase the data throughput further when the channel conditions allow. Before concluding this chapter in the next section let us now consider the generic problem of optimum power- and bit-allocation in the context of uncoded OFDM systems.

22.6 A fast algorithm for near-optimum power- and bit-allocation in OFDM systems [333]

22.6.1 State-of-the-art

In this section the problem of efficient OFDM symbol-by-symbol based power and bit allocation is analysed in the context of highly dispersive time-variant channels. A range of solutions published in the literature is reviewed briefly and Piazzo's [333] computationally efficient algorithm is exposed in somewhat more detail.

When OFDM is invoked over highly frequency-selective channels, each subcarrier can be allocated a different transmit power and a different modulation mode. This OFDM symbol-by-symbol based 'resource' allocation can be optimised with the aid of an algorithm which - if the channel is time-variant - has to be repeated on an OFDM symbol-by-symbol basis. Some of the existing algorithms [334] are mainly of theoretical interest due to their high complexity. Amongst the practical algorithms [321, 322, 333, 335, 336] the Hughes-Hartog Algorithm (HHA) [336, 337] is perhaps best known, but its complexity is somewhat high, especially for real-time OFDM symbol-by-symbol based applications at high bitrates. Hence the HHA has stimulated extensive research for computationally more efficient algorithms [322, 334, 336, 337]. The most efficient appears to be that of Lai et al. [336], which is a fast version of the HHA and and that of Piazzo [333].

22.6.2 Problem description

Piazzo [333] considered an OFDM system using N subcarriers, each employing a potentially different modulation mode and transmit power. Below we follow the notation and approach proposed by Piazzo [333]. The different modes use different modem constellations and thus carry a different number of bits per subcarrier, ranging from 1 to I bits per subcarrier, corresponding to BPSK and 2^I-ary QAM. We denote the transmit power and the number of bits allocated to subcarrier k ($k = 0 \ldots N-1$) by p_k and b_k, respectively. If $b_k = 0$, subcarrier k is allocated no power and no bits, hence it is disabled. The total transmit power is $P = \frac{1}{N}\sum_{k=0}^{N-1} p_k$ and the number of transmitted bits per OFDM symbol is $B = \sum_{k=0}^{N-1} b_k$. The i-bit modulation mode is characterized by the function $R_i(S)$, denoting the SNR required at the input of the detector, in order to achieve a target Bit Error Rate (BER) equal to S. Finally, we denote the channel's power attenuation at subcarrier k by a_k, and the power of the Gaussian noise by P_N, so that the SNR os subcarrier k is $r_k = p_k/(a_k \cdot P_N)$.

We consider the problem of minimising the transmit power for a fixed target BER of S and for a fixed number of transmitted bits B per OFDM symbol. We impose an additional constraint, namely that the BER of every carrier has to be equal to S. This constraint simplifies the problem, while producing a system close to the unconstrained optimum system [322,334,336,337]. Furthermore - from an important practical point of view - it produces a near-constant BER at the input of the channel decoder, if FEC is used, which maximises the achievable coding gain, since the channel does not become overwhelmed by the plethora of transmission errors, which would be the case for a more bursty error statistics without this constraint. In order to satisfy this constraint, the power transmitted on subcarrier k has to be $p_k = P_N a_k R_{b_k}(S)$, and the total power to be minimised is given by the sum of the N subcarriers' powers across the OFDM symbol:

$$P = \frac{P_N}{N}\sum_{k=0}^{k=N-1} a_k \cdot R_{b_k}(S). \tag{22.6}$$

We now state a property of the optimum system. Namely, in the optimum system if a subcarrier has a lower attenuation than another one - ie it exhibits a higher frequency-domain transfer function value and hence experiences a higher received SNR - then it must carry at least as many bits as the lower-SNR subcarrier. More explicitly:

$$a_k < a_h \;\Rightarrow\; b_k \geq b_h. \tag{22.7}$$

The above property in Equation 22.7 can be readily proven. Let us briefly consider a system, which does not satisfy Equation 22.7, where for subcarriers k and h the above condition is violated and hence we have $a_k < a_h$ and $b_k = i_1 < b_h = i_2$. In other words, although the attenuation a_k is lower than a_h, $i_1 < i_2$. Consider now a second system, where the lower-attenuation subcarrier was assigned was assigned the higher number of bits, ie $b_k = i_2$ and $b_h = i_1$. Since the required SNR for maintaining the target BER of S is lower for a lower number of bits - ie we have $R_{i_1}(S) < R_{i_2}(S)$ - upon substituting these SNR values in Equation 22.6 we can infer that the second system requires a lower total power P per OFDM symbol for maintaining the target BER S. Thus the first system is not optimum in this sense.

Equation 22.7 states a necessary condition of optimality, which was also exploited by Lai *et al.* in [336], but it can be exploited further, as we will demonstrate below.

From now on, we consider the channel's transfer function or attenuation vector sorted in the order of $a_0 \leq a_1 \leq a_2 \ldots$, which simplifies our forthcoming discussions.

22.6.3 Power- and Bit-allocation Algorithm

Piazzo's algorithm [333] solves the above resource allocation problem for the general system by repeteadly solving the problem for a simpler system. Explicitly, the simpler system employs only two modulation modes, those carrying J and $J-1$ bits. This system can be termed as the Twin-Mode System (TMS). On the basis of Equation 22.7 and since the channel's frequency-domain attenuation vector was sorted in the order of $a_0 \leq a_1 \leq a_2 \ldots$, for the Optimum TMS (OTMS) the OFDM subcarriers will be partitioned in three groups:

1) Group J comprises the first or lowest-attenuation OFDM subcarriers using a J-bit modulation mode;

2) Group 0 is constituted by the last or highest-attenuation OFDM subcarriers transmitting zero bits;

3) Lastly, group $(J-1)$ hosts the remaining OFDM subcarriers using a $(J-1)$-bit modem mode.

In order to find the OTMS - minimising the required transmit power of the OFDM symbol for a fixed target BER of S and for a fixed number of transmitted bits B per OFDM symbol - we initially assign all the B bits of the OFDM symbol to the highest-quality ie lowest-attenuation group J. This of course would be a suboptimum scheme, leaving the medium-quality subcarriers of group $J-1$ unused, since even the highest quality subcarriers would require an excessive SNR - ie transmit power - for maintaining the target BER, when transmitting B bits per OFDM symbol. We note furthermore that the above bit allocation may require padding of the OFDM symbol with dummy bits, if J is not an integer divisor of B.

Following the above initial bit allocation, Piazzo suggested performing a series of *bit reallocations, reducing the transmit power upon each reallocation*. Specifically, in each power and bit reallocation step we move the $J \cdot (J-1)$ number of bits allocated to the last - ie highest attenuation or lowest-quality - $(J-1)$ number of OFDM subcarriers of group J to group $(J-1)$. For example, if 1 bit/symbol BPSK and 2 bit/symbol 4QAM are used, then we move $2 \cdot 1$=2 bits, which were allocated to the highest-attenuation 4QAM subcarrier to two BPSK modulated subcarriers. The associated trade-off is that while previously the lowest-quality subcarrier had to carry 2 bits, it will now be conveying only 1 bit and additionally the highest quality previously unused subcarrier has to be assigned one bit. This reallocation was motivated by the fact that before reallocation the lowest-quality subcarrier would have required a higher power for meeting the target BER requirement of S than the regime generated by the reallocation step.

In general, for the sake of performing this power-reducing bit-reallocation we have to add J number of subcarriers to group $(J-1)$. Hence we assign the last - ie lowest-quality - $(J-1)$ number of OFDM subcarriers of group J and the first - ie highest-quality - unused subcarrier to group $(J-1)$. Based on Equation 22.6 and upon denoting the index of the last - ie lowest quality - subcarrier of group J before reallocation by M_J and the index of the first - ie highest-quality - unused subcarrier before reallocation by M_0, the condition of successful power reduction after the tentative bit-reallocation can be formulated. Specifically, the bit-reallocation results in a system using less power, if the sum of the subcarriers' attenuations carrying J bits weighted by their SNR $R_J(S)$ required for the J-bit modem mode for maintaining the target BER of S is higher than that of the corresponding constellation after the above-mentioned bit-reallocation process, when an extra previously unused subcarrier was invoked for transmission. This can be expressed in a more compact form as:

$$R_J(S)\sum_{k=0}^{J-2} a_{M_J-k} > R_{J-1}(S)(a_{M_0} + \sum_{k=0}^{J-2} a_{M_J-k}). \tag{22.8}$$

If Equation 22.8 is satisfied, the reallocation is performed and another tentative reallocation step is attempted. Otherwise the process is terminated, since the optimum twin-mode power- and bit-allocation scheme has been found.

According to Piazzo's proposition [333] the above procedure can be further accelerated. Since the attenuation vector was sorted, we have $a_{M_J-k} \approx a_{M_J}$ in Equation 22.8. Upon replacing a_{M_J-k} by a_{M_J}, after some manipulations Piazzo [333] reformulated Equation 22.8, ie the condition for the modem mode allocation after the bit reallocation to become more efficient as:

$$K_J(S)a_{M_J} - a_{M_0} > 0, \tag{22.9}$$

where $K_J(S) = (J-1)(\frac{R_J(S)}{R_{J-1}(S)} - 1)$ and $K_J(S) > 0$ holds, since $R_J(S) > R_{J-1}(S)$. Piazzo denoted the values of M_J and M_0 after m reallocation steps by $M_J(m)$ and $M_0(m)$. Since initially all the bits were allocated to group J, we have for the index of the last subcarrier of group J at the commencement of the bit reallocation steps $M_J(0) = \lfloor B/J \rfloor - 1$, while for the index of the first unused subcarrier is $M_0(0) = \lfloor B/J \rfloor$, where $\lfloor x \rfloor$ is the smallest integer greater than or equal to x. Furthermore, since in each bit reallocation step the last $(J-1)$ OFDM subcarriers of group J and the first subcarrier of group 0 are moved to group $(J-1)$, after m reallocations we have $M_J(m) = \lfloor B/J \rfloor - 1 - (J-1)m$ and $M_0(m) = \lfloor B/J \rfloor + m$. Upon substituting these values in Equation 22.9 the lefthand side becomes a function of m, namely $f(m) = K_J(S)a_{M_J(m)} - a_{M_0(m)}$. Because the frequency-domain channel transfer function's attenuation vector was ordered, we have $K_J(S) > 0$ and hence it is readily seen that $f(m)$ is a monotonically decreasing function of the reallocation index m. Therefore the method presented above essentially attempts to find the specific value of the reallocation index m, for which we have $f(m) > 0$ and $f(m+1) < 0$. In other words, when we have $f(m+1) < 0$, the last reallocation step resulted in a power increment, rather than decrement and hence the reallocation procedure is completed.

The search commences from $m = 0$ and increases m by one at each bit reallocation step. In order to accelerate the search procedure, Piazzo replaced the above mentioned linearly incremented search by a logarithmic search. This is possible, since the $f(m)$ function is monotonically decreasing upon increasing the reallocation index m. Piazzo [333] stipulated the search range by commencing from the minimum value of the reallocation index m, namely from $m_0 = 0$.

The maximum value, denoted by m_1, is determined by the number of OFDM subcarriers N or by the number of bits B to be transmitted per OFDM symbol, as it will be argued below. There are two limitations, which determine the maximum possible number of reallocation steps. Namely, the reallocations steps have to be curtailed, when there are no more bits left in the group of subcarriers associated with the J-bit modem mode group or when there are no more unused carriers left after iteratively invoking the best unused carrier from the group of disabled carriers. These limiting factors, which determine tha maximum possible number of bit reallocation steps are augmented further below.

Recall that at the commencement of the algorithm all the bits were assigned to the subcarrier group associated with the J-bit modem mode and hence there were $(\lfloor B/J \rfloor - 1)$ subcarriers in group J. Upon reallocating the $J \cdot (J-1)$ number of bits allocated to the last - ie highest attenuation or lowest-quality - $(J-1)$ number of OFDM subcarriers of group J to group $(J-1)$ until no more bits were left in the subcarrier group associated with the J-bit modem mode naturally constitutes an upper limit for the maximum number of reallocation steps m_1, which is given by $\lfloor B/J \rfloor/(J-1)$. Again, the other limiting factor of the maximum number of bit reallocation steps is the number of originally unused carriers, which was $N - 1 - \lfloor B/J \rfloor)$. Hence the maximum possible number of reallocations is given by $m_1 = min(\lceil \lfloor B/J \rfloor/(J-1) \rceil, N-1-\lfloor B/J \rfloor)$, where $\lceil x \rceil$ is the highest integer smaller than or equal to x.

The accelerated logarithmic search proposed by Piazzo [333] halves the above maximum possible range at each bit reallocation step, by testing the value of $f(m)$ at the centre of the range and by updating the range accordingly. In summary,Piazzo's proposed algorithm can be summarised in a compact form as follows [333]:

Algorithm 1 $OTMS(B, S, J, N, a_k)$
1) Initialize $m_0 = 0$, $m_1 = min(\lceil \lfloor B/J \rfloor/(J-1) \rceil, N-1-\lfloor B/J \rfloor)$.
2) Compute $m_x = m_0 + \lceil m_1 - m_0 \rceil /2$.
3) If $f(m_x) \geq 0$ *let* $m_0 = m_x$; *else let* $m_1 = m_x$.
4) If $m_1 = m_0 + 1$ *goto 5); else goto 2).*
5) Stop. The number of carriers in group J *is* $N_J = \lfloor B/J \rfloor - m_0(J-1)$.

When the algorithm is completed, the value N_J, specifying the number of OFDM subcarriers in the group J associated with the J-bit modem mode becomes known.

Having generated the optimum twin-mode system, Piazzo also considered the problem of finding the Optimum General System (OGS) employing OFDM subcarrier modulation modes carrying $1, ..., I$ bits. The procedure proposed initially invoked Algorithm 1 in order to find the optimumm twin-mode system carrying a total of B bits per OFDM symbol using the I-bit and the $(I-1)$-bit per subcarrier modulation modes. At the completion of Algorithm 1 we know N_I, the number of OFDM subcarriers carrying I bits. These subcarriers are now confirmed. These OFDM subcarriers as well as the associated $I \cdot N_I$ bits can now be eliminated from the resource-allocation problem, and the optimum system transmitting the remaining $B - I \cdot N_I$ bits of the remaining $(N - N_I)$ subcarriers can be sought, using subcarrier modulation modes transmitting $(I-1), (I-2), ...$ bits.

Again, Algorithm 1 can be applied to this new system, now using the modulation modes with $(I-1)$ and $(I-2)$ bits per subcarrier and repeating the procedure. After each application of Algorithm 1 a new group of subcarrier is confirmed. In summary, Piazzo's general algorithm can be summarised in a compact form as follows [333]:

Algorithm 2 $OGS(B, S, I, N, a_k)$
1) Initialize $\hat{B} = B$, $\hat{N} = N$, $\hat{a}_k = a_k$, $J = I$.
2) Perform $OTMS(\hat{B}, S, J, \hat{N}, \hat{a}_k)$ *to compute* N_J.
3) If $J = 2$, *let* $N_1 = \hat{B} - 2 \cdot N_2$ *and Stop.*
4) Remove the first N_J *carriers from* $\hat{a}_k$, *let* $\hat{B} = \hat{B} - J \cdot N_J$, $\hat{N} = \hat{N} - N_J$, $J = J - 1$ *and goto 2).*

When the algorithm is completed, the values N_i specifying the number of OFDM subcarriers conveying i bits, become known for all the legitimate mode modes carrying $i = I, (I-1), ..., 1$ bits per subcarrier. Hence we know the number of bits allocated to subcarrier k $(k = 0 \ldots N-1)$ expressed in terms of the b_k values as well as the associated minimum power requirements. Hence the system is specified in terms of $p_k = P_N a_k R_{b_k}(S)$. In closing it is worthwile noting that the algorithm can be readily modified also to handle the case where the two modes of the twin-mode system carry J and $K < J-1$ number of bits.

22.6.4 Conclusions

Piazzo noted [333] that Algorithm 2 is not guaranteed to produce an optimum solution. It produces a system satisfying Equation 22.7. However, Piazzo conducted simulations [333], comparing the results of Algorithm 2 with those of the Hughes-Hartog Algorithm presented in [336]. The results were nearly identical, where the maximum transmitted power difference was about $0.2dB$. The complexity of Algorithm 1 is determined by the range of m values, over which the search has to be conducted and it is upper-bounded by $O(log_2 B)$ [333]. Since Algorithm 1 is repeated $I-2$ times in Algorithm 2, and since a complexity of $O(N \cdot log_2 N)$ is required for sorting the channel's frequency-domain attenuation vector, the complexity of Algorithm 2 is upper-bounded by [333] $O(I \cdot log_2 B + N \cdot log_2 N)$, which is substantially lower than the $O(I \cdot B + N \cdot log_2 N)$ complexity of the fast Hughes-Hartog Algorithm of Lai *et al.* [336].

22.7 Summary

A range of adaptive modulation and spectral pre–distortion techniques has been presented in this chapter, all of which aim to react to the time– and frequency–dependent channel transfer function experienced by OFDM modems in fading time dispersive channels. It has been demonstrated that by exploiting the knowledge of the channel transfer function at the transmitter, the overall system performance can be increased substantially over the non–adaptive case. It has been pointed out that the prediction of the channel transfer function for the next transmission timeslot and the signalling of the parameters are the main practical problems in the context of employing adaptive techniques in duplex communications.

The channel prediction accuracy is dependent on the quality of the channel estimation at the receiver, as well as on the temporal correlation of the channel transfer function between the up– and downlink timeslots. Two–dimensional channel estimation techniques [128, 338] can be invoked in order to improve the channel prediction at the receivers.

It has been demonstrated that sub–band adaptivity instead of subcarrier–by–subcarrier adaptivity can significantly decrease the necessary signalling overhead, with a loss of system performance that is dependent on the channel's coherence bandwidth. We have seen that sub–band adaptivity allows the employment of blind–detection techniques in order to minimise the signalling overhead. Further work into blind detection algorithms as well as new signalling techniques is needed for improving the overall bandwidth efficiency of adaptive OFDM systems.

Pre–equalisation or spectral pre–distortion techniques have been demonstrated to significantly improve an OFDM system's performance in time dispersive channels, while not increasing the system's output power. It has been shown that spectral pre–distortion can integrate well with adaptive modulation techniques, improving the system's performance significantly. We have seen in Figure 22.1 that a data throughput of 0.5 bits/symbol has been achieved at 0dB average channel SNR with a BER of below 10^{-4}.

Chapter 24

Digital Terrestrial and Satellite-based Video Broadcasting to Mobile and Stationary Receivers

C. S. Lee, L. Hanzo, T. Keller, S. Vlahoyiannatos

24.1 OFDM-based Digital Terrestrial Video Broadcasting to Mobile Receivers[1][2]

24.1.1 Background and Motivation

Following the standardization of the Pan-European Digital Video Broadcasting (DVB) systems, we have begun to witness the arrival of digital television services to the home. However, for a high proportion of bussiness and leasure travellers it is desirable to have access to DVB services, while on the move. Although it is feasible to receive these services with the aid of dedicated DVB receivers, these receivers may also find their way into the laptop computers of the near future. These intelligent laptops may also become the portable DVB receivers of wireless in-home networks.

[1]This section is based on C. S. Lee, T. Keller and L. Hanzo: Turbo-coded Hierarchical and Non-hierarchical Mobile Digital Video Broadcasting, submitted to IEEE Tr. on Broadcasting, 1999

In recent years three DVB standards have emerged in Europe for terrestrial [135], cable-based [363] and satellite-oriented [364] delivery of DVB signals. The more hostile propagation environment of the terrestrial system requires concatenated Reed-Solomon [153,225] (RS) and rate compatible punctured convolutional coding [153,225] (RCPCC) combined with Orthogonal Frequency Division Multiplexing (OFDM) based modulation. By contrast, the more benign cable and satellite based media facilitates the employment of blind-equalised multi-level modems using upto 256 quadrature amplitude modulation (QAM) levels. These schemes are capable of delivering high-definition video at bitrates of upto 20 Mbits/s in stationary broadcast-mode distributive wireless scenarios.

Recently, there has been a range of DVB system performance studies in the literature [365–368]. Against this background in this section we have proposed turbo-coding based improvements to the terrestrial DVB system [135] and investigated its performance under hostile mobile channel conditions. We have also studied various partitioning and channel coding schemes both in the so-called hierarchical and non-hierarchical transceiver modes and compared their performance.

The rest of this section is divided into the following subsections. In Section 24.1.2 the bit error sensitivity of the MPEG-2 coding parameters [369] is characterised. A brief overview of the turbo-coded and standard DVB terrestrial scheme is presented in Section 24.1.3, while the channel model is described in Section 24.1.4. Following this, in Section 24.1.5 the reader is introduced to the MPEG-2 data partitioning scheme [370] used to split the input MPEG-2 video bitstream into two error protection classes, which can then be protected either equally or unequally. These two protection classes of data can then be communicated to the receiver using the so-called DVB terrestrial hierarchical transmission format. The performance of the data partitioning scheme was investigated by corrupting either the high or low priority data using randomly distributed errors for a range of system configurations in Section 24.1.6 and their effects on the overall reconstructed video quality was evaluated. Following this, the performance of the improved DVB terrestrial system employing the so-called non-hierarchical and hierarchical format was examined in a mobile environment in Sections 24.1.7 and 24.1.7, before our conclusions and future work areas were presented in Section 24.1.9. Let us now commence our discourse by quantifying the sensitivity of the MPEG-2 video parameters in the next section.

24.1.2 MPEG-2 Bit Error Sensitivity

In this section, we assume familiarity with the MPEG-2 standard [369]. The aim of our MPEG-2 error resilience study was to quantify the average PSNR degradation inflicted by each video codec parameter in the bitstream, so that appropriate protection can be assigned to them.

Most MPEG-2 parameters are encoded by several bits and they may occur in different positions in the video sequence. Furthermore, different encoded bits of the same parameter may exhibit different sensitivity to channel errors. Figure 24.1 shows such an example for the parameter known as intra_dc_precision [369], which is coded under the so-called Picture Coding Extension. In this example, the PSNR degradation profiles due to bit errors at Frame 28 showed that the degradation is dependent on

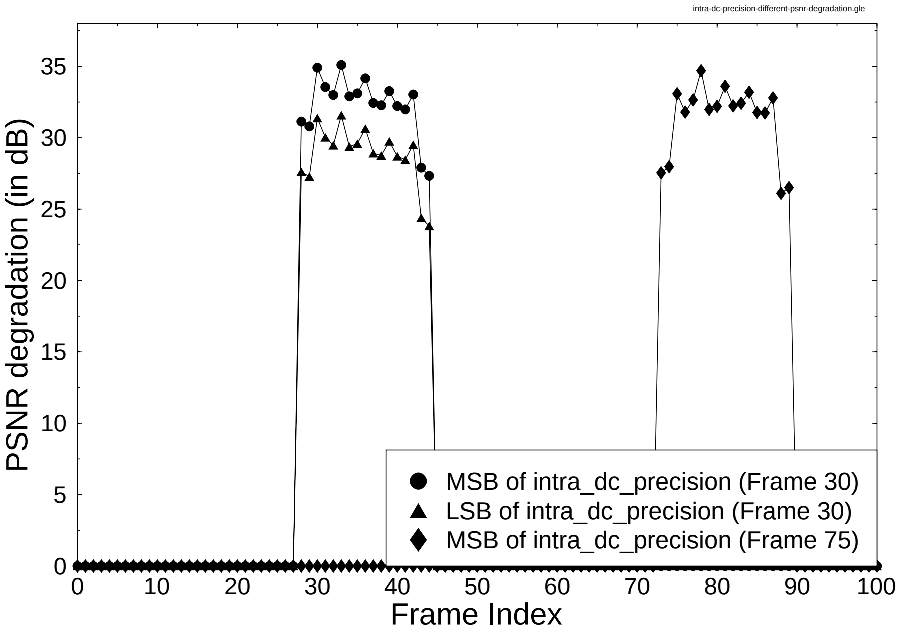

Figure 24.1: PSNR degradation profile for different bits encoding the so-called intra_dc_precision parameter in different corrupted video frames.

the significance of the bit, where errors in the most significant bit (MSB) inflicted approximately 3 dB higher PSNR degradation, than the least significant bit (LSB) errors. Furthermore, the PSNR degradation due to MSB errors in Frame 75 is similar to the PSNR degradation profile for the MSB of the intra_dc_precision parameter around Frame 30. Due to the variation of the PSNR degradation profile for the different significance bits of a particular parameter, as well as for the same parameter at its different occurences in the bitstream, it is necessary to determine the *average* PSNR degradation for each parameter in the MPEG-2 bitstream.

Our approach in obtaining the average PSNR degradation was similar to that suggested in References [371] and [372]. The average measure used here takes into account the significance of the bits corresponding to the parameter concerned, as well as the occurence of the same parameter at different locations in the encoded video bitstream. In order to acquire the average PSNR degradation for each MPEG-2 bitstream parameter, the different bits encoding the parameter, as well as the bits of the same parameter but occuring at different locations in the bitstream were corrupted and the associated PSNR degradation profile versus frame index was registered. The observed PSNR degradation profile for each case was then used to compute the average

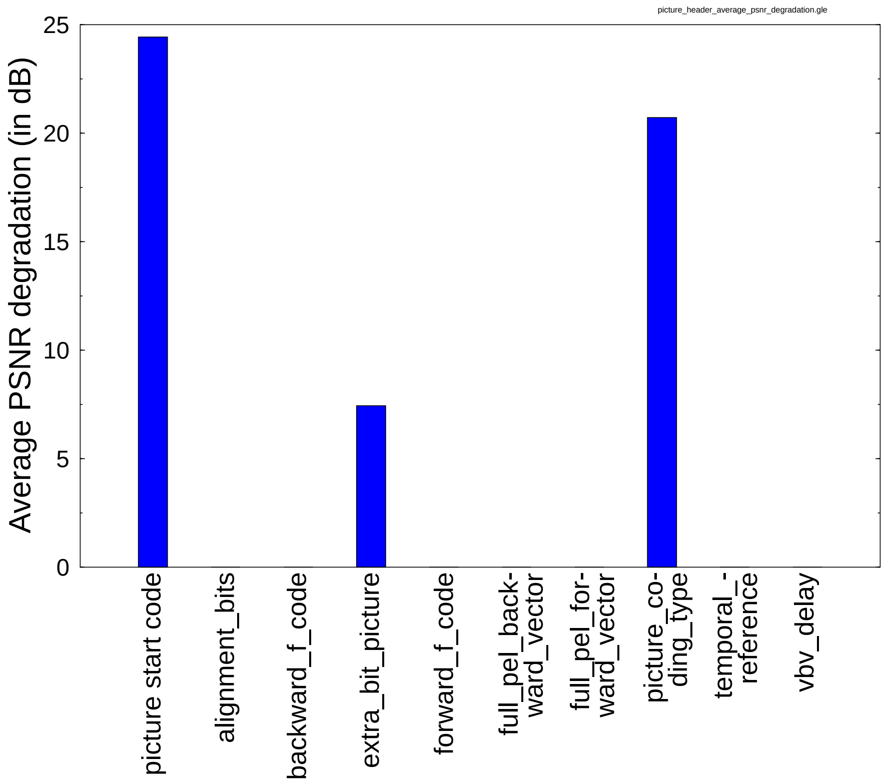

Figure 24.2: Average PSNR degradation for the various MPEG-2 parameters in the Picture Header Information

PSNR degradation. As an example, we shall use the PSNR degradation profile shown in Figure 24.1. In the figure there are three degradation profiles. The average PSNR degradation for each profile is first computed in order to produce three average PSNR degradation values. The mean of these three averages will then form the final average PSNR degradation for the intra_dc_precision parameter. The same process is repeated for all parameters from the Picture Layer up to the Block Layer. The difference with respect to the approach adopted in [371, 372] was that whilst in [371, 372] the average PSNR degradation was acquired for each bit of the output bitstream, due to the large number of different parameters within the MPEG-2 bitstream here a simpler approach was adopted. Figures 24.2 - 24.4 show the typical average PSNR degradation of the various parameters of the Picture Header Information, Picture Coding Extension, Slice Layer, Macroblock Layer and Block Layer, respectively, which was obtained using the QCIF Miss America video sequence at 30 frames/s and an average bitrate of 1.15 Mbits/s.

However, the different MPEG2 codewords occur with different probability and

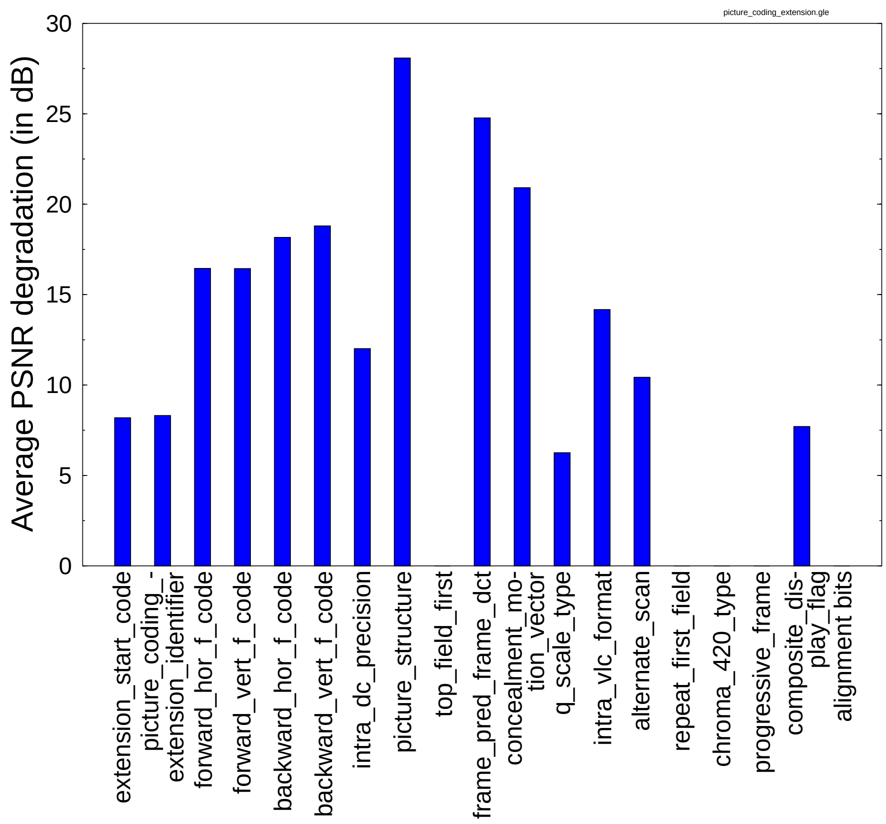

Figure 24.3: Average PSNR degradation for the various MPEG-2 parameters in the Picture Coding Extension

they are allocated different number of bits. Therefore, the average PSNR degradation registered in Figures 24.2 - 24.4 for each parameter was multiplied with the long-term probability of this parameter occuring in the bitstream and with the relative probability of bits being allocated to that parameter. Figure 24.5 and Figure 24.6 show the probability of occcurence of the various MPEG-2 parameters characterised in Figures 24.2 - 24.4 and the probability of bits allocated to the parameters in Picture Header Information, Picture Coding Extension, Slice-, Macroblock- and Block-Layers, respectively.

We shall concentrate first on Figure 24.5(a). It is observed that all parameters - except for full_pel_forward_vector, forward_f_code, full_pel_backward_vector and backward_f_code - have the same probability of occurence, since they appear once for every coded video frame. The parameters full_pel_forward_vector and forward_f_code have a higher probability of occurence than full_pel_backward_vector and backward_f_code, since the former two appear in both P-frames and B-frames, while the latter two only occur in B-frames and for every P-frame, there are two B-frames. However, when

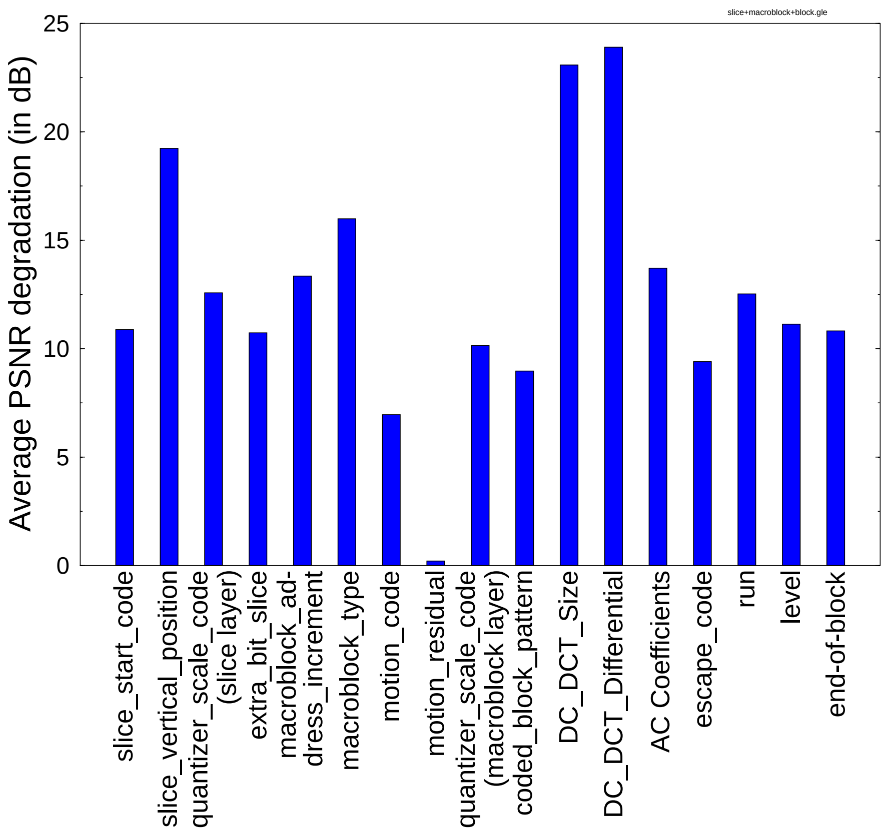

Figure 24.4: Average PSNR degradation for the various MPEG-2 parameters in the Slice-, Macroblock- and Block-Layers.

compared with the parameters from the Slice-Layer, Macroblock-Layer and Block-Layer, which is portrayed by the bar chart of Figure 24.5(b), the parameters of the Picture Header Information and Picture Coding Extension appeared less often.

If we compare the frequency of occurence of the parameters in the Slice-Layer with those in the Macroblock- and Block-Layers, the former appeared less often since there were 11 macroblocks and 44 blocks per slice. The parameter having the highest probability of occurence was constituted by the AC coefficients, having a probability of occurence exceeding eighty percent.

Figure 24.6 shows the probability of bits being allocated to the various parameters in the Picture Header Information, Picture Coding Extension, Slice-, Macroblock- and Block-Layers. Figure 24.7 was invoked in order to better illustrate the probability of bit allocation seen in Figure 24.6(b), with the probability of allocation of bits to the AC coefficients being omitted from the bar-chart. Considering Figure 24.6(a), the two dominant parameters which require the most encoding bits are the picture start code (PSC) and the picture coding extension start code (PCESC). However, comparing

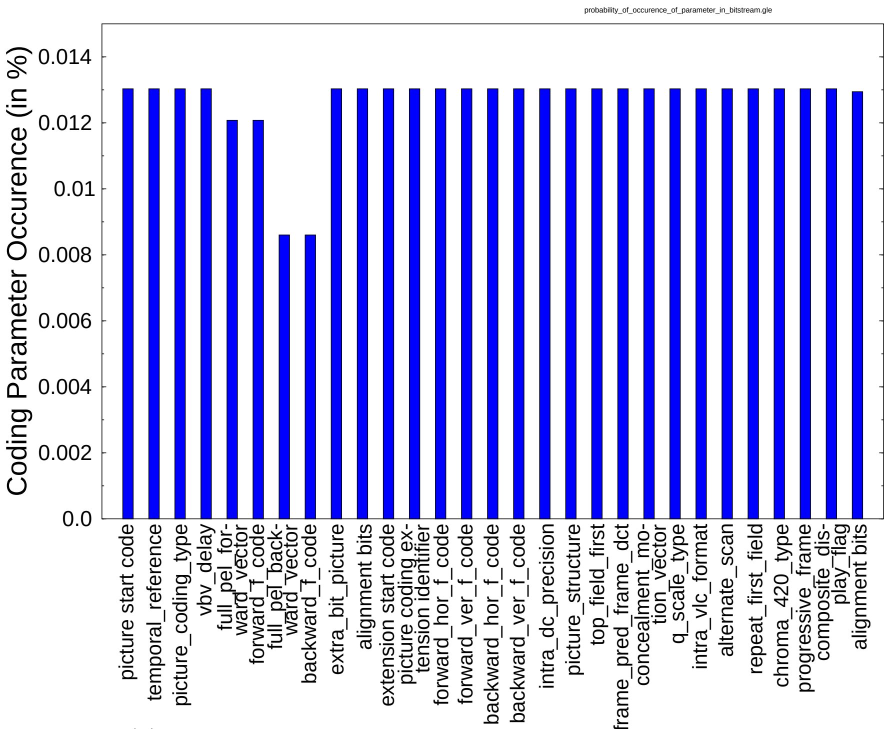

(a) Picture Header Information and Picture Coding Extension

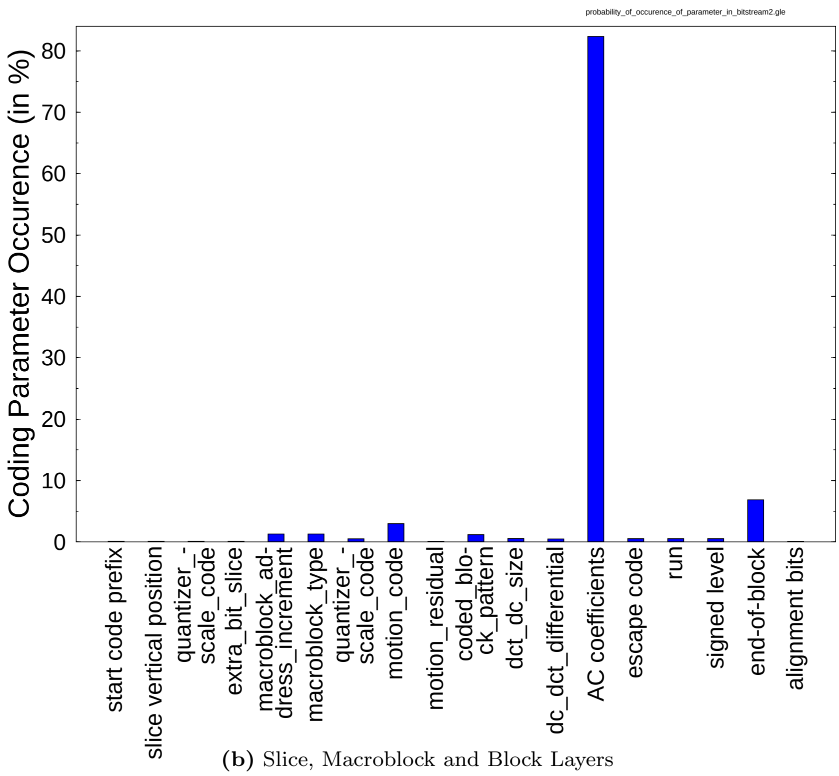

(b) Slice, Macroblock and Block Layers

Figure 24.5: Probability of occurence of the various MPEG-2 parameters characterised in Figures 24.2 - 24.4 (a) Picture Header Information and Picture Coding Extension (b) Slice-, Macroblock- and Block-Layers.

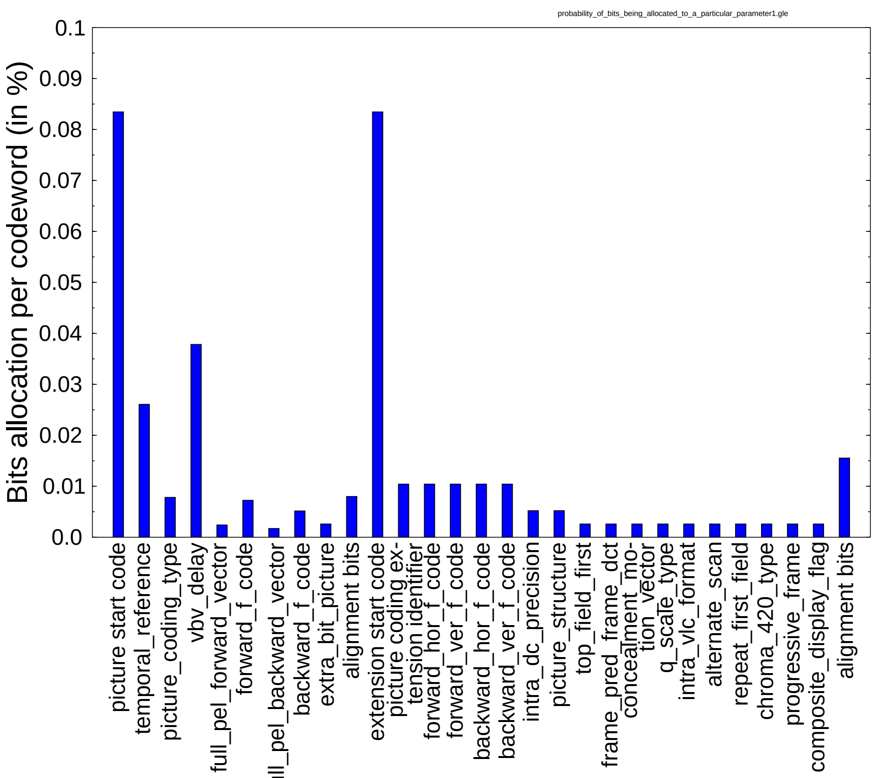

(a) Picture Header Information and Picture Coding Extension

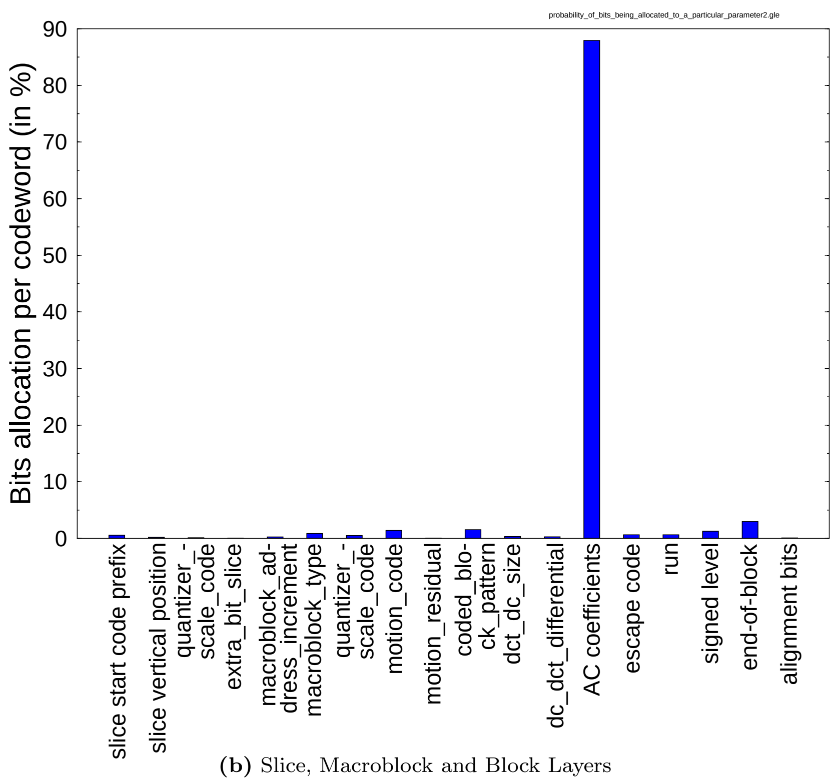

(b) Slice, Macroblock and Block Layers

Figure 24.6: Probability of bits being allocated to parameters in (a) Picture Header Information and Picture Coding Extension (b) Slice-, Macroblock- and Block-Layers.

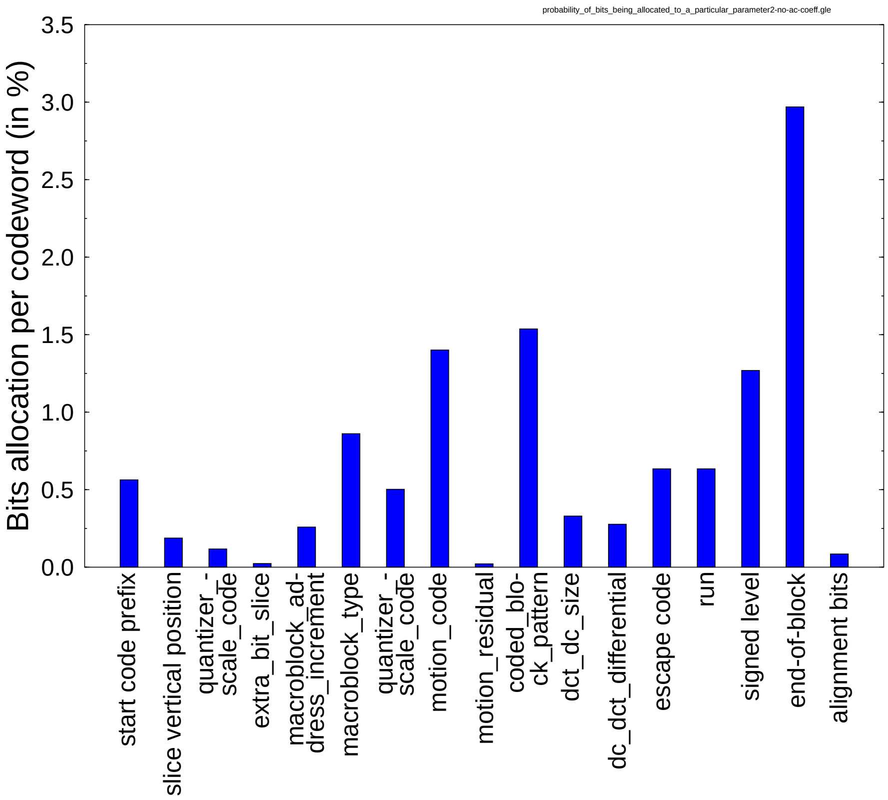

Figure 24.7: Probability of bits being allocated to the various MPEG-2 Slice-, Macroblock- and Block-Layer parameters, as seen in Figure 24.6(b), where the probability of bits allocated to the AC coefficients was omitted, in order to show the allocation of bits to the other parameters more clearly.

these probabilities with the probability of bits being allocated to the various parameters in the Slice-, Macroblock- and Block-Layers, the percentage of bits allocated can still be considered minimal. In the Block-Layer, the AC coefficients require in excess of 85 percent of the bits available for the whole video sequence. However, at lower bitrates the proportion of AC-coefficient encoding bits was significantly reduced, as illustrated by Figure 24.8. At 30 frames/s and 1.15 Mbits/s the average number of bits per video frame is about 38 000 and a given proportion of these bits is allocated to the control header information, motion information and to the DCT coefficients. Upon reducing the total bitrate budget - since the number of control header bits is more or less independent of the target bitrate - the proportion of bits allocated to the DCT coefficients is substantially reduced.

The next process, as discussed earlier, was to normalise the measured average PSNR degradation according to the probability of occurence of the respective parameters in the bitstream and the probability of bits being allocated to this parameter.

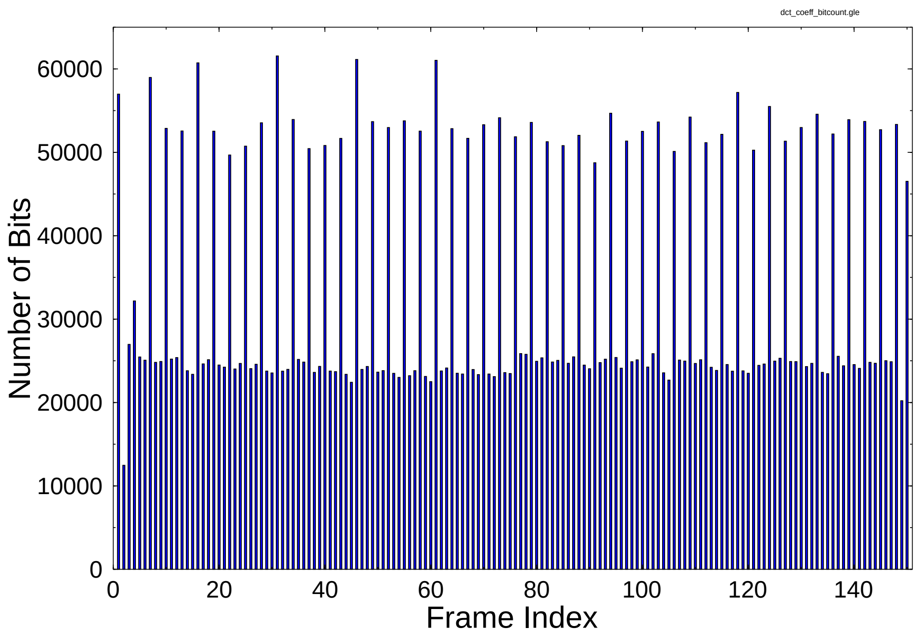

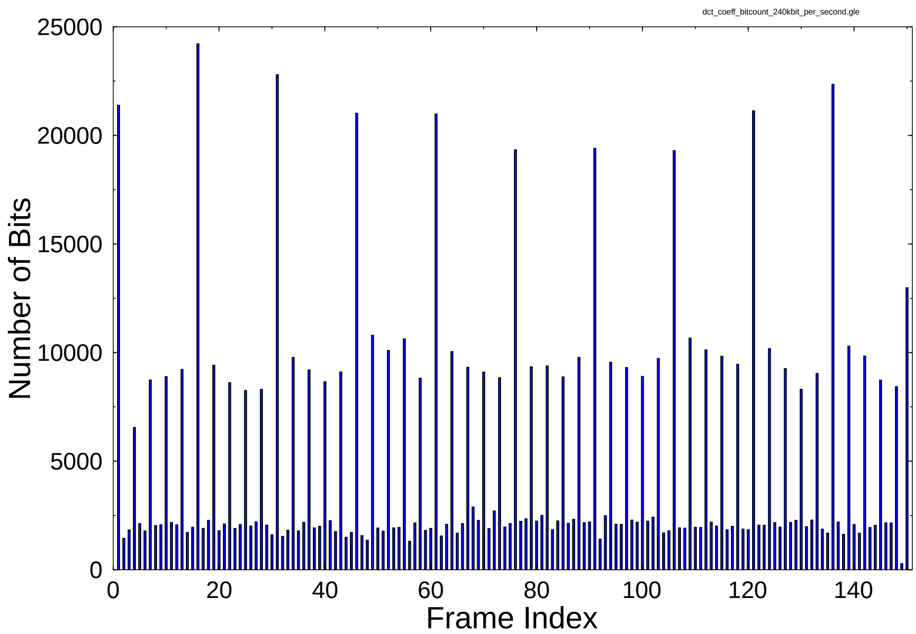

Figure 24.8: Profile of bits allocated to the DCT coefficients, when the Miss America video sequence is coded at (a) 1.15 Mbits/s (top) and (b) 240 kbits/s (bottom).

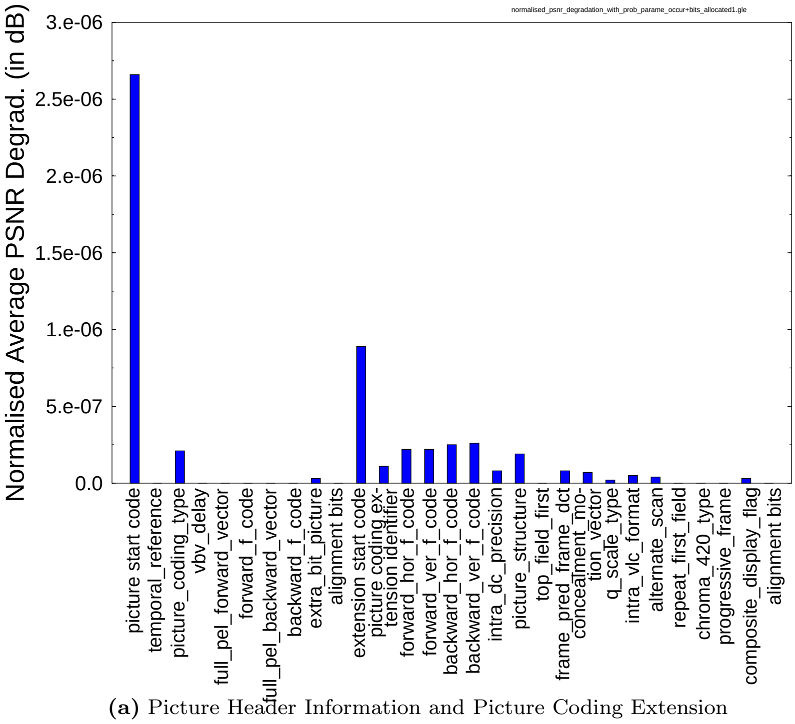

(a) Picture Header Information and Picture Coding Extension

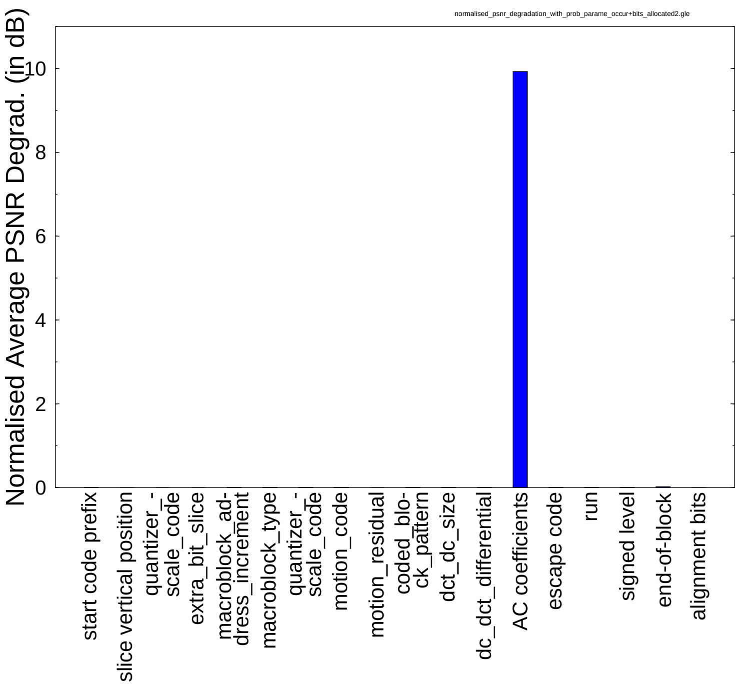

(b) Slice, Macroblock and Block Layers

Figure 24.9: Normalised average PSNR degradation for the various parameters in (a) Picture Header Information and Picture Coding Extension (b) Slice-, Macroblock- and Block-Layers, normalised to the probability of occurence of the respective parameters in the bitstream and the probability of bits being allocated to the parameter.

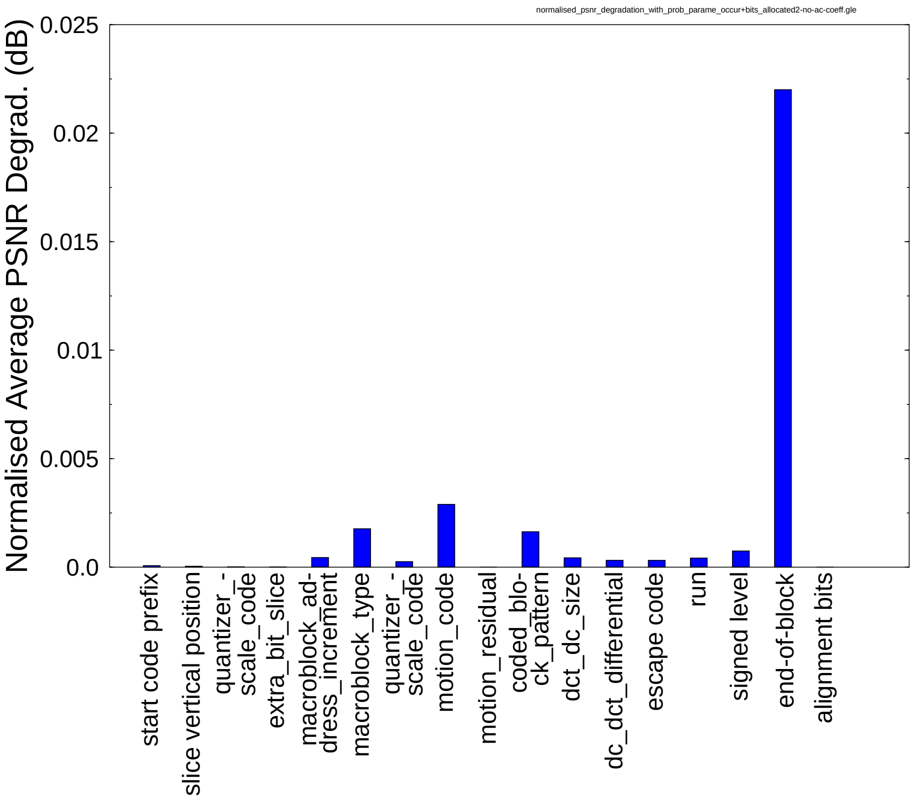

Figure 24.10: This bar chart is the same as Figure 24.9(b), although the normalised average PSNR degradation for the AC coefficients was omitted in order to show the average PSNR degradation of the other parameters.

The normalised average PSNR degradation inflicted by corrupting the parameters of the Picture Header Information and Picture Coding Extension is portrayed in Figure 24.9(a). Similarly, the normalised average PSNR degradation for the parameters of the Slice-, Macroblock- and Block-Layers is shown in Figure 24.9(b). In order to visually enhance Figure 24.9(b), the normalised average PSNR degradation for the AC coefficients was omitted in the bar-chart shown in Figure 24.10.

The highest PSNR degradation was inflicted by the AC coefficents, since these parameters occur most frequently and are allocated the highest number of bits. When a bit error occurs in the bitstream, the AC coefficients have a high probability of being corrupted. The other parameters, such as the DC_DCT_size and DC_DCT_differential, though exhibited high average PSNR degradations when corrupted, registered low normalised average PSNR degradations since their occurence in the bitstream is confined to intra-coded frames.

The end-of-block parameter exhibited the second highest normalised average PSNR degradation in this study. Although the average number of bits used for the

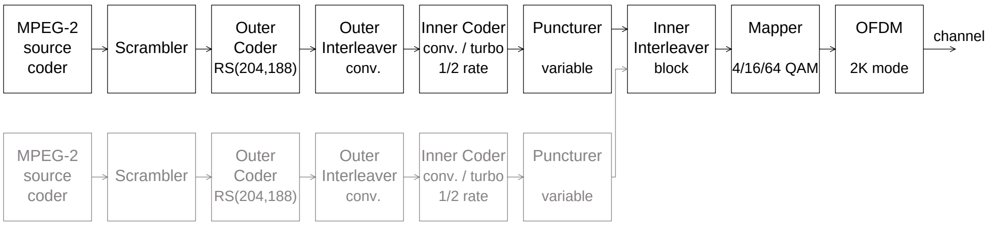

Figure 24.11: Schematic of the DVB terrestrial transmitter functions.

end-of-block is approximately 2.17 bits, the probability of occurence and the probability of bits being allocated to it is higher than those of other parameters, with the exception of the AC coefficients. Furthermore, in general, the parameters of the Slice-, Macroblock- and Block-Layers exhibit higher average normalised PSNR degradations due to their more frequent occurence in the bitstream than that due to the Picture Header Information and Picture Coding Extension. This also implies that the percentage of bits allocated to these parameters is higher.

If the comparison of the normalised average PSNR degradations is conducted in the context of the parameters in the Picture Header Information and Picture Coding Extension, the picture start code exhibits the highest normalised average PSNR degradation. Although most of the parameters here occur with equal probability as seen in Figure 24.5(b), the picture start code requires a higher portion of the bits compared to the other parameters here, with the exception of the extension start code. Despite having the same probability of occurence and the same allocation of bits, the extension start code exhibits a lower normalised PSNR degradation than the picture start code, since its average un-normalised degradation is lower, as it was shown in Figures 24.2 - 24.4.

From Figures 24.9 and 24.10, we observed that the video PSNR degradation was dominated by the erroneous decoding of the AC DCT coefficients, which appeared in the MPEG-2 video bitstream in the form of variable length codewords. This suggested invoking unequal error protection techniques for protecting the MPEG-2 parameters during transmission. In a low complexity implementation, two protection classes may be envisaged. The higher priority class would contain all the important header information and some of the more important low-frequency variable-length coded DCT coefficients. The lower priority class would then contain the remaining less important, higher frequency variable length coded DCT coefficients. This partitioning process will be detailed in Section 24.1.5 together with its associated performance in the context of the hierarchical digital video broadcasting (DVB) [135] transmission scheme in Section 24.1.8.

24.1.3 DVB Terrestrial Scheme

The block diagram of the DVB terrestrial (DVB-T) transmitter [135] is shown in Figure 24.11, which is constituted by an MPEG-2 video encoder, channel coding modules and an Orthogonal Frequency Division Multiplex (OFDM) modem [373].

Due to the poor error resilience of the MPEG-2 video codec, strong concatenated channel coding is employed, consisting of a shortened Reed-Solomon RS(204,188) outer code [153], which corrects up to eight erroneous bytes in a block of 204 bytes, and a half-rate inner convolutional encoder with a constraint length of 7 [153, 225]. The overall code rate can be adapted by the variable puncturer, which supports code rates of 1/2 (no puncturing) as well as 2/3, 3/4, 5/6, and 7/8. The parameters of the convolutional encoder are summarised in Table 24.1. If only one of the two branches of the transmitter in Figure 24.11 is utilised, the DVB-T modem is said to be operating in its non-hierarchical mode. In this mode, the modem can have a choice of QPSK, 16-QAM or 64-QAM modulation constellations.

Rate	1/2
Constraint Length	7
k	1
n	2
Polynomials (octal)	171,133

Table 24.1: Parameters of the CC(n,k,K) convolutional inner encoder in the DVB-T modem.

A second video bitstream can also be multiplexed with the first one by the inner interleaver, when the DVB modem is in its so-called hierarchical mode [135]. The choice of modulation constellations in this mode is between 16-QAM and 64-QAM. We shall be employing this transmission mode, when the so-called data partitioning scheme is used to split the incoming MPEG-2 video bitstream into two classes of data, as proposed in Section 24.1.5, with one class having a higher priority than the other one. The higher priority data will be multiplexed to the most significant bits (MSBs) of the modulation constellation points and the lower priority data to the least significant bits (LSBs). These different integrity subchannels were discussed earlier in Chapter 5. For 16-QAM and 64-QAM, the upper 2 bits of each 4- or 6-bit symbol will contain the more important video data. The lower priority data will then be multiplexed to the lower significance 2 bits and 4 bits of 16-QAM and 64-QAM, respectively.

Rate	1/2
Input block length	17952 bits
Interleaver	random
Number of iterations	8
Constraint Length	3
k	1
n	2
Polynomials	7,5

Table 24.2: Parameters of the inner turbo encoder used to replace the DVB-T system's convolutional coder.

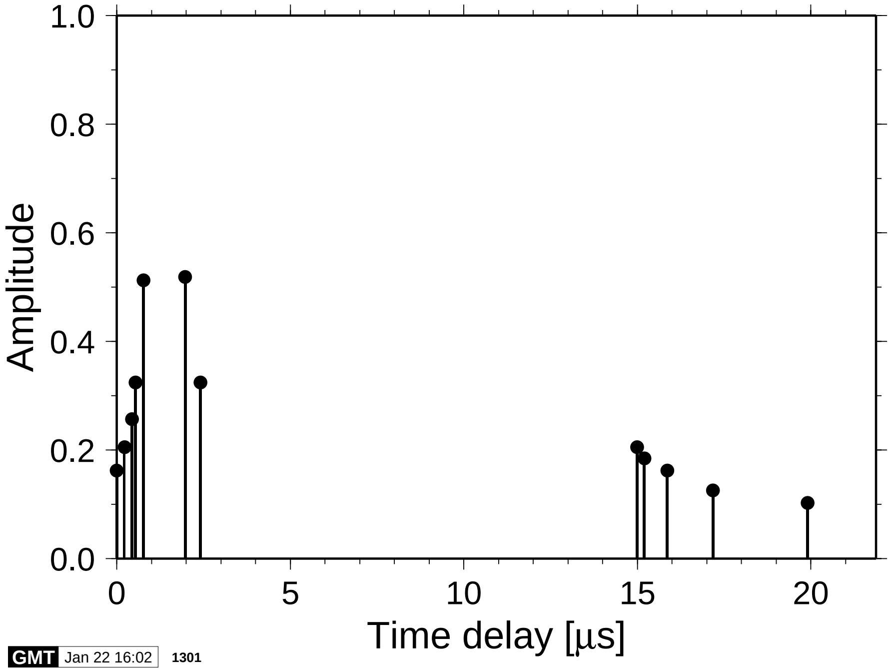

Figure 24.12: COST 207 hilly terrain (HT) type impulse response.

Beside implementing the standard DVB-T system as a benchmarker, we have improved the system by replacing the convolutional coder by a turbo codec [328]. The turbo codec's parameters used in the experiment are displayed by Table 24.2.

In this section, we have given an overview of the DVB-T system which we have used in our experiments. Readers interested in the details of the DVB-T system are referred to the DVB-T standard [135]. The performance of the standard DVB-T system and the turbo coded system is characterised in Section 24.1.7 and 24.1.8 for non-hierarchical and hierarchical transmissions, respectively. Let us now briefly consider the multipath channel model used in our experiments.

24.1.4 Terrestrial Mobile Broadcast Channel Model

In the system characterised here, we have used a carrier frequency of 500MHz and a sampling rate of $7/64\mu$s. The channel model employed in this study was the twelve-path COST 207 [374] hilly terrain (HT) type impulse response, with a maximal relative path delay of 19.9 μs. Each of the paths was faded independently obeying a Rayleigh fading distribution, according to a normalised Doppler frequency of 10^{-5}. This corresponds to a worst-case vehicular velocity of about 200 km/h. The unfaded impulse response is depicted in Figure 24.12. In order to facilitate un-equal error protection, let us now consider, how to partition the video data stream.

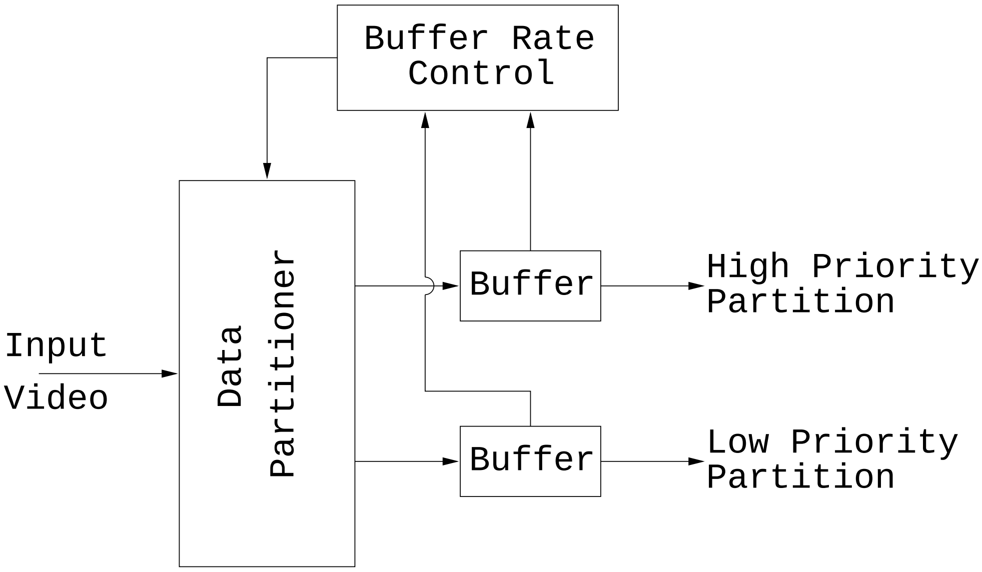

Figure 24.13: Block diagram of the data partitioner and rate controller.

24.1.5 Data Partitioning Scheme

As portrayed in Figures 24.9 and 24.10, the corrupted variable-length coded DCT coefficients inflict a high video PSNR degradation. Assuming that all header information is received correctly, the fidelity of the reconstructed images at the receiver side is dependent on the number of correctly decoded DCT coefficients. However, the effect of the loss of higher spatial frequency DCT coefficients are less dramatic compared to lower spatial frequency DCT coefficients. The splitting of the video bitstream into two different integrity bitstreams is termed as data partitioning [370]. Recall from Section 24.1.3 that the hierarchical DVB-T transmission scheme can enable us to multiplex two un-equal protected input bitstreams for transmission. This section describes the details of our proposed data partitioning scheme.

Figure 24.13 shows the block diagram of the data partitioning scheme, which splits a constant bitrate video bitstream into two resultant bitstreams. The position in which the input is split is based on a variable referred to here as the priority breakpoint (PBP). The PBP can be adjusted at the beginning of the encoding of every image slice, based on the buffer occupancy or 'fullness' of the two output buffers. For example, if the high priority buffer is 80 % full and the low priority buffer is only 40 % full, the rate control module would have to adjust the PBP such that more data is directed to the low priority partition. This measure is taken in order to avoid high priority buffer overflow and low priority buffer underflow events. The valid values for the PBP are summarized in Table 24.3 [370].

There are two main stages in updating the PBP. The first stage involves the rate control module in order to decide on the preferred new PBP value for each partition

PBP	Syntax elements in high priority partition
0	Low priority partition always has its PBP set to 0.
1	Sequence, GOP, Picture and Slice layer information upto extra bit slice.
2	Same as above and upto macroblock address increment.
3	Same as above plus including macroblock syntax elements but excluding coded block pattern.
4 . . . 63	Reserved for future use.
64	Same as above plus including DC coefficient and the first run-length coded DCT coefficient.
65	Same as above and up to the second runlength coded DCT coefficient.
64 + x	Same as above and up to x runlength coded DCT coefficient.
127	Same as above and up to 64 runlength coded DCT coefficient.

Table 24.3: Priority breakpoint values and the associated syntax elements that will be directed to the high priority partition [370].

based on their individual buffer fullness and on the current value of the PBP. The second stage then combines the two desired PBPs based on the buffer occupancy of both buffers in order to produce a new PBP.

The updating of the PBP in the first stage of the rate control module is based on a heuristic approach, similar to that suggested by Aravind *et.al.* [375]. The update procedure is detailed in Algorithm 1, which is discussed below and augmented by a numerical example at the end of this section.

The variable 'sign' is used in Algorithm 1, in order to indicate how the PBP has to be adjusted in the high- and low-priority partitions, so as to arrive at the required target buffer fullness. More explicitly, the variable 'sign' in Algorithm 1 is necessary, because the PBP values shown in Table 24.3 indicate the amount of information, which should be directed to the high priority partition. Therefore, if the low priority partition requires more data, then the new PBP must be lower than the current PBP, which is contrary to the requirements of the high priority partition, where a higher PBP implies obtaining more data.

Once the desired PBPs for both partitions have been acquired with the aid of Algorithm 1, Algorithm 2 is invoked, in order to compute the final PBP for the current image slice. The inner working of these algorithms will be augmented by a numerical example at the end of this section. There are two main cases to consider. The first one occurs, when both partitions have a buffer occupancy of less than 50%. By using the reciprocal of the buffer occupancy in Algorithm 2 as a weighting factor, the algorithm will favour the new PBP decision of the less occupied buffer, in order to fill the buffer with more data in the current image slice. This assists in preventing the particular buffer from under-flowing. On the other hand, when both buffers

Algorithm 1 Computes the desired PBP update for the high- and low-priority partitions which is then passed to Algorithm 2, in order to determine the PBP to be set for the current image slice.

```
Step 1: Initialize parameters
  if High Priority Partition then
    sign := +1
  else
    sign := −1
  end if

Step 2:
  if buffer occupancy ≥ 80% then
    diff := 64 − PBP
  end if

  if buffer occupancy ≥ 70% and buffer occupancy < 80% then
    if PBP ≥ 100 then
      diff := −9
    end if
    if PBP ≥ 80 and PBP < 100 then
      diff := −5
    end if
    if PBP ≥ 64 and PBP < 80 then
      diff := −2
    end if
  end if

  if buffer occupancy ≥ 50% and buffer occupancy < 70% then
    diff := +1
  end if

  if buffer occupancy < 50% then
    if PBP ≥ 80 then
      diff := +1
    end if
    if PBP ≥ 70 and PBP < 80 then
      diff := +2
    end if
    if PBP ≥ 2 and PBP < 70 then
      diff := +3
    end if
  end if

Step 3:
  diff := sign × diff
  Return diff
```

Algorithm 2 Compute new PBP for the current image slice based on current buffer occupancy of both partitions

Step 1:

$$
\begin{array}{lrcr}
\textbf{if} & \text{Occupancy}_{HighPriority} < 50\% & \textbf{and} & \text{Occupancy}_{LowPriority} < 50\% \\
\textbf{or} & \text{Occupancy}_{HighPriority} = 50\% & \textbf{and} & \text{Occupancy}_{LowPriority} < 50\% \\
\textbf{or} & \text{Occupancy}_{HighPriority} < 50\% & \textbf{and} & \text{Occupancy}_{LowPriority} = 50\% \\
\textbf{or} & \text{Occupancy}_{HighPriority} < 25\% & \textbf{and} & 50\% < \text{Occupancy}_{LowPriority} < 70\% \\
\textbf{or} & 50\% < \text{Occupancy}_{HighPriority} < 70\% & \textbf{and} & \text{Occupancy}_{LowPriority} < 25\%
\end{array}
$$

then

$$\text{delta} := \frac{\text{Occupancy}^{-1}_{HighPriority} \times \text{diff}_{HighPriority} + \text{Occupancy}^{-1}_{LowPriority} \times \text{diff}_{LowPriority}}{\text{Occupancy}^{-1}_{HighPriority} + \text{Occupancy}^{-1}_{LowPriority}}$$

else

$$\text{delta} := \frac{\text{Occupancy}_{HighPriority} \times \text{diff}_{HighPriority} + \text{Occupancy}_{LowPriority} \times \text{diff}_{LowPriority}}{\text{Occupancy}_{HighPriority} + \text{Occupancy}_{LowPriority}}$$

end if

Step 2:

New_PBP := Previous_PBP + $\lceil \text{delta} \rceil$ where $\lceil\rceil$ means rounding up to the nearest integer

Return New_PBP

experience a buffer fullness of more than 50%, the buffer occupancy itself is used as a weighting factor instead. Now, the algorithm will instruct the buffer having a higher fullness to have its desired PBP adjusted such that less data is inserted into it in the current image slice. Hence, the buffer overflow problems are prevented.

The new PBP value is then compared to its legitimate range tabulated in Table 24.3. Furthermore, we restricted the minimum PBP value such that I-, P- and B-pictures have minimum PBP values of 64, 3 and 2, respectively. Since B-pictures are not used for future predictions, it was decided that its data need not be protected as strongly as that of the I- and P-pictures. As for P-pictures, Ghanbari and Seferidis [376] showed that correctly decoded motion vectors can still provide a subjectively pleasing reconstruction of the image, even if the DCT coefficients were discarded. Hence, the minimum splitting location or PBP for P-pictures has been set to be just before the coded block pattern parameter, which would then ensure that the motion vectors would be mapped to the high priority partition. For I-pictures, the fidelity of the reconstructed image is dependent on the number of DCT coefficients that can be decoded successfully. Therefore, the minimum splitting location or PBP was set to include at least the first runlength coded DCT coefficient. The MPEG-2 syntax does not allow the split to be made after the first DC coefficient alone, which could lead to start code emulation, should decoding errors occur.

Below we demonstrate the operation of Algorithm 1 and Algorithm 2 with the aid of a simple numerical example. We shall assume that the PBP prior to the update is 75 and the buffer fullness for the high- and low-priority partition buffers is 40% and 10%, respectively. Considering the high priority partition, Algorithm 1 will set the

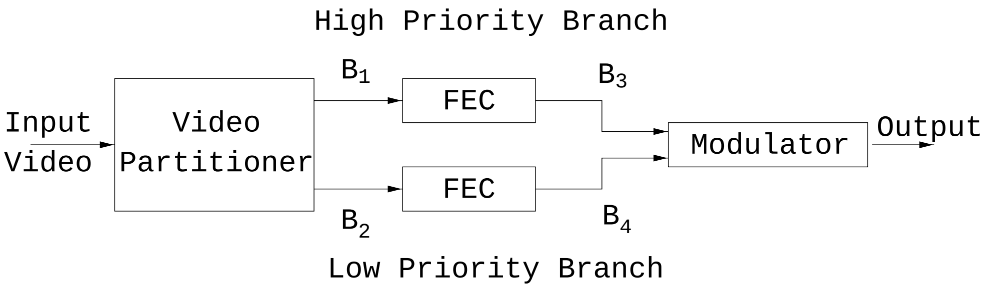

Figure 24.14: Video partitioning scheme for the DVB-T system operating in hierarchical mode.

desired update for PBP to +2 and this desired update is referred to as $\text{diff}_{HighPriority}$ in Algorithm 2. For the low priority partition, Algorithm 1 will set the desired update for PBP to -2. The desired PBP update for the low priority partition is referred to as $\text{diff}_{LowPriority}$ in Algorithm 2. Since both partition buffers' occupancy is less than 50%, Algorithm 2 will use the reciprocal of the buffer occupancy as the weighting factor, which will then favour the desired update of the low priority partition due to its 10 % occupancy. The final update value - which is denoted by delta in Algorithm 2 - is equal to -2 (after being rounded up). Hence, the new PBP is 73. This means that for the current image slice, more data will be directed into the low priority partition in order to prevent buffer underflow.

Apart from adjusting the PBP values from one image slice to another, in order to avoid buffer underflow or overflow, the output bitrate of each partition buffer has to be adjusted, such that the input bitrate of the inner interleaver and modulator in Figure 24.11 is properly matched between the two partitions. Hence, it is imperative to take into account the redundancy added by forward error correction (FEC), especially when the two partition's FECs operate at different code rate. Figure 24.14 shows a stylised block diagram of the DVB-T system operating in the hierarchical mode and receiving its input from the video partitioner. The FEC module represents the concatenated coding system, constituted by a Reed-Solomon codec and a convolutional codec. The modulator can invoke both 16-QAM and 64-QAM. We shall now use an example to illustrate the choice of the various partitioning ratios tabulated in Table 24.4.

We shall assume that 64-QAM is selected and the high- and low-priority partitions employ rate 1/2 and 3/4 convolutional codes, respectively. We do not have to take the Reed-Solomon code rate into account, since both partitions invoke the same Reed-Solomon codec. Based on these facts and upon referring to Figure 24.14, the input bitrates B_3 and B_4 of the modulator will have to obey the ratio 1:2 since the two MSBs of the 64-QAM constellation are assigned to the high priority partition and the remaining four bits to the low priority partition.

At the same time, the ratio of B_3 to B_4 is related to the ratio of B_1 to B_2 with the FEC redundancy taken into account, requiring:

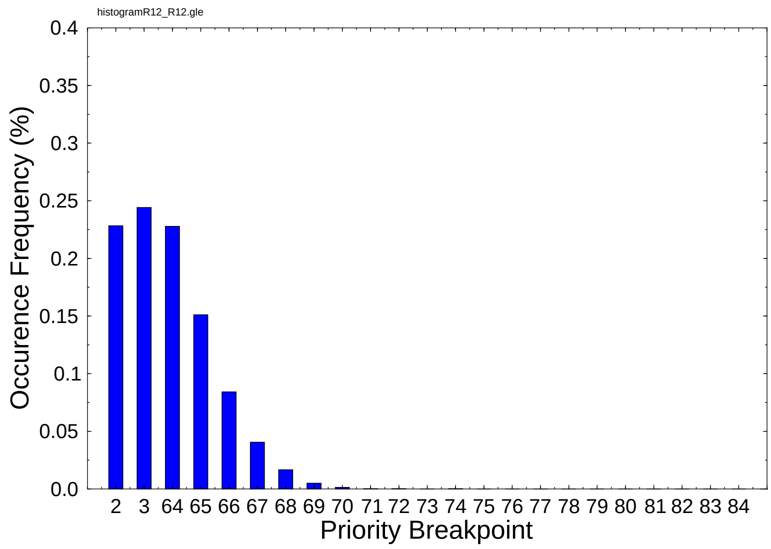

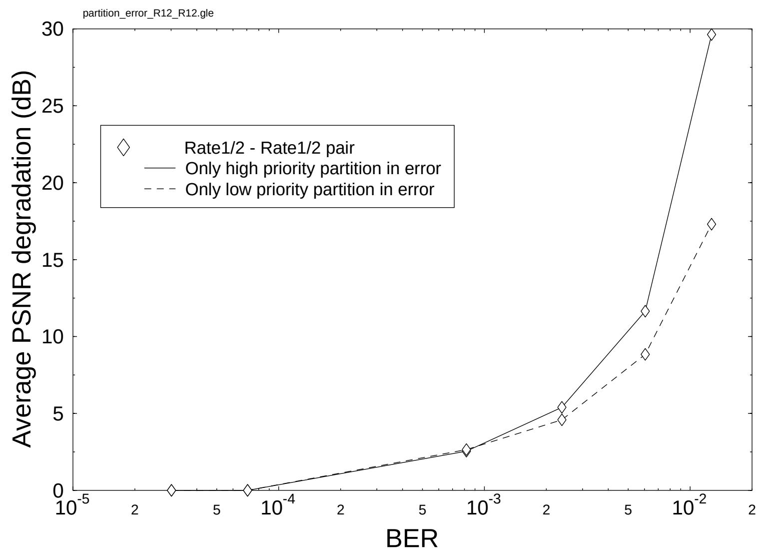

Figure 24.15: (a) Histogram of the probability of occurence for various priority breakpoints and (b) average PSNR degradation versus BER for rate-1/2 convolutional coded high and low priority data in Scheme 1.

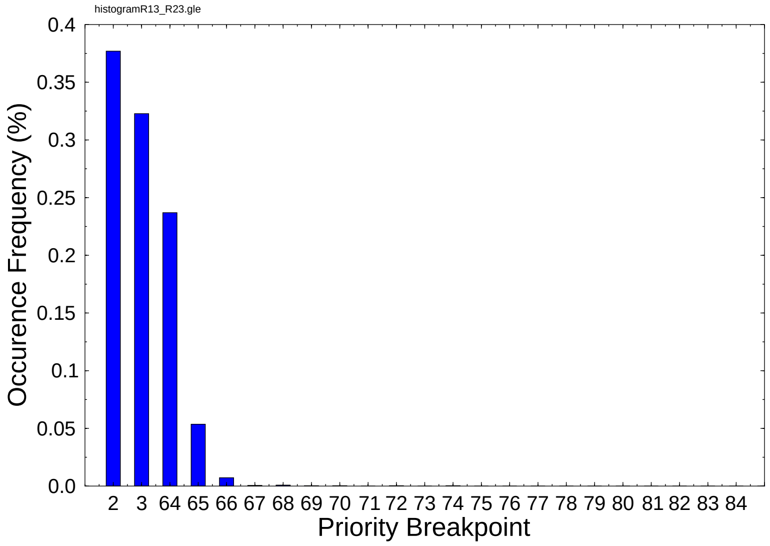

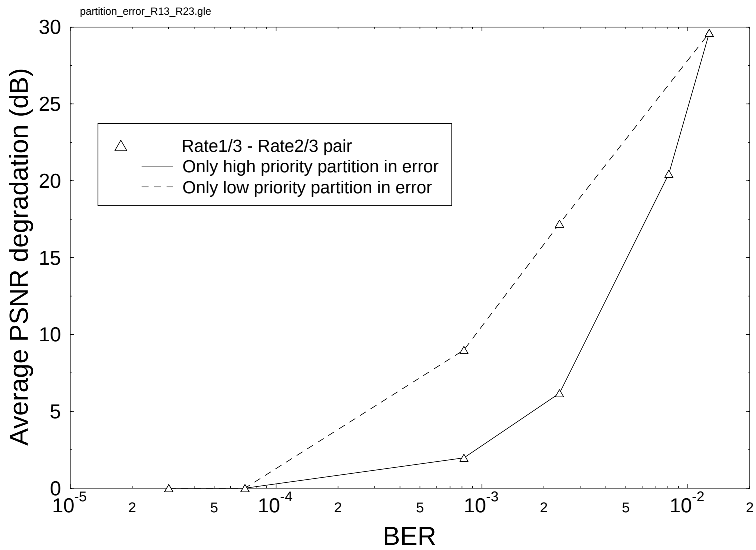

Figure 24.16: (a) Histogram of the probability of occurence for various priority breakpoints and (b) average PSNR degradation versus BER for the rate-1/3 convolutional coded high priority data and rate-2/3 convolutional coded low priority data in Scheme 2.

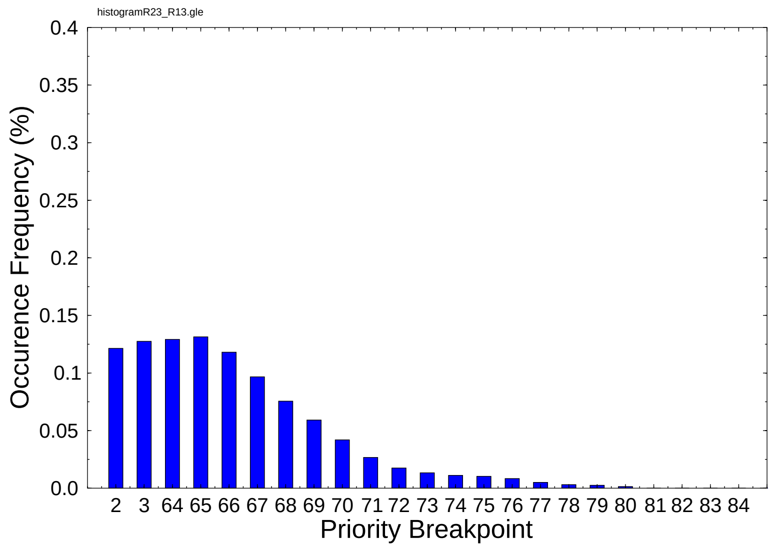

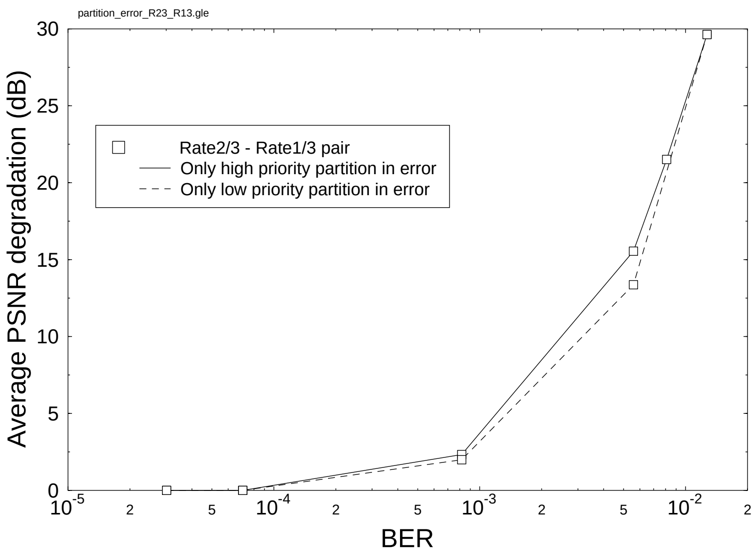

Figure 24.17: (a) Histogram of the probability of occurence for various priority breakpoints and (b) average PSNR degradation versus BER for the rate-2/3 convolutional coded high priority data and rate-1/3 convolutional coded low priority data in Scheme 3.

Modulation	Conv. Code Rate (High Priority)	Conv. Code Rate (Low Priority)	Bitrate Ratio (High Priority): Low Priority)
16-QAM	1/2	1/2	1 : 1
	1/2	2/3	3 : 4
	1/2	3/4	2 : 3
	1/2	5/6	3 : 5
	1/2	7/8	4 : 7
	2/3	1/2	4 : 3
64-QAM	1/2	2/3	1 : 2
	1/2	2/3	3 : 8
	1/2	3/4	1 : 3
	1/2	5/6	3 : 10
	1/2	7/8	2 : 7
	2/3	1/2	2 : 3

Table 24.4: The partitioning ratios for the high- and low-priority partition's output bitrate based on the modulation mode and code rates selected for the DVB-T hierarchical mode.

$$\begin{aligned} \frac{B_3}{B_4} &= \frac{2\times B_1}{\frac{4}{3}\times B_2} &= \frac{1}{2} \\ &= \frac{3}{2}\cdot\frac{B_1}{B_2} &= \frac{1}{2} \\ & \quad\ \frac{B_1}{B_2} &= \frac{1}{2}\times\frac{2}{3} \\ & &= \frac{1}{3} \end{aligned} \tag{24.1}$$

If, for example, the input video bitrate to the data partitioner module is 1 Mbit/s, the output bitrate of the high- and low-priority partition would be $B_1 = 250$ kbit/s and $B_2 = 750$ kbit/s respectively, according to the ratio indicated by Equation 24.1.

In this section, we have outlined the data partitioning scheme, which we used in the DVB-T hierarchical transmission scheme. Its performance in the overall system will be characterised in Section 24.1.8. Let us however first evaluate the BER-sensitivity of the partitioned MPEG-2 bitstream to randomly distributed bit errors using various partitioning ratios.

24.1.6 Performance of Data Partitioning Scheme

Let us refer to the equally split rate-1/2 convolutional coded high and low priority scenario as Scheme 1. Furthermore, the rate-1/3 convolutional coded high priority data and rate-2/3 convolutional coded low priority data based scenario is referred to here as Scheme 2. Lastly, the rate-2/3 convolutional coded high priority data and rate-1/3 coded low priority data based partitioning scheme is termed as Scheme 3. We then programmed the partitioning scheme of Figure 24.14 for maintaining the required splitting ratio. This was achieved by continuously adjusting the PBP using Algorithm 1 and Algorithm 2. The associated PBP histograms are

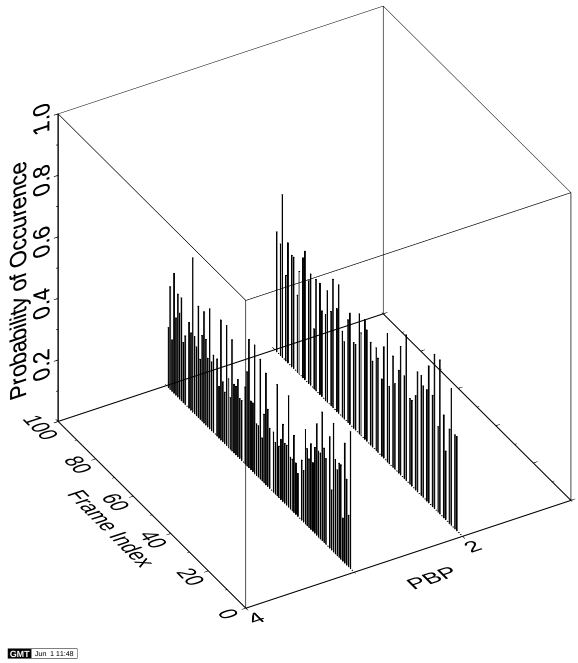

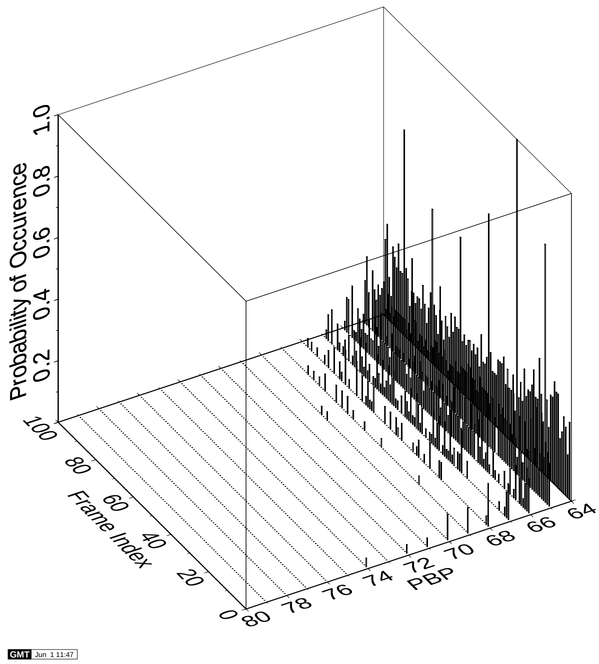

Figure 24.18: Evolution of the probability of occurence of PBP values from one picture to another for Scheme 1.

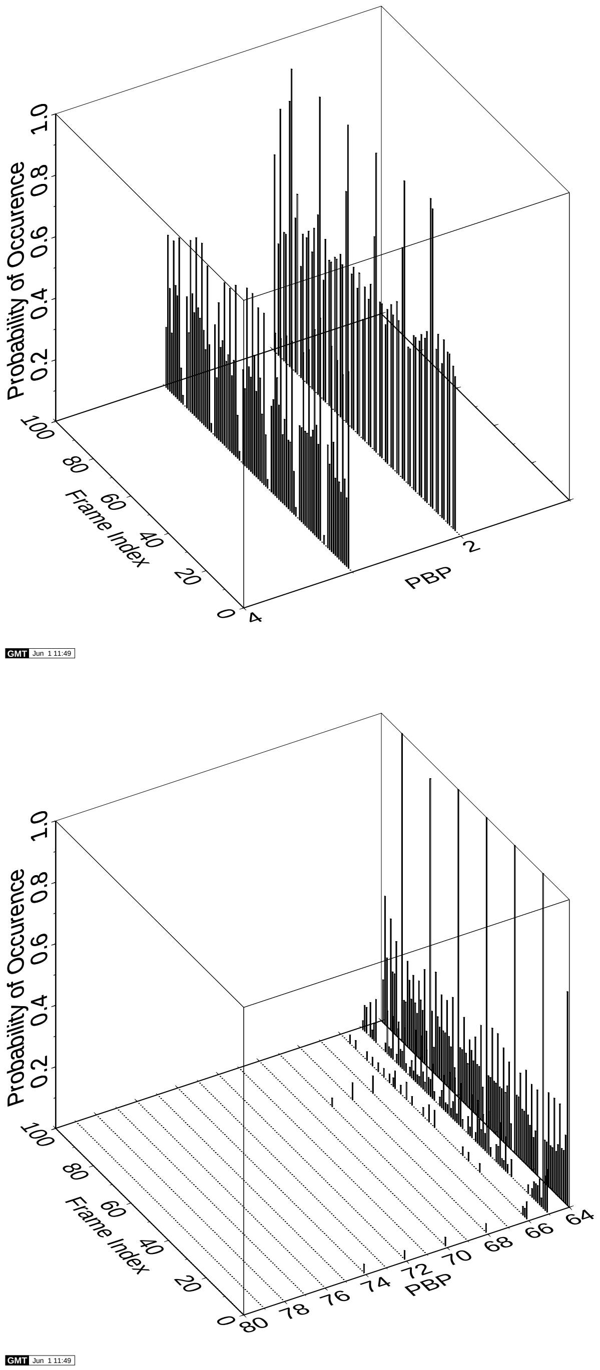

Figure 24.19: Evolution of the probability of occurence of PBP values from one picture to another for Scheme 2.

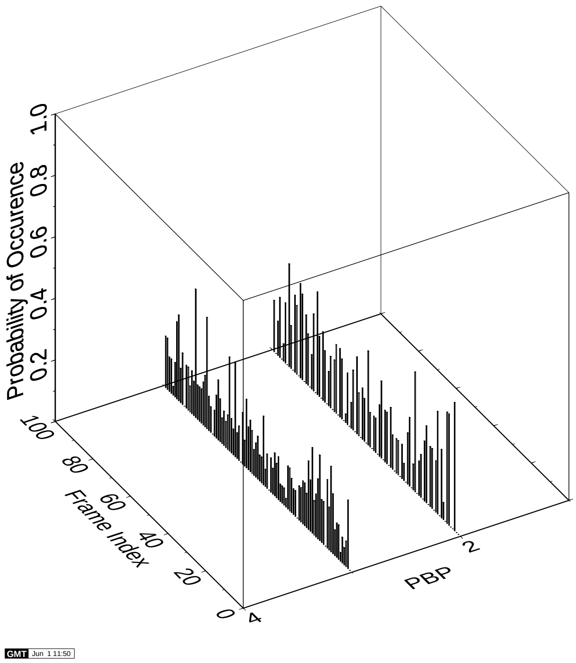

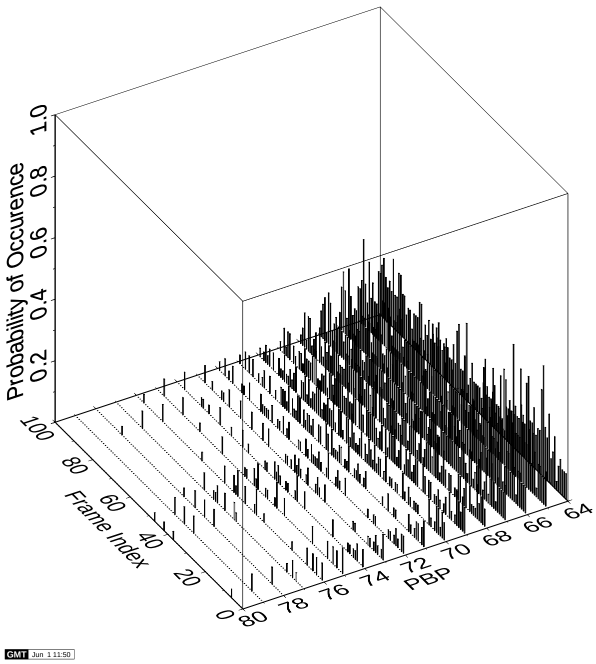

Figure 24.20: Evolution of the probability of occurence of PBP values from one picture to another for Scheme 3.

shown in Figures 24.15(a), 24.16(a) and 24.17(a). Comparing the histograms in Figure 24.15(a), 24.16(a) and Figure 24.17(a), we observed that as expected, Scheme 3 had the most data in the high priority partition, followed by Schemes 1 and 2.

We then embarked on quantifying the error sensitivity of the partitioning Schemes 1 to 3, when subjected to randomly distributed bit errors. Specifically, the previously defined average PSNR degradation was evaluated for given error probabilities inflicting random errors imposed on one of the partitions, while keeping the other partition error-free. These results are portrayed in Figures 24.15(b), 24.16(b) and 24.17(b), for Schemes 1 to 3. More explicitly, when aiming for $B_3 = B_4$ in Figure 24.14, the coding rate of the partitions predetermines the proportion of unprotected video data in the two partitions, i.e. the bitrates B_1 and B_2, as quantified by Equation 24.1. If instead of a 1/2-rate code we assume a strong 1/3-rate code for the high-sensitivity video partition, which we refer to as C1, more video data is directed to the lower sensitivity C2 subchannel, as in Scheme 2. Therefore the most error-sensitive 1/3 of the video data is expected to result in a higher PSNR degradation at a given BER, than the most sensitive rate-1/2 case. Furthermore, when assigning 2/3 of the bits to the less sensitive partition - again, as in Scheme 2 - the overall sensitivity is expected to increase in comparison to allocating only 1/2 of the bits to this class, since now a larger proportion of the higher-sensitivity bits belongs to this partition. We note however that the expected trends are strongly ameliorated by the fact that bit errors of any of the sensitivity classes influence the PSNR degradation of the reconstructed video through the reconstructed frame buffer of the remote decoder, while the encoder's local reconstructed frame buffer contains the error-free reconstructed video frames. Schemes 1 and 3 exhibited a higher PSNR degradation, when the high priority partitions were corrupted compared to corruption of the low priority partition only. The opposite was observed for Scheme 2. This showed that the average PSNR degradation was dependent on the amount of data in the partitions. In Scheme 2, there was more data in the low priority partition, inevitably increasing its sensitivity. Hence, when the low priority stream was corrupted, the amount of data left in the high priority partition was insufficient for concealing the effect of errors. Hence in Scheme 2 the dominant contributor to the average PSNR degradation was the low priority partition containing a large fraction of sensitive bits.

Furthermore, for Schemes 1 and 3 at BERs less than 10^{-3}, the PSNR degradation experienced by corrupting either the high or low priority partition was similar. These findings will assist us in explaining our observations in the context of the hierarchical transmission scheme of Section 24.1.8, suggesting that the data partitioning scheme did not provide overall gain in terms of error resilience over the non-partitioned case.

Figures 24.18, 24.19 and 24.20 show the evolution of the probability of occurence of the PBP values, as the video encoder progressed in encoding one picture after another for the "Football" HDTV video sequence. These figures again illustrate that Scheme 3 had the most data in the high priority partition, followed by Scheme 1 and Scheme 2.

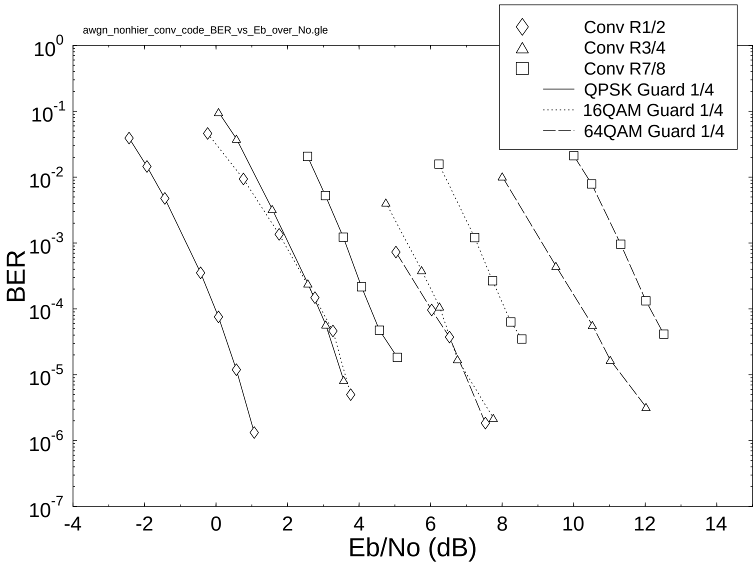

(a) Convolutional Code

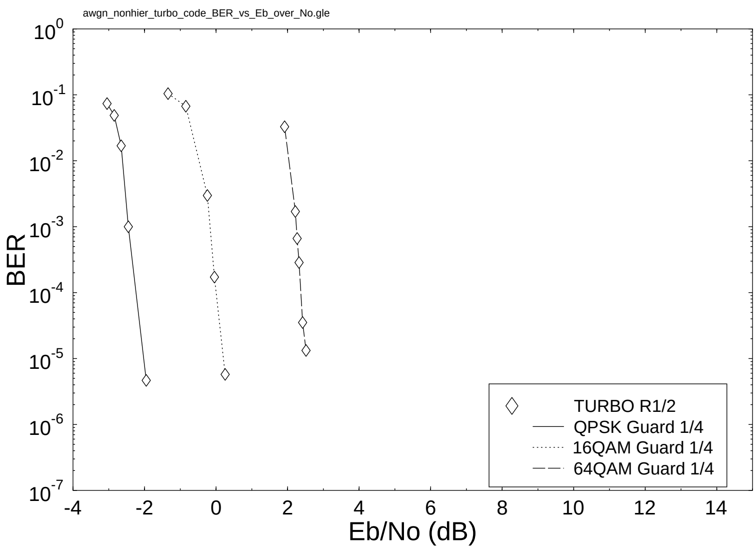

(b) Turbo Code

Figure 24.21: BER after (a) convolutional decoding and (b) turbo decoding for the DVB-T scheme over stationary, non-dispersive AWGN channels for non-hierarchical transmission.

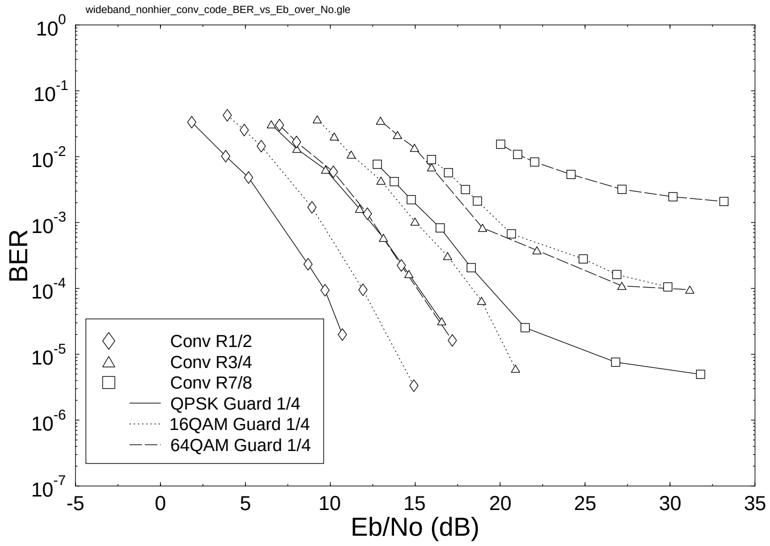

(a) Convolutional Code

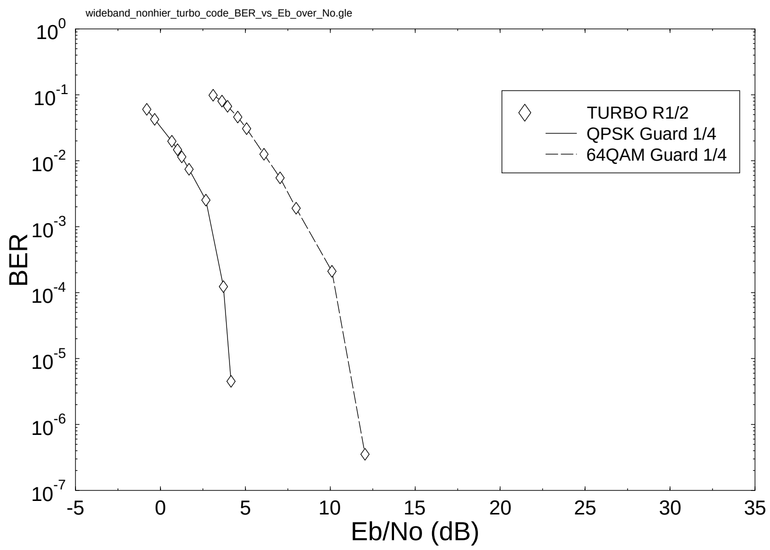

(b) Turbo Code

Figure 24.22: BER after (a) convolutional decoding and (b) turbo decoding for the DVB-T scheme over the wideband channel of Figure 24.12 for non-hierarchical transmission.

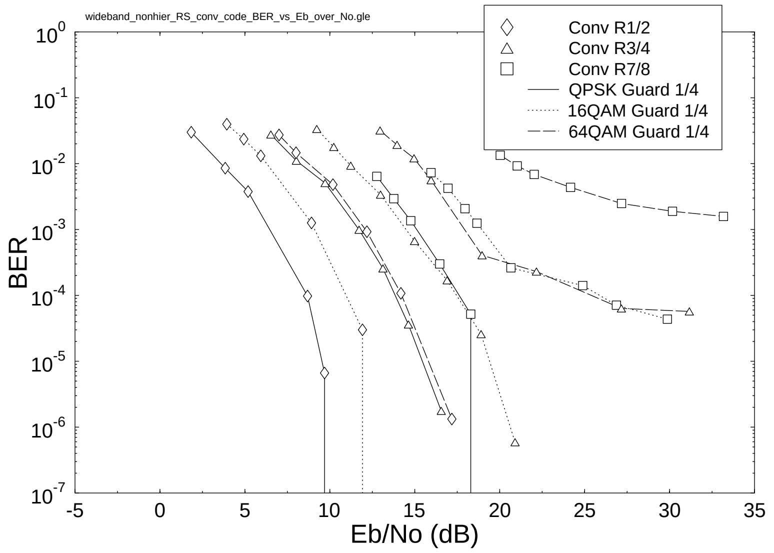

(a) RS and Convolutional Code

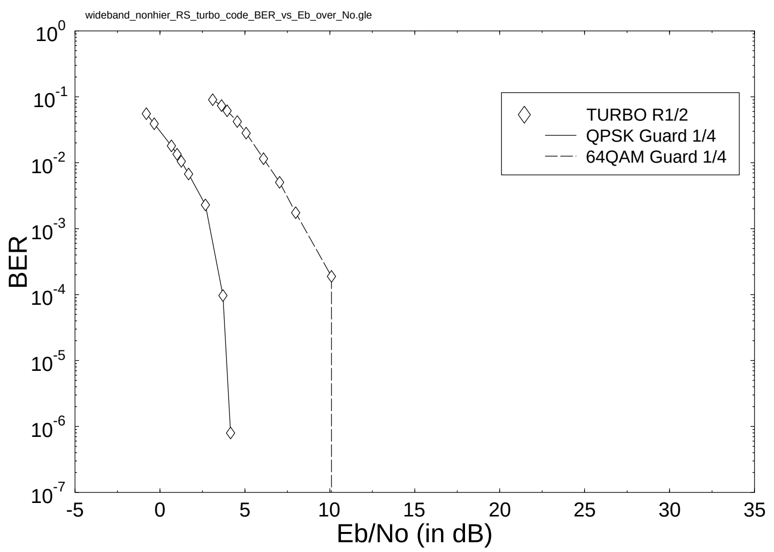

(b) RS and Turbo Code

Figure 24.23: BER after (a) RS and convolutional decoding and (b) RS and turbo decoding for the DVB-T scheme over the wideband channel of Figure 24.12 for non-hierarchical transmission.

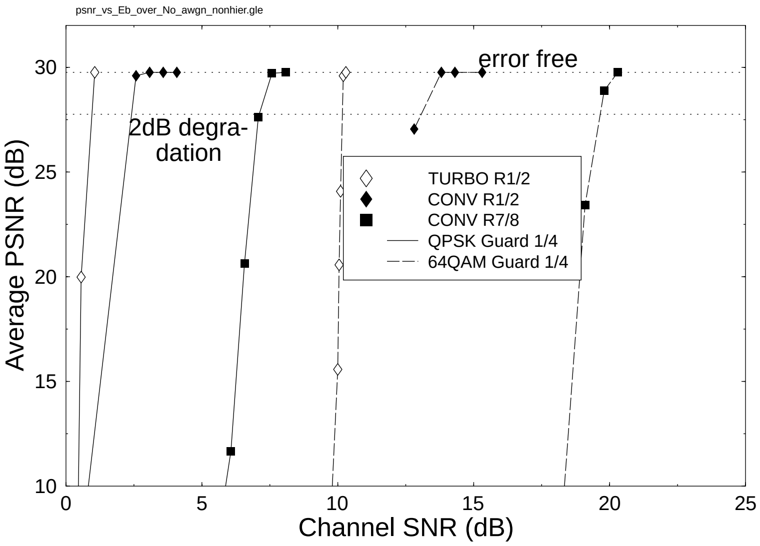

Figure 24.24: Average PSNR versus channel SNR of the DVB scheme [135] over non-dispersive AWGN channels for non-hierarchical transmission.

24.1.7 Performance of the Non-hierarchical DVB Terrestrial Scheme

In this section we shall elaborate on our findings, when replacing the convolutional code used in the standard DVB scheme [135] with a turbo code. We will invoke a range of standard-compliant schemes as benchmarkers. The "Football" HDTV video sequence was used in our experiments. In Figures 24.21(a) and 24.21(b) the bit error rate (BER) performance of the various modem modes in conjunction with the diverse channel coding schemes are portrayed over stationary, narrowband Additive White Gaussian Noise (AWGN) channels, where the turbo codec exhibits a significantly steeper BER reduction in comparison to the convolutionally coded arrangements.

Specifically, comparing the performance of the various turbo and convolutional codes for QPSK and 64-QAM at a BER of 10^{-4}, the turbo code exhibited an additional coding gain of about 2.24 dB and 3.7 dB respectively, when using half-rate codes in Figures 24.21(a) and 24.21(b). Hence the Peak Signal to Noise Ratio (PSNR) versus channel Signal to Noise Ratio (SNR) graphs in Figure 24.24 demonstrate that approximately 2 dB and 3.5 dB lower channel SNRs are required in conjunction with the rate 1/2 turbo codec for QPSK and 64-QAM, respectively, than for convolutional coding, in order to maintain error free video performance.

Comparing the BER performance of the 1/2-rate convolutional decoder in Figure 24.22(a) and the so-called Log-Map turbo decoder using eight iterations in Fig-

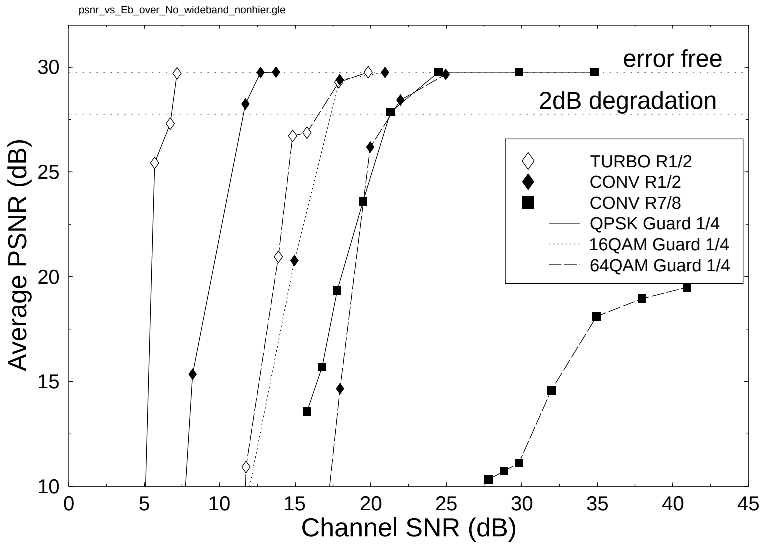

Figure 24.25: Average PSNR versus channel SNR of the DVB scheme [135] over the wideband fading channel of Figure 24.12 for non-hierarchical mobile transmission.

ure 24.22(b) for QPSK modulation over the worst-case fading mobile channel of Figure 24.12 we observe that the turbo code provided an additional coding gain of 6 dB in comparison to the convolutional code at a BER of about 10^{-4}. By contrast, for 64QAM using similar codes, a 5 dB coding gain was observed at this BER.

Similar observations were also made with respect to the average Peak Signal to Noise Ratio (PSNR) versus channel Signal to Noise Ratio (SNR) plots of Figure 24.25. For example, for the QPSK modulation mode and a 1/2 coding rate, the turbo code required an approximately 5.5 dB lower channel SNR, than the convolutional code for maintaining error free video transmission.

In conclusion, Tables 24.5 and 24.6 summarize the system performance in terms of the required channel SNR (CSNR) in order to maintain less than 2 dB PSNR video degradation. It was observed that at this PSNR degradation decoding errors were still perceptually unnoticable to the viewer due to the 30 frames/s refresh-rate, although the still-frame shown in Figure 24.26 exhibits some degradation. In the next section, we shall present the results of our experiments employing the DVB-T system [135] in a hierarchical transmission scenario.

Figure 24.26: Frame 79 of "Football" sequence, which illustrates the visual effects of minor decoding errors at a BER of 2.10^{-4} after convolutional decoding. The PSNR degradation observed is approximately 2 dB. The sequence was coded using a rate-7/8 convolutional code and transmitted emplying QPSK modulation.

Mod.	Code	CSNR (dB)	E_b/N_0	BER
QPSK	Turbo (1/2)	1.02	-1.99	$6{\cdot}10^{-6}$
64QAM	Turbo (1/2)	9.94	2.16	$2{\cdot}10^{-3}$
QPSK	Turbo (7/8)	8.58	5.57	$1.5{\cdot}10^{-4}$
64QAM	Turbo (7/8)	21.14	13.36	$4.3{\cdot}10^{-4}$
QPSK	Conv (1/2)	2.16	-0.85	$1.1{\cdot}10^{-3}$
64QAM	Conv (1/2)	12.84	5.06	$6{\cdot}10^{-4}$
QPSK	Conv (7/8)	6.99	3.98	$2{\cdot}10^{-4}$
64QAM	Conv (7/8)	19.43	11.65	$3{\cdot}10^{-4}$

Table 24.5: Summary of performance results over non-dispersive AWGN channels tolerating a PSNR degradation of 2dB.

Mod.	Code	CSNR (dB)	E_b/N_0	BER
QPSK	Turbo (1/2)	6.63	3.62	$2.5{\cdot}10^{-4}$
64QAM	Turbo (1/2)	15.82	8.03	$2{\cdot}10^{-3}$
QPSK	Turbo (7/8)	28.47	25.46	10^{-6}
QPSK	Conv (1/2)	10.82	7.81	$6{\cdot}10^{-4}$
64QAM	Conv (1/2)	20.92	13.14	$7{\cdot}10^{-4}$
QPSK	Conv (7/8)	20.92	17.91	$3{\cdot}10^{-4}$

Table 24.6: Summary of performance results over fading wideband channels tolerating a PSNR degradation of 2dB.

24.1.8 Performance of the Hierarchical DVB Terrestrial Scheme

Below we will invoke the DVB-T hierarchical scheme in a mobile broadcasting scenario. We shall also show the improvements which turbo codes offer, when replacing the convolutional code in the standard scheme. Hence, the convolutional codec in both the high and low priority partitions was replaced by the turbo codec. We have also investigated replacing only the high priority convolutional codec with the turbo codec, pairing the 1/2-rate turbo codec in the high priority partition with the convolutional codec in the low priority partition. Such a hybrid arrangement would constitute a reduced-complexity compromise scheme. Again, the "Football" sequence was used in these experiments. Partitioning was carried out using the schematic of Figure 24.14 as well as Algorithms 1 and 2.

Referring to Figure 24.27 and comparing the performance of the 1/2-rate convolutional code and turbo code at a BER of 10^{-4} for the low priority partition, the turbo code, employing 8 iterations, exhibited a coding gain of about 6.6 dB and 5.97 dB for 16-QAM and 64-QAM, respectively. When the number of iterations was reduced to 4, the coding gains offered by the turbo code over that of the convolutional code were 6.23 dB and 5.7 dB for 16-QAM and 64-QAM respectively. We observed that by reducing the number of iterations to 4 halved the associated complexity but the turbo code exhibited a coding loss of only about 0.37 dB and 0.27 dB in comparison to the 8-iteration scenario for 16-QAM and 64-QAM, respectively. Hence, the computational complexity of the turbo codec can be halved by sacrificing only a small amount of coding gain. The substantial coding gain provided by turbo coding is also reflected in the PSNR versus channel SNR graphs of Figure 24.29. In order to achieve error free transmission, Figure 24.29 demonstrated that approximately 5.72 dB and 4.56 dB higher channel SNRs are required by the standard scheme compared to the scheme employing turbo coding, using 4 iterations in both partitions. We have only shown the performance of turbo coding for the low priority partition in Figures 24.27(b) and 24.28(b), since the high priority partition experienced error-free reception after Reed-Solomon decoding for the range of SNRs used.

We also observed that the rates 3/4 and 7/8 convolutional codes in the low priority partition were unable to provide sufficient protection to the transmitted data, as it

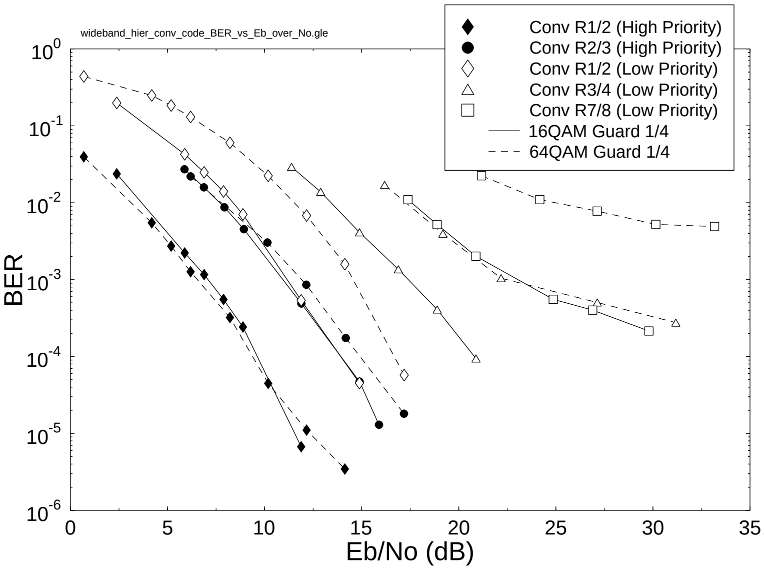

(a) Convolutional Code

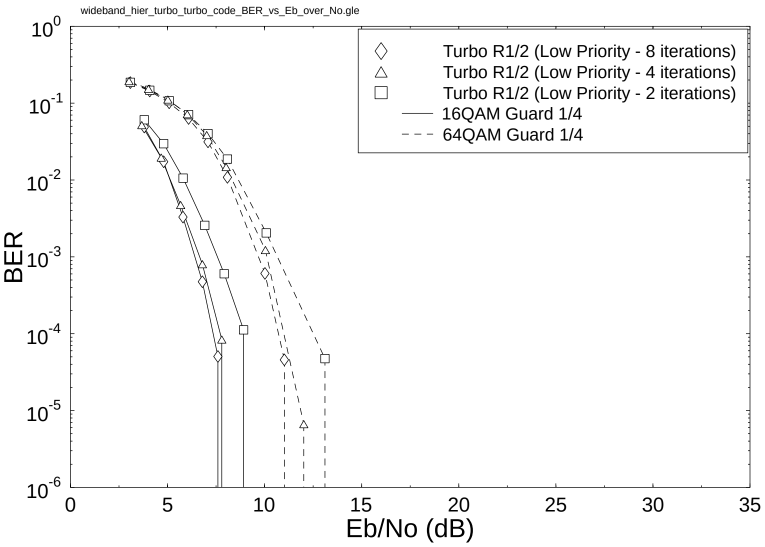

(b) Turbo Code

Figure 24.27: BER after (a) convolutional decoding and (b) turbo decoding for the DVB-T hierarchical scheme over the wideband fading channel of Figure 24.12 using the schematic of Figure 24.14 as well as Algorithms 1 and 2.

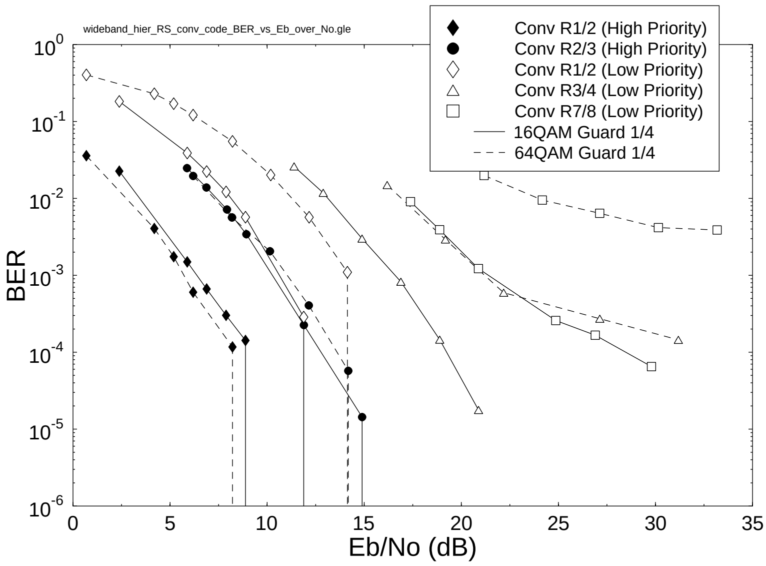

(a) RS and Convolutional Code

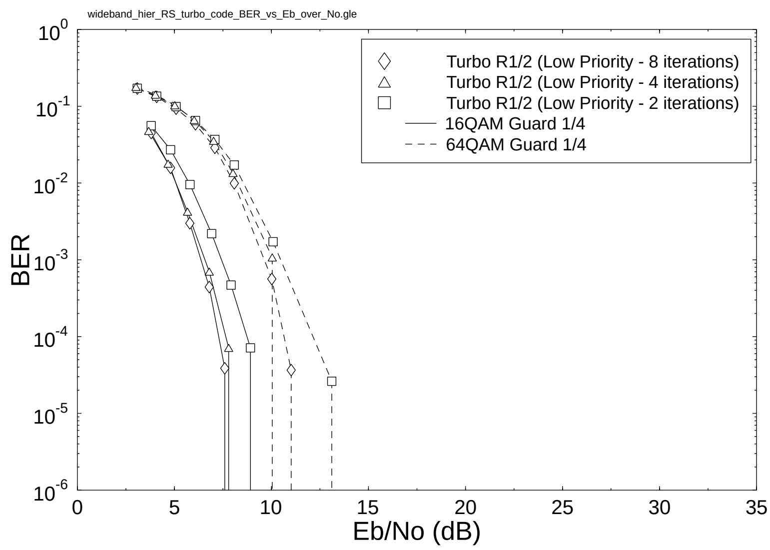

(b) RS and Turbo Code

Figure 24.28: BER after (a) RS and convolutional decoding and (b) RS and turbo decoding for the DVB-T hierarchical scheme over the wideband fading channel of Figure 24.12 using the schematic of Figure 24.14 as well as Algorithms 1 and 2.

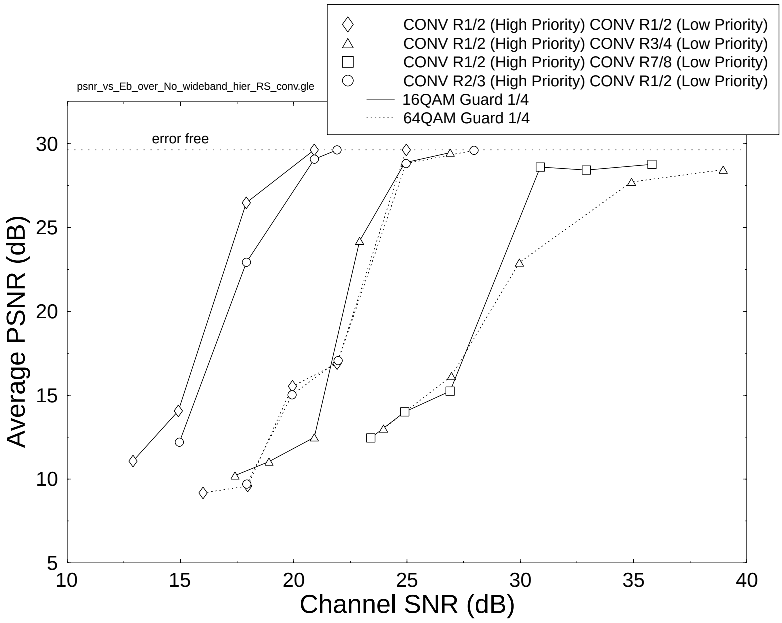

(a) Standard Scheme

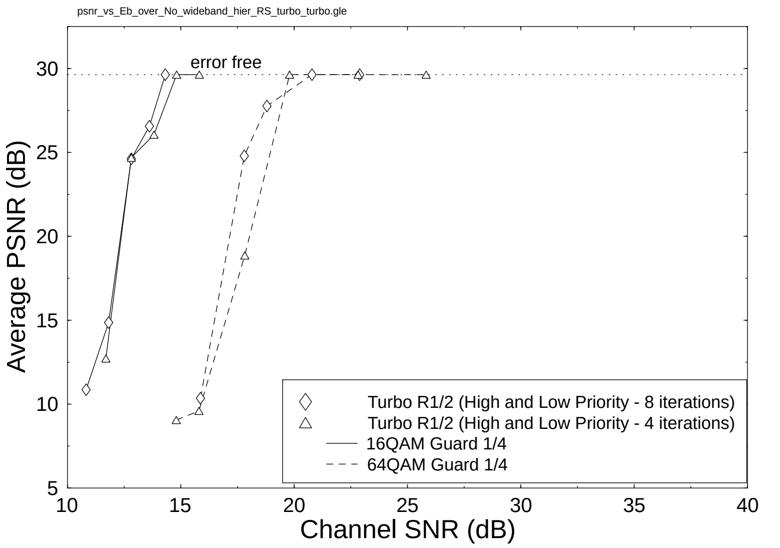

(b) Turbo Code in both partitions

Figure 24.29: Average PSNR versus channel SNR for (a) standard DVB scheme [135] and (b) system with turbo coding employed in both partitions, for transmission over the wideband fading channel of Figure 24.12 for hierarchical transmission using the schematic of Figure 24.14 as well as Algorithms 1 and 2.

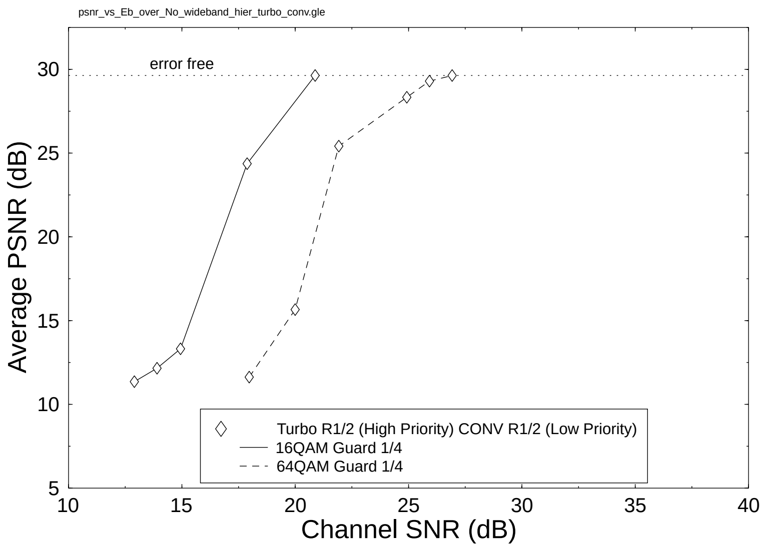

Figure 24.30: Average PSNR versus channel SNR of the DVB scheme, employing turbo coding in the high priority partition and convolutional coding in the low priority partition, over the wideband fading channel of Figure 24.12 for hierarchical transmission using the schematic of Figure 24.14 as well as Algorithms 1 and 2.

becomes evident in Figures 24.27(a) and 24.28(a). Due to the presence of residual errors even after the Reed-Solomon decoder, the decoded video always exhibited some decoding errors, which is shown by the flattening of the PSNR versus channel SNR curves in Figure 24.29(a), before reaching the error free PSNR.

A specific problem faced, when using the data partitioning scheme in conjunction with the high priority partition being protected by the rate 1/2 code and the low priority partition protected by the rate 3/4 and 7/8 codes was that when the low priority partition data was corrupted, the error-free high priority data available was insufficient for concealing the errors. We have also experimented with the combination of rate 2/3 convolutional coding and rate 1/2 convolutional coding, in order to protect the high and low priority data, respectively. From Figure 24.29(a) we observed that the performance of this combination approached that of the rate 1/2 convolutional code in both partitions. This was expected, since now more data can be inserted into the high priority partition. Hence, in the event of decoding errors in the low priority data we had more error-free high priority data that can be used to reconstruct the received image.

Our last combination investigated involved using rate 1/2 turbo coding and convolutional coding for the high- and low-priority partitions, respectively. Comparing

Figures 24.30 and 24.29(a), the channel SNR required for achieving error free transmission in both cases were similar. This was expected, since the turbo-convolutional combination's performance is dependent on the convolutional code's performance in the low priority partition.

Lastly, comparing Figures 24.29 and 24.25, we found that the error-free condition was achieved at similar channel SNRs suggesting that the data partitioning scheme had not provided sufficient performance improvements in the context of the mobile DVB scheme, in order to justify its added complexity.

24.1.9 Conclusions and Future Work

In this section we have investigated the performance of a turbo-coded DVB system in a mobile environment. A range of system performance results was presented based on the standard scheme as well as on a turbo-coded scheme. The convolutional code specified in the standard system was substituted with turbo coding, which resulted in a substantial coding gain of around 5 dB. We have also applied data partitioning to the MPEG-2 video stream in order to gauge its effectiveness in increasing the error resilience of the video codec. However, from these experiments we found that the data partitioning scheme did not provide substantial improvements compared to the non-partitioned video transmitted over the non-hierarchical DVB-T system. Our future work in this field will be focused on improving the system's robustness by invoking a range of so-called maximum-minimum distance Redundant Residue Number System (RRNS) codes and turbo BCH codes. Let us now in the next section consider a variety of satellite-based turbo-coded blind-equalised multi-level modulation assisted video broadcasting schemes.

24.2 Satellite Based Turbo-coded, Blind-equalised 4-QAM and 16-QAM Digital Video Broadcasting [3] [4]

24.2.1 Background and Motivation

In recent years three harmonised Digital Video Broadcasting (DVB) standards have emerged in Europe for terrestrial [135], cable-based [363] and satellite-oriented [364] delivery of video signals. The dispersive wireless propagation environment of the terrestrial system requires concatenated Reed-Solomon [225, 377] (RS) and rate compatible punctured convolutional coding [225, 377] (RCPCC) combined with Orthogonal Frequency Division Multiplexing (OFDM) based modulation. The satellite-based

[3]This section is based on C. S. Lee, S. Vlahoyiannatos and L. Hanzo: Satellite Based Turbo-coded, Blind-equalised 4-QAM and 16-QAM Digital Video Broadcasting, submitted to IEEE Tr. on Broadcasting, 1999

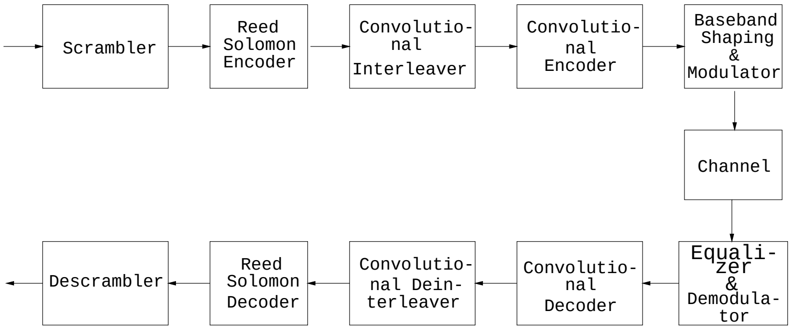

Figure 24.31: Schematic of the DVB satellite transmitter functions.

system employs the same concatenated channel coding arrangement, as the terrestrial schem, while the cable-based system refrains from using concatenated channel coding, opting for RS coding only. Both of the latter schemes employ furthermore blind-equalised multi-level modems. Lastly, the video codec in all three systems is the Motion Pictures Expert Group's MPEG-2 codec. These standardisation activities were followed by a variety of system performance studies in the open literature [378–381]. Against this backcloth, in this treatise we suggested turbo-coding based improvements to the satellite-based DVB system [364] and studied the performance of the proposed system under dispersive channel conditions in conjunction with a variety of blind channel equalisation algorithms. The transmitted power requirements of the standard convolutional codecs can be reduced upon invoking the more complex turbo codec. Alternatively, the standard system's bit error rate (BER) versus signal-to-noise-ratio (SNR) performance can be almost matched by a turbo-coded 16-level quadrature amplitude modulation (16QAM) based scheme, whilst doubling the achievable bit rate within the same bandwidth and hence improving the associated video quality. This is achieved at the cost of an increased system complexity.

The remainder of this section is organised as follows. A terse overview of the turbo-coded and standard DVB satellite scheme is presented in Subsection 24.2.2, while our channel model is described in Section 24.2.3. A brief digest of the blind equaliser algorithms employed is presented in Subsection 24.2.4. Following this, the performance of the improved DVB satellite system was examined over a dispersive two-path channel in Subsection 24.2.5, before our conclusions and future work areas were presented in Subsection 24.2.6.

24.2.2 DVB Satellite Scheme

The block diagram of the DVB satellite (DVB-S) transmitter [364] is shown in Figure 24.31, which is constituted by an MPEG-2 video encoder, channel coding modules and a QPSK modem. Due to the poor error resilience of the MPEG-2 video codec, strong concatenated channel coding is employed, consisting of a shortened Reed-Solomon RS(204,188) outer code [377], which corrects up to eight erroneous bytes in a block of 204 bytes, and a half-rate inner convolutional encoder with a constraint length of 7 [225, 377]. The overall code rate can be adapted by a variable puncturer, not shown in the figure, which supports code rates of 1/2 (no puncturing) as well as 2/3, 3/4, 5/6 and 7/8. The parameters of the convolutional encoder are summarised in Table 24.7.

Rate	1/2
Constraint Length	7
k	1
n	2
Polynomials (octal)	171,133

Table 24.7: Parameters of the CC(n,k,K) convolutional inner encoder in the DVB-S modem.

Rate	1/2
Input block length	17952 bits
Interleaver	random
Number of iterations	8
Constraint Length	3
k	1
n	2
Polynomials (octal)	7,5

Table 24.8: Parameters of the inner turbo encoder used to replace the DVB-S system's convolutional coder.

In addition to implementing the standard DVB-S system as a benchmarker, we have improved the system upon replacing the convolutional codec by a turbo codec [328]. The turbo codec's [382] parameters used in our studies are displayed in Table 24.8.

Readers interested in further details of the DVB-S system are referred to the DVB-S standard [364]. The performance of the standard DVB-S system and that of the turbo coded 16QAM system is characterised in Section 24.2.5. Let us now briefly consider the multipath channel model used in our investigations.

24.2.3 DVB-S Channel Model

The properties of the satellite channel have been characterised for example by Vogel and his colleagues [383–386]. The channel model employed in this study was the two-path (nT)-symbol spaced impulse response, where T is the symbol-duration and in our studies we used $n = 1$ and $n = 2$. This corresponds to a stationary dispersive transmission channel. Our channel model assumed that the receiver had a direct line-of-sight with the satellite as well as a second path caused by a single reflector. In our work, we studied the ability of a range of 4QAM/16QAM blind equaliser algorithms to converge under various path delay conditions. In the next section we provide a

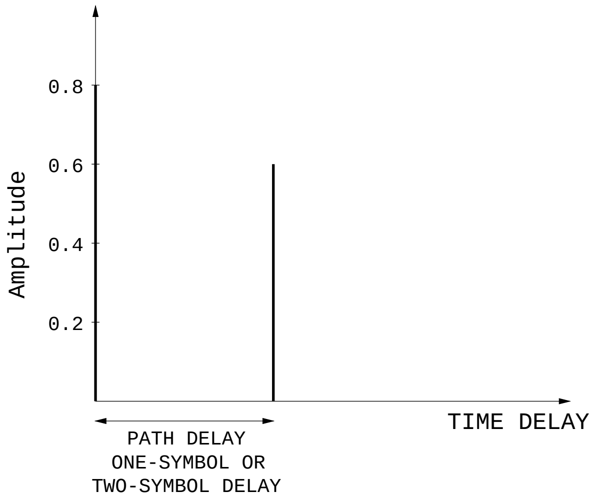

Figure 24.32: Two-path satellite channel model with either a one-symbol or two-symbol delay.

brief overview of the various blind equalisers employed in our experiments, noting that readers mainly interested in the system's performance may proceed directly to our performance analysis section, namely to Section 24.2.5.

In the following section, we will present the performance results of our satellite-based DVB system.

24.2.4 The blind equalisers

In this section the blind equalisers used in the system are presented. The following blind equalisers have been studied:

- The Modified Constant Modulus Algorithm (or Modified CMA) [387]
- The Benveniste-Goursat Algorithm (or B-G) [388]
- The Stop-and-Go algorithm [389]
- The Per-Survivor Processing (PSP) Algorithm [390]

We will now briefly introduce these algorithms.

The **Modified CMA** (MCMA) is an improved version of Godard's well-known constant modulus algorithm [391] which was proposed by Wesolowsky [387]. This algorithm, unlike the CMA, equalises both the real and imaginary parts of the complex signal, according to the equaliser tap update equation of [387]:

$$\begin{aligned}\mathbf{c}^{(n+1)} = \mathbf{c}^{(n)} - \lambda \cdot \mathbf{y}^*(n) \cdot (Re[z(n)] \cdot \big((Re[z(n)])^2 - R_{2,R}\big) + \\ +j \cdot Im\{z(n)\} \cdot \big((Im\{z(n)\})^2 - R_{2,I}\big))\end{aligned}$$

where $\mathbf{c}^{(n)}$ is the equaliser tap vector at the nth iteration, $\mathbf{y}(n)$ is the received signal vector at time n, $z(n)$ is the equalised signal at time n, λ is the step-size parameter and $R_{2,R}$, $R_{2,I}$ are constant parameters of the algorithm, the values of which depend on the QAM signal constellation.

The **Benveniste-Goursat** (B-G) algorithm [388] is an amalgam of Sato's algorithm [392] and the decision-directed algorithm. The decision-directed algorithm is not a blind equalisation technique, since its convergence is highly dependent on the channel. The B-G algorithm combines the above two algorithms into one using the following equaliser coefficient update equations:

$$\mathbf{c}^{(n+1)} = \mathbf{c}^{(n)} - \lambda \cdot \mathbf{y}^*(n) \cdot \epsilon^G(n) \tag{24.2}$$

where

$$\epsilon^G(n) = k_1 \cdot \epsilon(n) + k_2 \cdot |\epsilon(n)| \cdot \epsilon^S(n) \tag{24.3}$$

is the B-G error term, which consists of the combination of the decision-directed error

$$\epsilon(n) = z(n) - \hat{z}(n), \tag{24.4}$$

($\hat{z}(n)$ is the estimated symbol) and the Sato-type error

$$\epsilon^S(n) = z(n) - \gamma \cdot csgn(z(n), \tag{24.5}$$

γ being a constant Sato-algorithm parameter and $csgn(x) = sign(Re\{x\}) + j \cdot sign(Im\{x\})$ is the complex sign function. The two error terms are suitably weighted by the constant parameters k_1 and k_2 in Equation (24.3).

The **Stop-and-Go** (S-a-G) algorithm [389] is a variant of the decision-directed algorithm, where at each equaliser coefficient adjustment iteration the update is enabled or disabled, depending on whether the update is likely to be correct. The update equations of this algorithm are given by:

$$\mathbf{c}^{(n+1)} = \mathbf{c}^{(n)} - \lambda \mathbf{y}^*(n)(f_{n,R} Re\{\epsilon(n)\} + j f_{n,I} Im\{\epsilon(n)\}) \tag{24.6}$$

where $\epsilon(n)$ is the decision-directed error as in Equation (24.4) and the functions $f_{n,R}$, $f_{n,I}$ enable or disable the update of the equaliser according to the following rule: if the sign of the Sato-error (the real or the imaginary part independently) is the same as the sign of the decision-directed error, then the update takes place, otherwise it does not. In a blind equaliser, this condition provides us with a measure of the probability of the coefficient update being correct.

The **PSP algorithm** [390] is a sequence estimation technique, in which the channel is not known “a priori”. Hence, an iterative channel estimation technique is employed in order to estimate the channel jointly with the symbol estimation. In this sense, an initial channel estimation is used and the estimation is updated at each new symbol's arrival. Each of the surviving paths in the trellis carries not only its own signal estimation, but also its own channel estimation. Moreover, convolutional decoding can take place jointly with this procedure, leading to an improved Bit Error Rate (BER) performance.

The summary of the equalisers' parameters is given in Table 24.9.

	Step-size λ	No. of Equal. Taps	Initial Tap–Vector
Benveniste-Goursat	$5 \cdot 10^{-4}$	10	$(1.2, 0, \cdots, 0)$
Modified-CMA	$5 \cdot 10^{-4}$	10	$(1.2, 0, \cdots, 0)$
Stop-and-Go	$5 \cdot 10^{-4}$	10	$(1.2, 0, \cdots, 0)$
PSP (1 sym delay)	10^{-2}	2	$(1.2, 0)$
PSP (2 sym delay)	10^{-2}	3	$(1.2, 0, 0)$

Table 24.9: Summary of the equaliser parameters used in the simulations. The tap–vector $(1.2, 0, \cdots, 0)$ indicates that the first equaliser coefficient is initialised to the value of 1.2, while the others to 0.

Following the above brief overview of the blind equaliser algorithms studied, let us now consider the overall system performance.

24.2.5 Performance of the DVB Satellite Scheme

In this section, the performance of the DVB-S system was evaluated by means of simulations. Two modulation types were used, i.e. QPSK and 16-QAM, and the channel model of Figure 24.32 was employed. The first channel model had a one-symbol second-path delay, while in the second one the path-delay corresponded to the period of two symbols. The average BER versus SNR per bit performance is presented after the equalisation and demodulation process, as well as after Viterbi [377] or turbo decoding [382]. The SNR per bit is defined as follows:

$$\text{SNR per bit} = 10log_{10}\frac{\bar{S}}{\bar{N}} + \delta, \tag{24.7}$$

where $\bar{S}$ is the average received signal amplitude, $\bar{N}$ is the average received noise amplitude and δ is the adjustment required to transform average signal-to-noise ratio into bit energy or SNR per bit. The adjustment is dependent on the type of modulation and channel code rate used in the system. In Figure 24.33, the linear equalisers' performance was quantified and compared for QPSK modulation over the one-symbol delay two-path channel model of Figure 24.32. Since all the equalisers' BER performance is similar, only the Modified CMA results are shown in the figure.

The equalised performance was inferior to that over the non-dispersive AWGN channel. However, as expected, it was better than without any equalisation. Another observation for Figure 24.33 was that the different punctured channel coding rates appeared to give slightly different bit error rates after equalisation. This is because the linear blind equalisers require uncorrelated input bits in order to converge. However, the input bits were not entirely random, when convolutional coding was used. The consequences of violating the zero-correlation constraint are not generally known. Nevertheless, two potential problems are apparent. Firstly, the equaliser may diverge from the desired equaliser equilibrium [393].

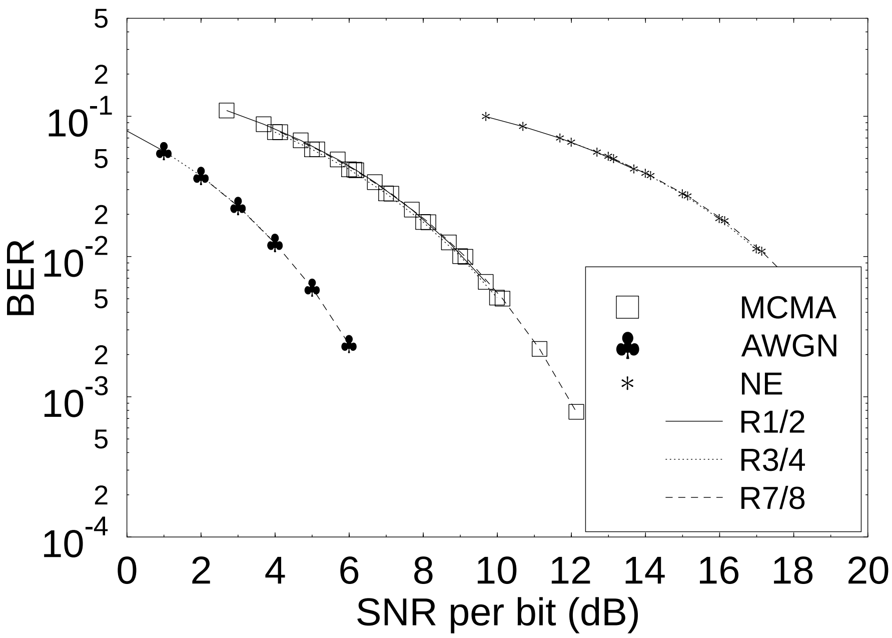

Figure 24.33: Average BER versus SNR per bit performance after equalisation and demodulation but before channel decoding employing QPSK modulation and one-symbol delay channel (NE:Non-Equalised).

Secondly, the performance of the equaliser is expected to degrade, owing to the violation of the randomness requirement, which is imposed on the input bits in order to ensure that the blind equalisers will converge.

Since the channel used in our investigations was static, the first problem was not encountered. Instead, the second problem was what we actually observed. Figure 24.34 quantifies the equalisers' performance degradation due to the correlation introduced by convolutional coding. We can observe a 0.1 dB SNR degradation, when the convolutional codec creates correlation among the bits for this specific case.

The average BER curves after equalisation and demodulation are shown in Figure 24.35(a). In this figure, the average BER over the non-dispersive AWGN channel after turbo decoding constitutes the best performance, while the average BER of the one-symbol delay two-path unequalised channel after turbo decoding exhibits the worst performance. Again, in this figure only the Modified-CMA was featured for simplicity. The performance of the remaining equalisers was characterised in Figure 24.35(b). Clearly, the performance of the linear equalisers is similar.

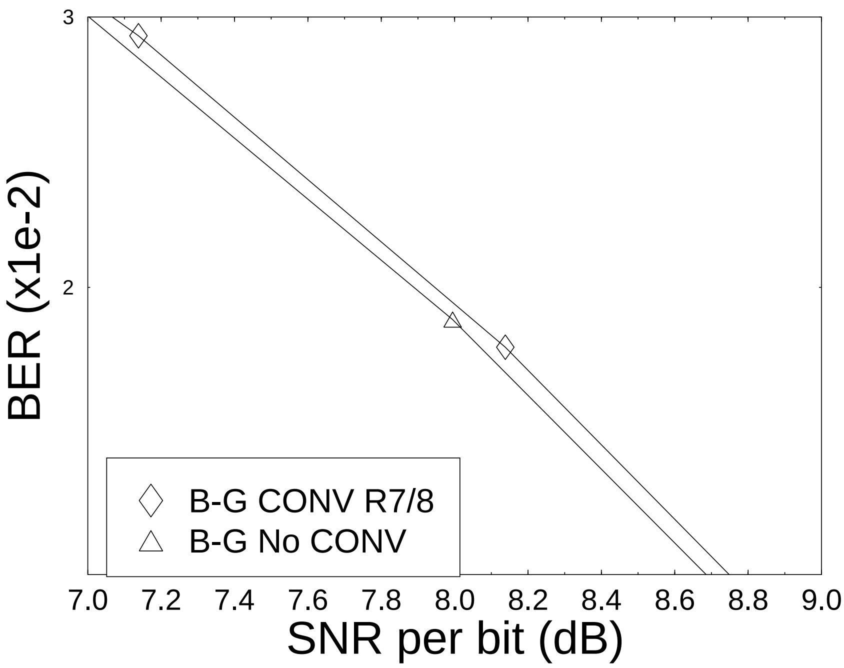

Figure 24.34: Average BER versus SNR per bit performance after equalisation and demodulation but before channel decoding employing QPSK modulation and the one-symbol delay two-path channel of Figure 24.32, for the Benveniste-Goursat algorithm, where the input bits are random (No CONV) or correlated (CONV 7/8) as a result of convolutional coding having a coding rate of 7/8.

It is observed in Figure 24.35(a) that the combination of the MCMA-based blind equaliser with turbo decoding exhibited the best SNR performance. The only comparable alternative was the PSP algorithm. Although the performance of the PSP algorithm is better at low SNRs, the associated curves cross over and the PSP algorithm's performance becomes inferior after the average BER becomes approximately 10^{-3}. Although not shown in Figure 24.35, the Reed-Solomon decoder, which was concatenated to either the convolutional or the turbo decoder, gave an error-free output after the average BER of its input reached approximately 10^{-4}. In this case, the PSP algorithm's performed worse by at least 1 dB in the area of interest, which is at an average BER of 10^{-4}.

A final observation in the context of Figure 24.35(a) is that when convolutional decoding was used, the associated E_b/N_0 performance of rate 1/2 convolutional coding appears inferior to that of the rate 3/4 and the rate 7/8 scenarios beyond certain E_b/N_0 values.

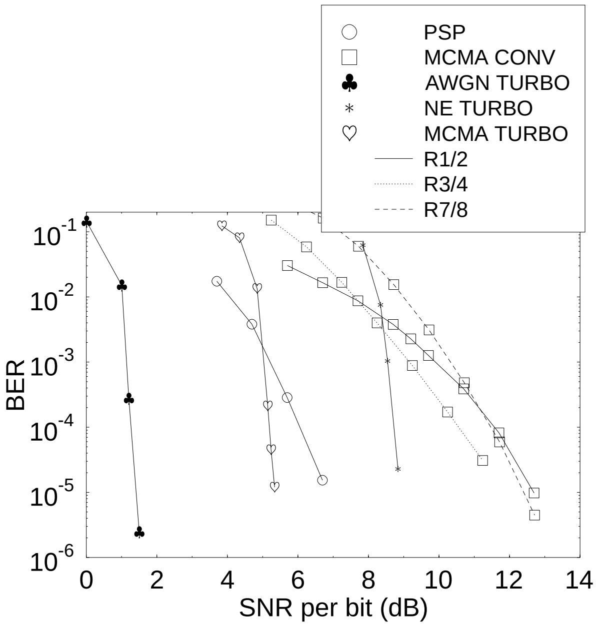

(a) PSP and linear equalisers

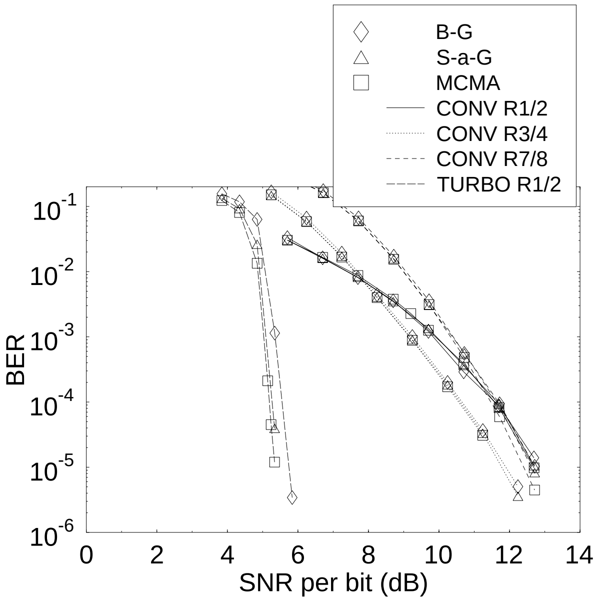

(b) Linear equalisers only

Figure 24.35: Average BER versus SNR per bit performance after convolutional or turbo decoding but before RS(204,188) decoding for QPSK modulation over the one-symbol delay channel (NE:Non-Equalised B-G:Benveniste-Goursat S-a-G:Stop-and-Go MCMA:Modified Constant Modulus Algorithm PSP:Per-Survivor-Processing).

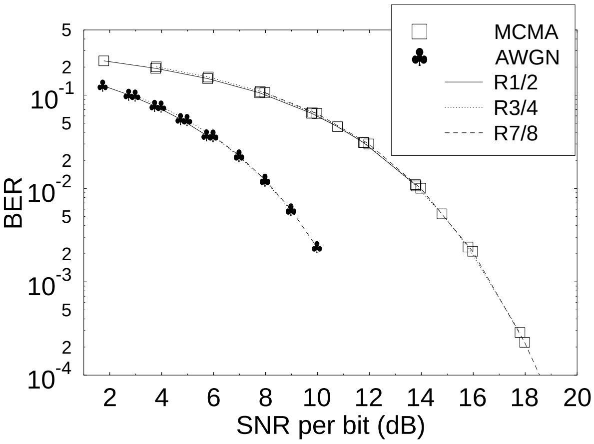

(a) After equalisation and demodulation

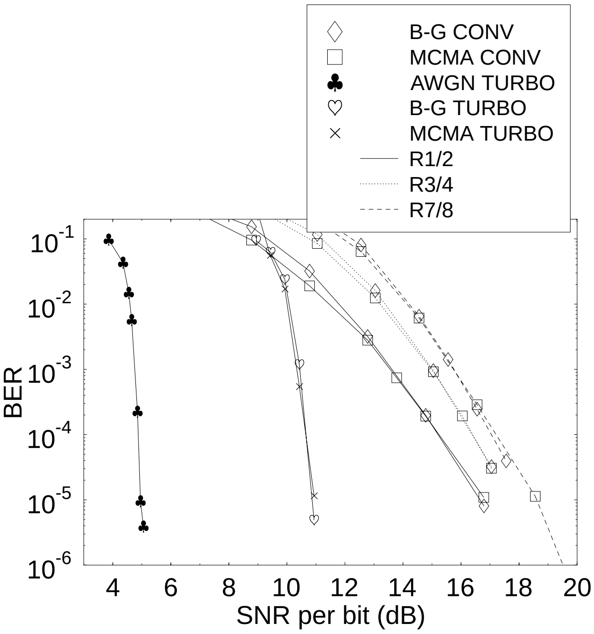

(b) After viterbi or turbo decoding

Figure 24.36: Average BER versus SNR per bit (a) after equalisation and demodulation but before channel decoding and (b) after Viterbi or turbo decoding but before RS(204,188) decoding for 16-QAM modulation over the one-symbol delay two-path channel of Figure 24.32.

In Figure 24.36, the corresponding BER curves are given for 16-QAM, under the same channel and equaliser conditions. Again, for simplicity, only the Modified CMA results are given. In this case the ranking order of the different coding rates follows our expectations more closely in the sense that the lowest coding rate of 1/2 is the best performer, followed by the rate 3/4 codec, in turn followed by the weakest rate 7/8 codec.

The Stop-and-Go algorithm has not been included in these results. The reason is that this algorithm does not converge for high SNR values. This happens because this procedure is only activated when there is a high probability of correct update. In our case, the equaliser is initialised far from its convergence point and hence the decision–directed updates are unlikely to provide correct updates. In the absence of noise this leads to the algorithm being permanently de-activated. If noise is present though, then some random perturbations from the point of the equaliser's initialization can activate the algorithm and can lead to convergence. This is what we observe at medium SNR values. For high SNR values though, the algorithm does not converge.

It is also interesting to compare the performance of the system for the QPSK and 16-QAM schemes. When the one-symbol delay two-path channel model of Figure 24.32 was considered, the system was capable of supporting the use of 16-QAM with the provision of an additional SNR per bit of 5 dB. Although the original DVB-Satellite system only employs QPSK modulation, our simulations had shown that 16-QAM can be employed equally well for the range of blind equalisers that we have used in our work. This allows us to double the video bitrate and hence to substantially improve the video quality. The comparison of Figures 24.35 and 24.36 also reveals that the extra SNR requirement of 5 dB of 16QAM over 4QAM can be eliminated by employing turbo coding at the cost of a higher implementational complexity. This allowed us to accommodate a doubled bitrate within a given bandwidth, which improved the video quality.

In Figures 24.37 (only for Benveniste-Goursat for simplicity) and 24.38 the corresponding BER results for the two-symbol delay two-path channel of Figure 24.32 are given for QPSK. They are similar to Figures 24.33 and 24.35 in terms of their trends, although we observed some differences:

- The "cross-over point", beyond which the performance of the PSP algorithm becomes worse than that of the Modified CMA in conjunction with turbo decoding is now at 10^{-4}, which is in the area where the RS decoder provides an error-free output.
- The rate 1/2 convolutional decoding is now the best performer, while the rate 3/4 scheme exhibited the worst performance.

Finally, in Figure 24.39, the associated 16-QAM results are presented. Notice that the Stop-and-Go algorithm was again excluded from the results. We can observe a high performance difference between the B-G and the Modified CMA.

In the previous cases we did not observe such a significant difference. The difference in this case is that the channel exhibits an increased delay spread. In fact, what we observe here is the capability of the equalisers to cope with more wide–spread multipaths, while keeping their length constant. The Benveniste-Goursat equaliser is more efficient, than the Modified CMA in this case.

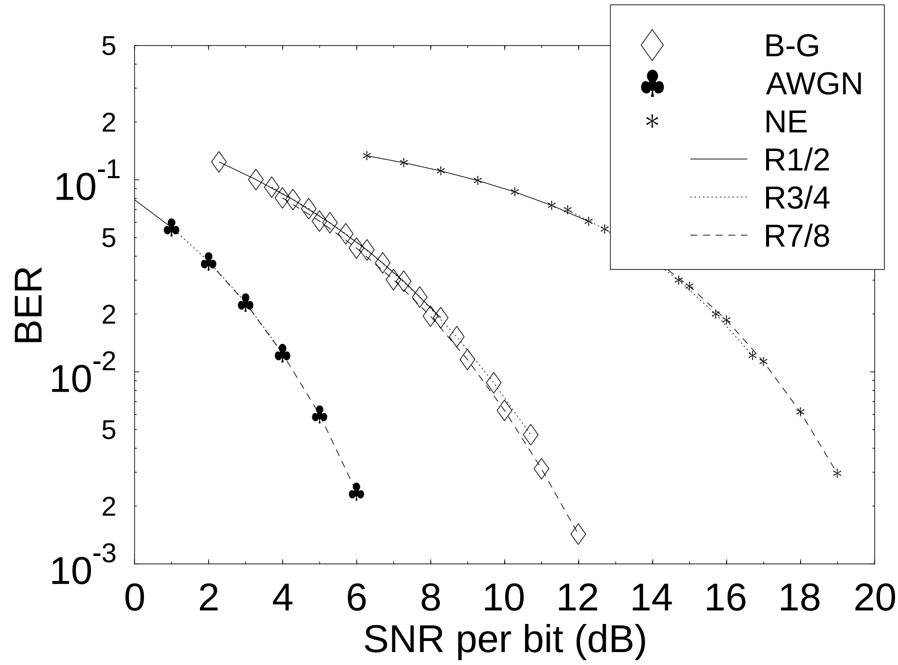

Figure 24.37: Average BER versus SNR per bit performance after equalisation and demodulation but before channel decoding for QPSK modulation over the two-symbol delay two-path channel of Figure 24.32.

It is interesting to note that in this case, the performance of the different coding rates is again in the expected order, the rate 1/2 being the best, followed by the rate 3/4 and then the rate 7/8 scheme.

If we compare the performance of the system employing QPSK and 16-QAM under the two-symbol delay two-path channel model of Figure 24.32, we again observe that 16-QAM can be incorporated into the DVB system if an extra 5 dB of SNR per bit is affordable in power budget terms. However, only the B-G algorithm is worthwhile considering here out of the three linear equalisers used in our work.

Figure 24.40 portrays the corresponding reconstructed video performance in terms of the average peak signal-to-noise ratio (PSNR) versus channel SNR for the one-symbol delay and two-symbol delay two-path channel model of Figure 24.32. The average PSNR is defined as follows:

$$\text{PSNR} = 10log_{10}\frac{\sum_{n=0}^{N}\sum_{m=0}^{M}255^2}{\sum_{n=0}^{N}\sum_{m=0}^{M}\Delta^2} \tag{24.8}$$

where Δ is the difference between the uncoded pixel value and the reconstructed pixel value.

Tables 24.10 and 24.11 provide a summary of the DVB-Satellite system's perfor-

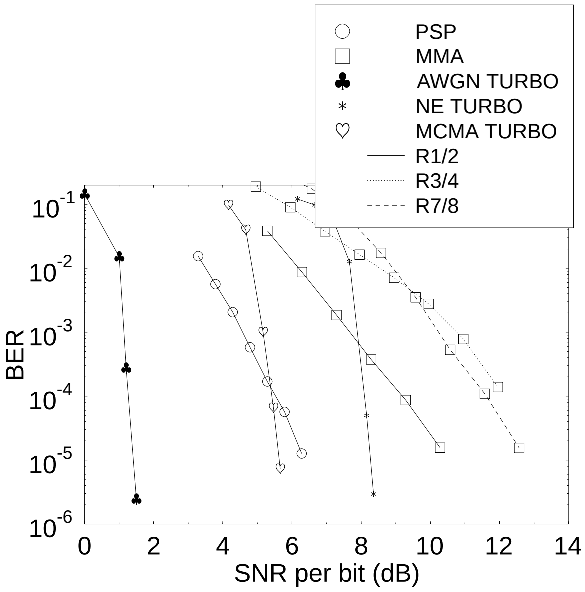

(a) PSP and linear equalisers

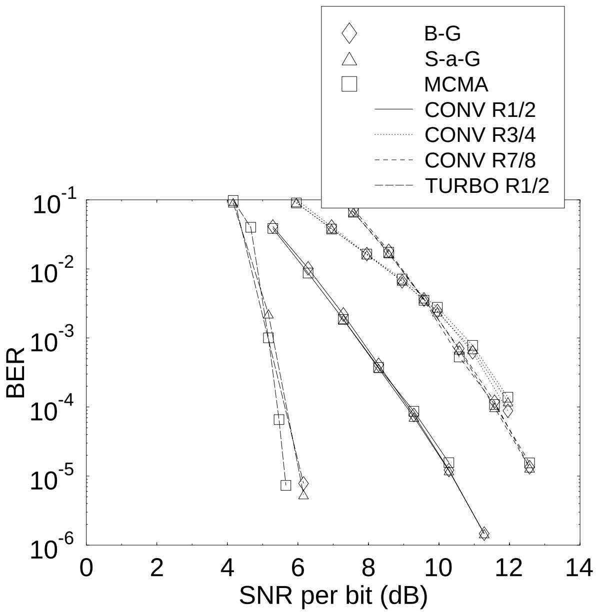

(b) Linear equalisers only

Figure 24.38: Average BER versus SNR per bit performance after convolutional or turbo decoding but before RS(204,188) decoding for QPSK modulation over the two-symbol delay two-path channel of Figure 24.32.

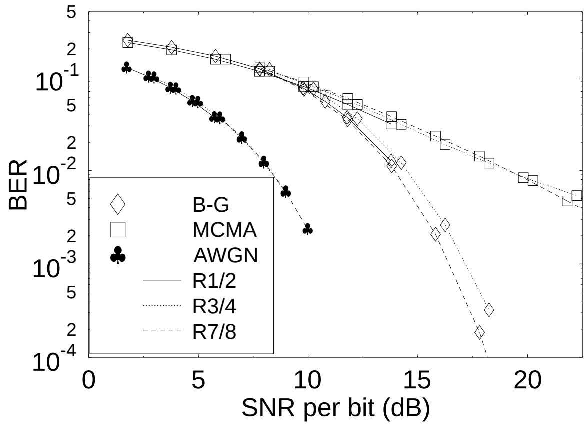

(a) After equalisation and demodulation

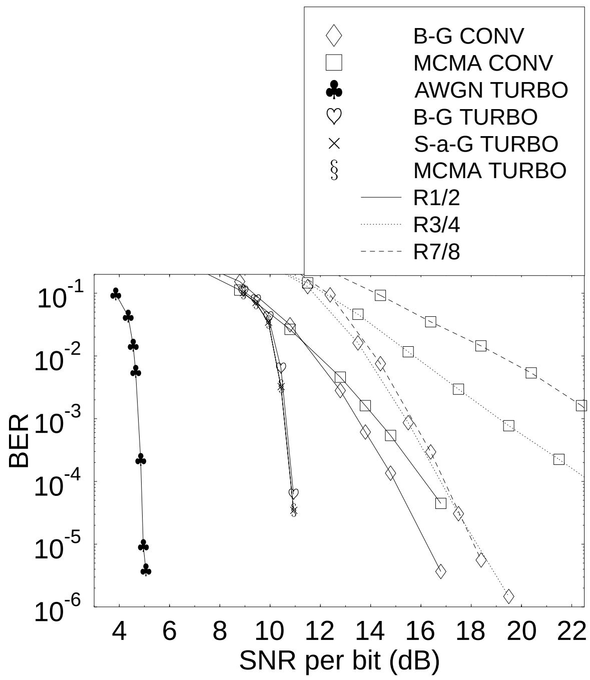

(b) After viterbi or turbo decoding

Figure 24.39: Average BER versus SNR per bit performance (a) after equalisation and demodulation but before channel decoding and (b) after Viterbi or turbo decoding but before RS(204,188) decoding for 16-QAM over the two-symbol delay two-path channel of Figure 24.32.

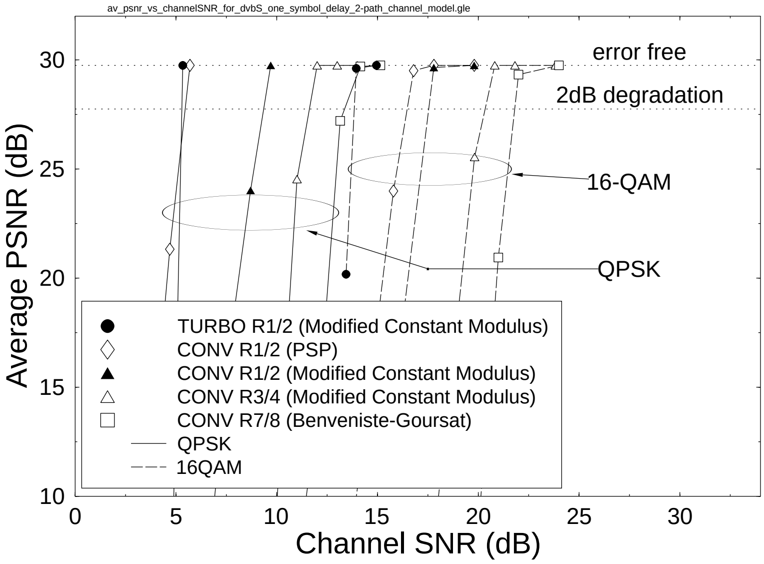

(a) One-symbol delay two-path channel model

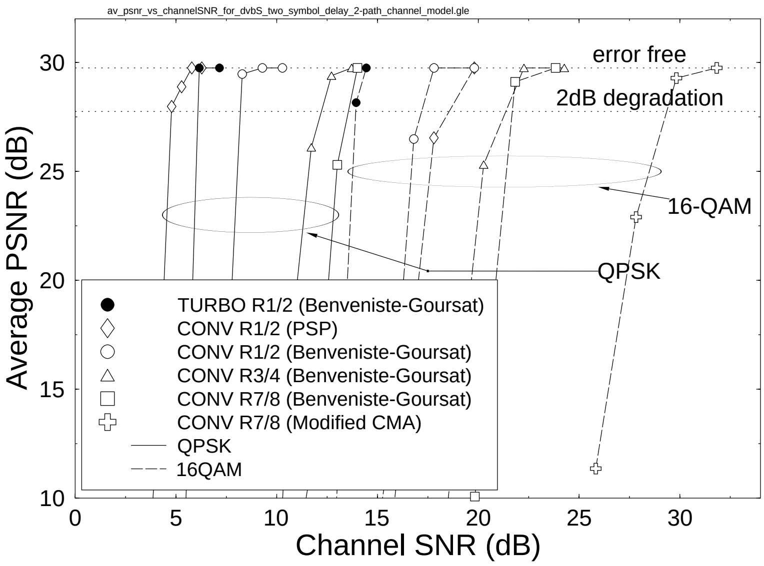

(b) Two-symbol delay two-path channel model

Figure 24.40: Average PSNR versus channel SNR for (a) one-symbol delay two-path channel model after concatenated channel decoding and (b) two-symbol delay two-path channel model of Figure 24.32 after concatenated channel decoding.

mance tolerating a PSNR degradation of 2 dB, which was deemed to be imperceptible in terms of subjective video degradations. The average BER values quoted in the tables refer to the average BER achieved after Viterbi or turbo decoding. The channel SNR (CSNR) is quoted in association with the 2 dB average PSNR degradation since the viewer will begin to perceive video degradations due to erroneous decoding of the received video at this threshold, as noted in [394].

Mod.	Equaliser	Code	CSNR (dB)	E_b/N_0
QPSK	PSP(R=1/2)		5.3	5.3
QPSK	MCMA	Turbo (1/2)	5.2	5.2
16QAM	MCMA	Turbo (1/2)	13.6	10.6
QPSK	MCMA	Conv (1/2)	9.1	9.1
16QAM	MCMA	Conv (1/2)	17.2	14.2
QPSK	MCMA	Conv (3/4)	11.5	9.7
16QAM	MCMA	Conv (3/4)	20.2	15.4
QPSK	B-G	Conv (7/8)	13.2	10.8
16QAM	B-G	Conv (7/8)	21.6	16.2

Table 24.10: Summary of performance results over the dispersive one-symbol delay two-path AWGN channel of Figure 24.32 tolerating a PSNR degradation of 2 dB. The average BER was evaluated after Viterbi or turbo decoding and concatenated RS(204,188) decoding.

Mod.	Equaliser	Code	CSNR (dB)	E_b/N_0
QPSK	PSP(R=1/2)		4.7	4.7
QPSK	B-G	Turbo (1/2)	5.9	5.9
16QAM	B-G	Turbo (1/2)	13.7	10.7
QPSK	B-G	Conv (1/2)	8.0	8.0
16QAM	B-G	Conv (1/2)	17.0	14.0
QPSK	B-G	Conv (3/4)	12.1	10.3
16QAM	B-G	Conv (3/4)	21.1	16.3
QPSK	B-G	Conv (7/8)	13.4	11.0
16QAM	MCMA	Conv (7/8)	29.2	23.8

Table 24.11: Summary of performance results over the dispersive two-symbol delay two-path AWGN channel of Figure 24.32 tolerating a PSNR degradation of 2 dB. The average BER was evaluated after Viterbi or turbo decoding and concatenated RS(204,188) decoding.

Table 24.14 provides an approximation of the convergence speed of each blind equalisation algorithm for each case. It is clear that PSP converges significantly faster than any of the other techniques. On the other hand, the Benveniste-Goursat

Mod.	Equaliser	Code	E_b/N_0
QPSK	PSP(R=1/2)		6.1
QPSK	MCMA	Turbo (1/2)	5.2
16QAM	MCMA	Turbo (1/2)	10.7
QPSK	MCMA	Conv (1/2)	11.6
16QAM	MCMA	Conv (1/2)	15.3
QPSK	MCMA	Conv (3/4)	10.5
16QAM	MCMA	Conv (3/4)	16.4
QPSK	B-G	Conv (7/8)	11.8
16QAM	B-G	Conv (7/8)	17.2

Table 24.12: Summary of system performance results over the dispersive one-symbol delay two-path AWGN channel of Figure 24.32 tolerating an average BER of 10^{-4}. The average BER was evaluated after Viterbi or turbo decoding but before RS(204,188) decoding.

Mod.	Equaliser	Code	E_b/N_0
QPSK	PSP(R=1/2)		5.6
QPSK	B-G	Turbo (1/2)	5.7
16QAM	B-G	Turbo (1/2)	10.7
QPSK	B-G	Conv (1/2)	9.2
16QAM	B-G	Conv (1/2)	15.0
QPSK	B-G	Conv (3/4)	12.0
16QAM	B-G	Conv (3/4)	16.8
QPSK	B-G	Conv (7/8)	11.7
16QAM	MCMA	Conv (7/8)	26.0

Table 24.13: Summary of system performance results over the dispersive two-symbol delay two-path AWGN channel of Figure 24.32 tolerating an average BER of 10^{-4}. The average BER was evaluated after Viterbi or turbo decoding but before RS(204,188) decoding.

	B-G	MCMA	S-a-G	PSP
QPSK 1-sym	$2 \cdot 10^5$	$4.4 \cdot 10^5$	$2.6 \cdot 10^5$	380
QPSK 2-sym	$2 \cdot 10^5$	$3.9 \cdot 10^5$	$2.1 \cdot 10^5$	380
16-QAM 1-sym	$5.6 \cdot 10^5$	$8.8 \cdot 10^5$	$19 \cdot 10^5$	
16-QAM 2-sym	$4.9 \cdot 10^5$	$5.6 \cdot 10^5$	$18 \cdot 10^5$	

Table 24.14: Equaliser convergence speed measured in the simulations, given as the number of bits required for convergence (x-sym: x-symbol delay two-path channel).

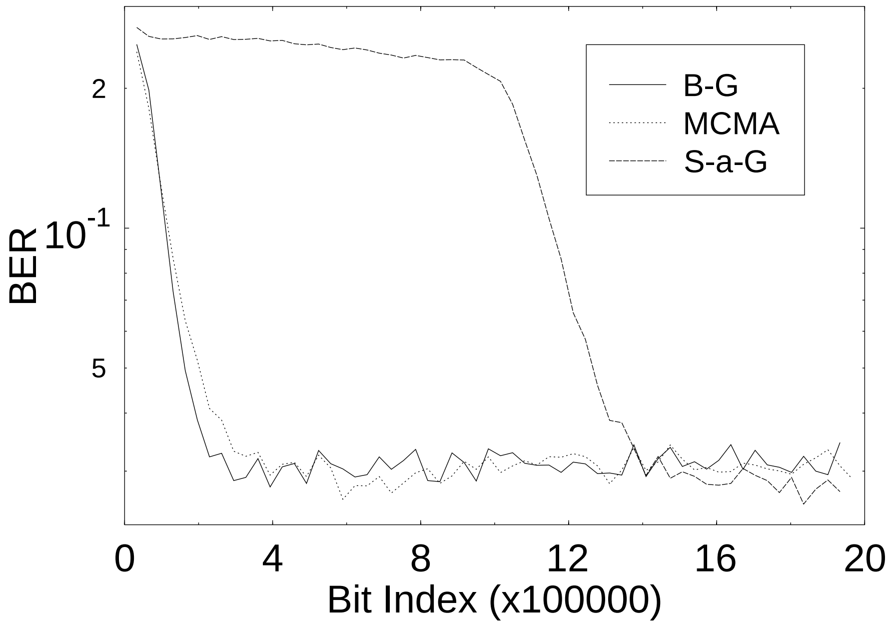

Figure 24.41: Learning curves for 16-QAM, one-symbol delay two-path channel at SNR=18dB.

algorithm is the fastest of the other techniques. In our simulations the convergence was quantified by measuring the slope of the BER curve, as this curve was reaching the associated residual BER. Convergence was established, when this slope gradient became smaller than a threshold value, implying that the BER has reached its steady–state. Figure 24.41 gives an illustrative example of the equaliser convergence for the case of 16-QAM. It is observed that the Stop-and-Go algorithm converges significantly slower than the other algorithms, which can also be seen from Table 24.14. This happens because, during the startup, the algorithm is de-activated most of the time, an effect which becomes more severe with an increasing QAM order.

Tables 24.12 and 24.13 provide a summary of the SNR per bit required for the various system configurations. The threshold of 10^{-4} is selected here, since at this average BER after Viterbi or turbo decoding the RS decoder becomes effective. This means that the output bits have a high probability of being error free. This also translates into error-free video decoding.

24.2.6 Conclusions and Future Work

In this section, we have investigated the performance of a turbo-coded DVB system in a satellite broadcast environment. A range of system performance results was presented based on the standard DVB-S scheme, as well as on a turbo-coded scheme in conjunction with blind equalised 4QAM/16QAM. The convolutional code specified in the standard system was substituted by turbo coding, which resulted in a substantial coding gain of around 4-5 dB. We have also shown that 16-QAM can be utilised instead of QPSK, if an extra 5 dB SNR per bit gain is added to the link budget. This extra transmitted power requirement can be eliminated upon invoking the more complex turbo codec, which requires lower transmitted power for attaining the same performance as the standard convolutional codecs. Our future work will be focused on extending the DVB-Satellite system to supporting mobile users for the reception of satellite broadcast video signals. The use of turbo equalisers will also be investigated in comparison to blind equalisers. Further work will also be dedicated to trellis coded modulation (TCM) and turbo trellis coded modulation (TTCM) based OFDM and single-carrier equalised modems.

Bibliography

[1] S. Stapleton and F. Costescu, "An adaptive predistorter for a power amplifier based on adjacent channel emissions," *IEEE Tr. on VT*, vol. 41, pp. 49–57, February 1992.

[2] S. L.D.Quach, "A post-distortion receiver for mobile communications," *IEEE Tr. on VT*, vol. 42, pp. 604–616, November 1993.

[3] S. Haykin, *Adaptive Filter Theory.* Prentice Hall, 1991.

[4] J. McGeehan and A. Bateman, "Phase-locked transparent tone in band (TTIB): A new spectrum configuration particularly suited to the transmission of data over SSB mobile radio networks," *IEEE Transactions on Communications*, vol. COM-32, no. 1, pp. 81–87, 1984.

[5] J. Cavers, "The performance of phase locked transparent tone in band with symmetric phase detection," *IEEE Trans. on Comms.*, vol. 39, pp. 1389–1399, September 1991.

[6] P.M.Martin and A.Bateman, "Practical results for a modem using linear mobile radio channels," in *Proceedings of IEEE Vehicular Technology Conference (VTC'91)*, (St. Louis, MO, USA), pp. 386–392, IEEE, 19–22 May 1991.

[7] J. Cavers, "An analysis of pilot symbol assisted modulation for rayleigh fading channels," *IEEE Transactions on Vehicular Technology*, vol. 40, pp. 686–693, Nov 1991.

[8] C.R.Cahn, "Performance of digital phase modulation communication systems," *IRE Trans Comms*, vol. CS-7, pp. 3–6, May 1959.

[9] C.R.Cahn, "Combined digital phase and amplitude modulation communication system," *IRE Trans Comms*, vol. CS-8, pp. 150–155, Sept 1960.

[10] J.C.Hancock and R.W.Lucky, "Performance of combined amplitude and phase modulated communications system," *IRE Trans Comms*, vol. CS-8, pp. 232–237, December 1960.

[11] C. Campopiano and B. Glazer, "A coherent digital amplitude and phase modulation scheme," *IRE Trans. Commun. Systems*, vol. CS-10, pp. 90– 95, 1962.

[12] R.W.Lucky and J.C.Hancock, "On the optimum performance of n-ary systems having two degrees of freedom," *IRE Trans Comms*, vol. CS-10, pp. 185–192, June 1962.

[13] R. Lucky, J. Salz, and E. Weldon, *Principles of Data Communication*. New York: McGraw-Hill, 1968.

[14] J.Salz, J.R.Sheenhan, and D.J.Paris, "Data transmission by combined AM and PM," *Bell Systems Technical Journal*, vol. 50, pp. 2399–2419, September 1971.

[15] E.Y.Ho and Y.S.Yeh, "Error probability of a multilevel digital system with intersymbol interference and gaussian noise," *Bell Systems Technical Journal*, vol. 50, pp. 1017–1023, March 1971.

[16] G.J.Foschini, R.D.Gitlin, and S.B.Weinstein, "Optimization of two-dimensional signal constellations in the presence of gaussian noise," *IEEE Trans Comms*, vol. COM-22, pp. 28–38, January 1974.

[17] C.M.Thomas, M.Y.Weidner, and S.H.Durrani, "Digital amplitude-phase keying with m-ary alphabets," *IEEE Trans Comms*, vol. COM-22, pp. 168–180, February 1974.

[18] M.K.Simon and J.G.Smith, "Carrier synchronization and detection of QASK signal sets," *IEEE Trans Comms*, vol. COM-22, pp. 98–106, February 1974.

[19] M.K.Simon and J.G.Smith, "Offset quadrature communications with decision feedback carrier synchronization," *IEEE Trans Comms*, vol. COM-22, pp. 1576–1584, October 1974.

[20] J.G.Smith, "Odd-bit quadrature amplitude-shift keying," *IEEE Trans Comms*, vol. COM-23, pp. 385–389, March 1975.

[21] K.Miyauchi, S.Seki, and H.Ishio, "New techniques for generating and detecting multilevel signal formats," *IEEE Trans Comms*, vol. COM-24, pp. 263–267, February 1976.

[22] W.J.Weber, "Differential encoding for multiple amplitude and phase shift keying systems," *IEEE Trans Comms*, vol. COM-26, pp. 385–391, March 1978.

[23] P.Dupuis, M.Joindot, A.Leclert, and D.Soufflet, "16 QAM modulation for high capacity digital radio system," *IEEE Trans Comms*, vol. COM-27, pp. 1771–1781, December 1979.

[24] I.Horikawa, T.Murase, and Y.Saito, "Design and performance of a 200mbit/s 16 QAM digital radio system," *IEEE Trans Comms*, vol. COM-27, pp. 1953–1958, December 1979.

[25] V.K.Prabhu, "The detection efficiency of 16-ary QAM," *Bell Systems Technical Journal*, vol. 59, pp. 639–656, April 1980.

[26] D.H.Morais and K.Feher, "NLA-QAM: A method for generating high power QAM signals through non-linear amplification," *IEEE Trans Comms*, vol. COM-30, pp. 517–522, March 1982.

[27] T.Hill and K.Feher, "A performance study of NLA 64-state QAM," *IEEE Trans Comms*, vol. COM-31, pp. 821–826, June 1983.

[28] K. Feher, "Digital communications - satellite/earth station engineering," in *Digital communications - satellite/earth station engineering* [176], pp. 118–120.

[29] K.-T. Wu and K.Feher, "256-QAM modem performance in distorted channels," *IEEE Trans Comms*, vol. COM-33, pp. 487–491, May 1985.

[30] P.Mathiopoulos and K.Feher, "Performance evaluation of a 512-QAM system in distorted channels," *Proc Pt F*, vol. 133, pp. 199–204, April 1986.

[31] M.Borgne, "Comparison of high level modulation schemes for high capacity digital radio systems," *IEEE Trans Comms*, vol. COM-33, pp. 442–449, May 1985.

[32] M.Shafi and D.J.Moore, "Further results on adaptive equalizer improvements for 16 QAM and 64 QAM digital radio," *IEEE Trans Comms*, vol. COM-34, pp. pp59–66, January 1986.

[33] Y.Saito and Y.Nakamura, "256 QAM modem for high capacity digital radio system," *IEEE Trans Comms*, vol. COM-34, pp. 799–805, August 1986.

[34] A.J.Rustako, L.J.Greenstein, R.S.Roman, and A.A.Saleh, "Using times four carrier recovery in M-QAM digital radio receivers," *IEEE J-SAC*, pp. 524–533, April 1987.

[35] C-E.W.Sundberg, W.C.Wong, and R.Steele, "Logarithmic PCM weighted QAM transmission over gaussian and rayleigh fading channels," *IEE Proc Pt. F*, vol. 134, pp. 557–570, October 1987.

[36] R. Steele, C.-E. Sundberg, and W. Wong, "Transmission of log-PCM via QAM over Gaussian and Rayleigh fading channels," *IEE Proc.*, vol. 134, Pt. F, pp. 539–556, October 1987.

[37] L. Hanzo, R. Steele, and P. Fortune, "A subband coding, BCH coding and 16-QAM system for mobile radio speech communication," *IEEE Trans. on Vehicular Technology*, vol. 39, pp. 327–340, November 1990.

[38] H.Sari and S.Moridi, "New phase and frequency detectors for carrier recovery in PSK and QAM systems," *IEEE Trans Comms*, vol. COM-36, pp. 1035–1043, September 1988.

[39] J. C. I. Chuang, "The effects of time-delay spread on QAM with non-linearly switched filters in a portable radio communications channel," *IEEE Trans Comms*, vol. 38, pp. 9–13, February 1989.

[40] J.M.Matthews, "Cochannel performance of 16-level QAM with phase locked TTIB/FFSR processing," *IEE colloquium on multi-level modulation*, March 1990.

[41] P.W.Huish and G.D.Richman, "Increasing the capacity and quality of digital microwave radio," *IEE colloquium on multi-level modulation*, March 1990.

[42] W.T.Webb and R.Steele, "16-level circular QAM transmissions over a rayleigh fading channel," *IEE colloquium on multi-level modulation*, March 1990.

[43] E.Issman and W.T.Webb, "Carrier recovery for 16-level QAM in mobile radio," *IEE colloquium on multi-level modulation*, March 1990.

[44] W. Peterson and E. Weldon, Jr, *Error correcting codes.* MIT. Press, 2nd ed., August 1972. ISBN: 0262160390.

[45] W.T.Webb and R.Steele, "Equaliser techniques for QAM transmissions over dispersive mobile radio channels," *IEE Proc Pt. I*, vol. 138, pp. 566–576, December 1991.

[46] W.T.Webb, "QAM, the modulation scheme for future mobile radio communications?," *IEE Electronics & Communications Journal*, vol. 4, pp. 1167–176, August 1992.

[47] W.T.Webb, "Modulation methods for PCNs," *IEEE Communications magazine*, vol. 30, pp. 90–95, December 1992.

[48] R. Steele and W. Webb, "Variable rate QAM for data transmission over Rayleigh fading channels," in *Proceeedings of Wireless '91*, (Calgary, Alberta), pp. 1–14, IEEE, 1991.

[49] K. Feher, "Modems for emerging digital cellular mobile systems," *IEEE Tr. on VT*, vol. 40, pp. 355–365, May 1991.

[50] M. Iida and K. Sakniwa, "Frequency selective compensation technology of digital 16-QAM for microcellular mobile radio communication systems," in *Proceedings of IEEE VTC '92*, (Denver, Colorado, USA), pp. 662–665, IEEE, 10-13 May 1992.

[51] R. Castle and J. McGeehan, "A multilevel differential modem for narrowband fading channels," in *Proceedings of IEEE VTC '92*, (Denver, Colorado, USA), pp. 104–109, IEEE, 10-13 May 1992.

[52] D. Purle, A. Nix, M. Beach, and J. McGeehan, "A preliminary performance evaluation of a linear frequency hopped modem," in *Proceedings of IEEE VTC '92*, (Denver, Colorado, USA), pp. 120–124, IEEE, 10-13 May 1992.

[53] Y. Kamio and S. Sampei, "Performance of reduced complexity DFE using bidirectional equalizing in land mobile communications," in *Proceedings of IEEE VTC '92*, (Denver, Colorado, USA), pp. 372–376, IEEE, 10-13 May 1992.

[54] S. S. T. Nagayasu and Y. Kamio, "Performance of 16-QAM with decision feedback equalizer using interpolation for land mobile communications," in *Proceedings of IEEE VTC '92*, (Denver, Colorado, USA), pp. 384–387, IEEE, 10-13 May 1992.

[55] E. Malkamaki, "Binary and multilevel offset QAM, spectrum efficient modulation schemes for personal communications," in *Proceedings of IEEE VTC '92*, (Denver, Colorado, USA), pp. 325–328, IEEE, 10-13 May 1992.

[56] Z. Wan and K. Feher, "Improved efficiency CDMA by constant envelope SQAM," in *Proceedings of IEEE VTC '92*, (Denver, Colorado, USA), pp. 51–55, IEEE, 10-13 May 1992.

[57] H. Sasaoka, "Block coded 16-QAM/TDMA cellular radio system using cyclical slow frequency hopping," in *Proceedings of IEEE VTC '92*, (Denver, Colorado, USA), pp. 405–408, IEEE, 10-13 May 1992.

[58] P. Kenington, R. Wilkinson, and J. Marvill, "Broadband linear amplifier design for a PCN base-station," in *Proceedings of IEEE Vehicular Technology Conference (VTC'91)*, (St. Louis, MO, USA), pp. 155–160, IEEE, 19–22 May 1991.

[59] R. Wilkinson et al, "Linear transmitter design for MSAT terminals," in *Proc. of 2nd Int. Mobile Satellite Conference*, June 1990.

[60] S. Stapleton, G. Kandola, and J. Cavers, "Simulation and analysis of an adaptive predistorter utilizing a complex spectral convolution," *IEEE Tr. on VT*, vol. 41, pp. 387–394, November 1992.

[61] A. Wright and W. Durtler, "Experimental performance of an adaptive digital linearized power amplifier," *IEEE Tr. on VT*, vol. 41, pp. 395– 400, November 1992.

[62] M. Faulkner and T. Mattson, "Spectral sensitivity of power amplifiers to quadrature modulator misalignment," *IEEE Tr. on VT*, vol. 41, pp. 516–525, November 1992.

[63] S. Sampei and T. Sunaga, "Rayleigh fading compensation for QAM in land mobile radio communications," *IEEE Transactions on Vehicular Technology*, vol. 42, pp. 137–147, May 1993.

[64] T. Sunaga and S. Sampei, "Performance of multi-level QAM with post-detection maximal ratio combining space diversity for digital land-mobile radio communications," *IEEE Tr. on VT*, vol. 42, pp. 294–301, August 1993.

[65] F. Adachi and M. Sawahashi, "Performance analysis of various 16 level modulation schemes under rayleigh fading," *Electronics Letters*, vol. 28, pp. 1579–1581, November 1992.

[66] R. Chang, "Synthesis of band-limited orthogonal signals for multichannel data transmission," *BSTJ*, vol. 46, pp. 1775–1796, December 1966.

[67] M. Zimmermann and A. Kirsch, "The AN/GSC-10/KATHRYN/ variable rate data modem for HF radio," *IEEE Trans. Commun.Techn.*, vol. CCM–15, pp. 197–205, April 1967.

[68] S. Weinstein and P. Ebert, "Data transmission by frequency division multiplexing using the discrete fourier transform," *IEEE Trans. Commun. Techn.*, vol. COM–19, pp. 628–634, October 1971.

[69] L. J. Cimini, "Analysis and simulation of a digital mobile channel using orthogonal frequency division multiplexing," *IEEE Transactions on Communications*, vol. 33, pp. 665–675, July 1985.

[70] M. Alard and R. Lassalle, "Principles of modulation and channel coding for digital broadcasting for mobile receivers," *EBU Review, Technical No. 224*, pp. 47–69, August 1987.

[71] *Proc. 1st Int. Symp.,DAB*, (Montreux, Switzerland), June 1992.

[72] Peled and A. Ruiz, "Frequency domain data transmission using reduced computational complexity algorithms," in *Proceedings of International Conference on Acoustics, Speech, and Signal Processing, ICASSP'80*, (Denver, Colorado, USA), pp. 964–967, IEEE, 9–11 April 1980.

[73] B. Hirosaki, "An orthogonally multiplexed QAM system using the discrete fourier transform," *IEEE Trans. Commun.*, vol. COM-29, pp. 983–989, July 1981.

[74] H. Kolb, "Untersuchungen über ein digitales mehrfrequenzverfahren zur datenübertragung," in *Ausgewählte Arbeiten über Nachrichtensysteme*, no. 50, Universität Erlangen-Nürnberg, 1982.

[75] H. Schüssler, "Ein digitales Mehrfrequenzverfahren zur Datenübertragung," in *Professoren-Konferenz, Stand und Entwicklungsaussichten der Daten und Telekommunikation*, (Darmstadt, Germany), pp. 179–196, 1983.

[76] K. Preuss, "Ein Parallelverfahren zur schnellen Datenübertragung Im Ortsnetz," in *Ausgewählte Arbeiten über Nachrichtensysteme*, no. 56, Universität Erlangen-Nürnberg, 1984.

[77] R. Rückriem, "Realisierung und messtechnische Untersuchung an einem digitalen Parallelverfahren zur Datenübertragung im Fernsprechkanal," in *Ausgewählte Arbeiten über Nachrichtensysteme*, no. 59, Universität Erlangen-Nürnberg, 1985.

[78] I. Kalet, "The multitone channel," *IEEE Tran. on Comms*, vol. 37, pp. 119–124, February 1989.

[79] B. Hirosaki, "An analysis of automatic equalizers for orthogonally multiplexed qam systems," *IEEE Transactions on Communications*, vol. COM-28, pp. 73–83, January 1980.

[80] L. Hanzo, R. A. Salami, R. Steele, and P. Fortune, "Transmission of digitally encoded speech at 1.2 kbaud for PCN," *IEE Proceedings, Part I*, vol. 139, pp. 437–447, August 1992.

[81] P. Fortune, L. Hanzo, and R. Steele, "On the computation of 16-QAM and 64-QAM performance in rayleigh-fading channels," *IEICE Tr. on Comms.*, vol. E75-B, pp. 466–475, June 1992.

[82] R. Stedman, H. Gharavi, L. Hanzo, and R. Steele, "Transmission of subband-coded images via mobile channels," *IEEE Tr. on Circuits and Systems for Video Technology*, vol. 3, pp. 15–27, Feb 1993.

[83] X. Lin, L. Hanzo, R. Steele, and W. Webb, "A subband-multipulse digital audio broadcasting scheme for mobile receivers," *IEEE Tr. on Broadcasting*, vol. 39, pp. 373–382, December 1993.

[84] W. Webb, R. Steele, J. Cheung, and L. Hanzo, "A packet reservation multiple access assisted cordless telecommunications scheme," *IEEE Transactions on Veh. Technology*, vol. 43, pp. 234–245, May 1994.

[85] L. Hanzo, W. Webb, R. A. Salami, and R. Steele, "On QAM speech transmission schemes for microcellular mobile PCNs," *European Transactions on Communications*, pp. 495–510, Sept/Oct 1993.

[86] L. Hanzo, J. Streit, R. A. Salami, and W. Webb, "A low-rate multi-level voice/video transceiver for personal communications," *Wireless Personal Communications, Kluwer Academic Publishers*, vol. 2, no. 3, pp. 217–234, 1995.

[87] L. Hanzo, R. Stedman, R. Steele, and J. Cheung, "A mobile speech/video/data transceiver scheme," in *Proceedings of IEEE VTC '94*, (Stockholm, Sweden), pp. 452–456, IEEE, June 8-10 1994.

[88] L. Hanzo, X. Lin, R. Steele, and W. Webb, "A mobile hi-fi digital audio broadcasting scheme," in *Proceedings of IEEE VTC '94*, (Stockholm, Sweden), pp. 1035–1039, IEEE, June 8-10 1994.

[89] J. Woodard and L. Hanzo, "A dual-rate algebraic CELP-based speech transceiver," in *Proceedings of IEEE VTC '94*, vol. 3, (Stockholm, Sweden), pp. 1690–1694, IEEE, June 8-10 1994.

[90] J. Streit and L. Hanzo, "A fractal video communicator," in *Proceedings of IEEE VTC '94*, (Stockholm, Sweden), pp. 1030–1034, IEEE, June 8-10 1994.

[91] P. A. Bello, "Selective fading limitations of the KATHRYN modem and some system design considerations," *IEEE Trabsactions on Communications Technology*, vol. COM–13, pp. 320–333, September 1965.

[92] E. Powers and M. Zimmermann, "A digital implementation of a multichannel data modem," in *Proc. of the IEEE Int. Conf. on Commun.*, (Philadelphia, USA), 1968.

[93] R. Chang and R. Gibby, "A theoretical study of performance of an orthogonal multiplexing data transmission scheme," *IEEE Trans. Commun. Techn.*, vol. COM–16, pp. 529–540, August 1968.

[94] B. Saltzberg, "Performance of an efficient parallel data transmission system," *IEEE Trans. Commun. Techn.*, pp. 805–813, December 1967.

[95] K. Fazel and G. Fettweis, eds., *Multi-carrier spread-spectrum.* Kluwer, 1997. p260, ISBN 0-7923-9973-0.

[96] F. Classen and H. Meyr, "Synchronisation algorithms for an ofdm system for mobile communications," in *Codierung für Quelle, Kanal und Übertragung*, no. 130 in ITG Fachbericht, (Berlin), pp. 105–113, VDE–Verlag, 1994.

[97] F. Classen and H. Meyr, "Frequency synchronisation algorithms for ofdm systems suitable for communication over frequency selective fading channels," in *Proceedings of IEEE VTC '94*, (Stockholm, Sweden), pp. 1655–1659, IEEE, June 8-10 1994.

[98] S. J. Shepherd, P. W. J. van Eetvelt, C. W. Wyatt-Millington, and S. K. Barton, "Simple coding scheme to reduce peak factor in QPSK multicarrier modulation," *Electronics Letters*, vol. 31, pp. 1131–1132, July 1995.

[99] A. E. Jones, T. A. Wilkinson, and S. K. Barton, "Block coding scheme for reductioon of peak to mean envelope power ratio of multicarrier transmission schemes," *Electronics Letters*, vol. 30, pp. 2098–2099, 1994.

[100] D. Wulich, "Reduction of peak to mean ratio of multicarrier modulation by cyclic coding," *Electronics Letters*, vol. 32, pp. 432–433, 1996.

[101] S. H. Müller and J. B. Huber, "Vergleich von OFDM–Verfahren mit reduzierter Spitzenleistung," in *2. OFDM–Fachgespräch in Braunschweig*, 1997.

[102] M. Pauli and H.-P. Kuchenbecker, "Neue Aspekte zur Reduzierung der durch Nichtlinearitäten hervorgerufenen Außerbandstrahlung eines OFDM–Signals," in *2. OFDM–Fachgespräch in Braunschweig*, 1997.

[103] T. May and H. Rohling, "Reduktion von Nachbarkanalstörungen in OFDM–Funkübertragungssystemen," in *2. OFDM–Fachgespräch in Braunschweig*, 1997.

[104] D. Wulich, "Peak factor in orthogonal multicarrier modulation with variable levels," *Electronics Letters*, vol. 32, no. 20, pp. 1859–1861, 1996.

[105] H. Schmidt and K. D. Kammeyer, "Adaptive Subträgerselektion zur Reduktion des Crest faktors bei OFDM," in *3. OFDM Fachgespräch in Braunschweig*, 1998.

[106] R. Dinis and A. Gusmão, "Performance evaluation of OFDM transmission with conventional and 2-branch combining power amplification schemes," in *Proceeding of IEEE Global Telecommunications Conference, Globecom 96*, (London, UK), pp. 734–739, IEEE, 18–22 Nov 1996.

[107] R. Dinis, P. Montezuma, and A. Gusmão, "Performance trade-offs with quasi-linearly amplified OFDM through a 2-branch combining technique," in *Proceedings of IEEE VTC '96*, (Atlanta, GA, USA), pp. 899–903, IEEE, 1996.

[108] R. Dinis, A. Gusmão, and J. Fernandes, "Adaptive transmission techniques for the mobile broadband system," in *Proceeding of ACTS Mobile Communication Summit '97*, (Aalborg, Denmark), pp. 757–762, ACTS, 7-10 October 1997.

[109] B. Daneshrad, L. J. C. Jr., and M. Carloni, "Clustered-OFDM transmitter implementation," in *Proc. of IEEE International Symposium on Personal, Indoor, and Mobile Radio Communications (PIMRC'96)*, (Taipei, Taiwan), pp. 1064–1068, IEEE, 15-18 October 1996.

[110] M. Okada, H. Nishijima, and S. Komaki, "A maximum likelihood decision based nonlinear distortion compensator for multi-carrier modulated signals," *IEICE Trans. On Communications*, vol. E81B, no. 4, pp. 737–744, 1998.

[111] R. Dinis and A. Gusmão, "Performance evaluation of a multicarrier modulation technique allowing strongly nonlinear amplification," in *Proc. ICC 1998*, pp. 791–796, IEEE, 1998.

[112] T. Pollet, M. van Bladel, and M. Moeneclaey, "BER sensitivity of PFDM systems to carrier frequency offset and wiener phase noise," *IEEE Transactions on Communications*, vol. 43, pp. 191–193, February/March/April 1995.

[113] H. Nikookar and R. Prasad, "On the sensitivity of multicarrier transmission over multipath channels to phase noise and frequency offset," in *Proc. of IEEE International Symposium on Personal, Indoor, and Mobile Radio Communications (PIMRC'96)*, (Taipei, Taiwan), pp. 68–72, IEEE, 15-18 October 1996.

[114] W. D. Warner and C. Leung, "OFDM/FM frame synchronization for mobile radio data communication," *IEEE Transactions on Vehicular Technology*, vol. 42, pp. 302–313, August 1993.

[115] H. Sari, G. Karam, and I. Jeanclaude, "Transmission techniques for digital terrestrial tv broadcasting," *IEEE Communications Magazine*, pp. 100–109, February 1995.

[116] P. H. Moose, "A technique for orthogonal frequency division multiplexing frequency offset correction," *IEEE Trans. on Communications*, vol. 42, pp. 2908–2914, October 1994.

[117] K. Brüninghaus and H. Rohling, "Verfahren zur Rahmensynchronisation in einem OFDM-System," in *3. OFDM Fachgespräch in Braunschweig*, 1998.

[118] F. Daffara and O. Adami, "A new frequency detector for orthogonal multicarrier transmission techniques," in *Proceedings of IEEE Vehicular Technology Conference (VTC'95)*, (Chicago, USA), pp. 804–809, IEEE, July 15–28 1995.

[119] M. Sandell, J.-J. van de Beek, and P. O. Börjesson, "Timing and frequency synchronisation in OFDM systems using the cyclic prefix," in *Proceedings of International Symposium on Synchronisation*, (Essen, Germany), pp. 16–19, 14–15 Dec 1995.

[120] N. Yee, J.-P. Linnartz, and G. Fettweis, "Multicarrier CDMA in indoor wireless radio networks," in *PIMRC'93*, pp. 109–113, 1993.

[121] A. Chouly, A. Brajal, and S. Jourdan, "Orthogonal multicarrier techniques applied to direct sequence spread spectrum CDMA systems," in *Proceedings of the IEEE GLOBECOM '93*, (Houston, USA), pp. 1723–1728, November 1993.

[122] G. Fettweis, A. S. Bahai, and K. Anvari, "On multi-carrier code division multiple access (MC-CDMA) modem design," in *Proceedings of IEEE VTC '94*, (Stockholm, Sweden), pp. 1670–1674, IEEE, June 8-10 1994.

[123] K. Fazel and L. Papke, "On the performance of convolutionally-coded CDMA/OFDM for mobile communication system," in *PIMRC'93*, pp. 468–472, 1993.

[124] R. Prasad and S. Hara, "Overview of multicarrier CDMA," *IEEE Communications Magazine*, pp. 126–133, December 1997.

[125] B.-J. Choi, E.-L. Kuan, and L. Hanzo, "Crest–factor study of MC–CDMA and OFDM," in *Proceeding of VTC'99 (Fall)*, vol. 1, (Amsterdam, Netherlands), pp. 233–237, IEEE, 19–22 September 1999.

[126] Y. Li and N. R. Sollenberger, "Interference suppression in OFDM systems using adaptive antenna arrays," in *Proceeding of Globecom'98*, (Sydney, Australia), pp. 213–218, IEEE, 8–12 Nov 1998.

[127] Y. Li and N. R. Sollenberger, "Adaptive antenna arrays for OFDM systems with cochannel interference," *IEEE Trans. on. Comms.*, vol. 47, pp. 217–229, Feb 1999.

[128] Y. Li, L. J. Cimini, and N. R. Sollenberger, "Robust channel estimation for OFDM systems with rapid dispersive fading channels," *IEEE Trans. on. Comms.*, vol. 46, pp. 902–915, Apr 1998.

[129] C. K. Kim, S. Choi, and Y. S. Cho, "Adaptive beamforming for an OFDM sytem," in *Proceeding of VTC'99 (Spring)*, (Houston, Texas, USA), IEEE, 16–20 May 1999.

[130] L. Lin, L. J. C. Jr., and J. C.-I. Chuang, "Turbo codes for OFDM with antenna diversity," in *Proceeding of VTC'99 (Spring)*, (Houston, Texas, USA), IEEE, 16–20 May 1999.

[131] M. Münster, T. Keller, and L. Hanzo, "Co–channel interference suppression assisted adaptive OFDM in interference limited environments," in *Proceeding of VTC'99 (Fall)*, vol. 1, (Amsterdam, Netherlands), pp. 284–288, IEEE, 19–22 September 1999.

[132] F. Mueller-Roemer, "Directions in audio broadcasting," *Jnl Audio Eng. Soc.*, vol. 41, pp. 158–173, March 1993.

[133] G. Plenge, "DAB - a new radio broadcasting system - state of development and ways for its introduction," *Rundfunktech. Mitt.*, vol. 35, no. 2, 1991.

[134] ETSI, *Digital Audio Broadcasting (DAB)*, 2nd ed., May 1997. ETS 300 401.

[135] ETSI, *Digital Video Broadcasting (DVB); Framing structure, channel coding and modulation for digital terrestrial television*, August 1997. EN 300 744 V1.1.2.

[136] P. S. Chow, J. C. Tu, and J. M. Cioffi, "A discrete multitone transceiver system for HDSL applications," *IEEE journal on selected areas in communications*, vol. 9, pp. 895–908, August 1991.

[137] P. S. Chow, J. C. Tu, and J. M. Cioffi, "Performance evaluation of a multi-channel transceiver system for ADSL and VHDSL services," *IEEE journal on selected areas in communications*, vol. 9, pp. 909–919, August 1991.

[138] K. Sistanizadeh, P. S. Chow, and J. M. Cioffi, "Multi-tone transmission for asymmetric digital subscriber lines (ADSL)," in *Proc. ICC93*, pp. 756–760, IEEE, 1993.

[139] ANSI, *ANSI/T1E1.4/94-007, Asymmetric Digital Subscriber Line (ADSL) Metallic Interface.*, August 1997.

[140] A. G. Burr and P. A. Brown, "Application of OFDM to powerline telecommunications," in *3rd International Symposium On Power-Line Communications*, (Lancaster), 30 March – 1 April 1999.

[141] M. Deinzer and M. Stoger, "Integrated PLC-modem based on OFDM," in *3rd International Symposium On Power-Line Communications*, (Lancaster), 30 March – 1 April 1999.

[142] R. Prasad and H. Harada, "A novel OFDM based wireless ATM system for future broadband multimedia communications," in *Proceeding of ACTS Mobile Communication Summit '97*, (Aalborg, Denmark), pp. 757–762, ACTS, 7-10 October 1997.

[143] C. Ciotti and J. Borowski, "The AC006 MEDIAN project — overview and state–of–the–art," in *Proc. ACTS Summit '96*, (Granada, Spain), pp. 362–367, 27–29 November 1996.

[144] J. Borowski, S. Zeisberg, J. Hübner, K. Koora, E. Bogenfeld, and B. Kull, "Performance of OFDM and comparable single carrier system in MEDIAN demonstrator 60GHz channel," in *Proceeding of ACTS Mobile Communication Summit '97*, (Aalborg, Denmark), pp. 653–658, ACTS, 7-10 October 1997.

[145] M. G. D. Benedetto, P. Mandarini, and L. Piazzo, "Effects of a mismatch in the in–phase and in–quadrature paths, and of phase noise, in QDCPSK-OFDM modems," in *Proceeding of ACTS Mobile Communication Summit '97*, (Aalborg, Denmark), pp. 769–774, ACTS, 7-10 October 1997.

[146] T. Rautio, M. Pietikainen, J. Niemi, J. Rautio, K. Rautiola, and A. Mammela, "Architecture and implementation of the 150 Mbit/s OFDM modem (invited paper)," in *IEEE Benelux Joint Chapter on Communications and Vehicular Technology, 6th Symposium on Vehicular Technology and Communications*, (Helsinki, Finland), p. 11, Oct 12–13 1998.

[147] J. Ala-Laurila and G. Awater, "The magic WAND — wireless ATM network demondtrator system," in *Proceeding of ACTS Mobile Communication Summit '97*, (Aalborg, Denmark), pp. 356–362, ACTS, 7-10 October 1997.

[148] J. Aldis, E. Busking, T. Kleijne, R. Kopmeiners, R. van Nee, R. Mann-Pelz, and T. Mark, "Magic into reality, building the WAND modem," in *Proceeding of ACTS Mobile Communication Summit '97*, (Aalborg, Denmark), pp. 775–780, ACTS, 7-10 October 1997.

[149] E. Hallmann and H. Rohling, "OFDM-Vorschläge für UMTS," in *3. OFDM Fachgespräch in Braunschweig*, 1998.

[150] "Universal mobile telecommunications system (UMTS); UMTS terrestrial radio access (UTRA); concept evaluation," tech. rep., ETSI, 1997. TR 101 146.

[151] W. C. Jakes, ed., *Microwave Mobile Communications.* John Wiley and Sons, 1974. ISBN 0-471-43720-4.

[152] W. Lee, *Mobile cellular communications.* New York: McGraw Hill, 1989.

[153] R. Steele, ed., *Mobile Radio Communications.* IEEE Press-Pentech Press, 1992.

[154] D. Parsons, *The mobile radio propagation channel.* London: Pentech Press, 1992.

[155] D. Greenwood and L. Hanzo, "Characterisation of mobile radio channels," in Steele [153], ch. 2, pp. 92–185.

[156] J. C. Cheung, *Adaptive Equalisers for Wideband TDMA Mobile Radio.* PhD thesis, Dept. of Electronics and Computer Science, Univ. of Southampton, UK, 1991.

[157] R.Steele and V.K.Prabhu, "Mobile radio cellular structures for high user density and large data rates," *Proc. of the IEE*, pp. 396–404, August 1985. Pt F.

[158] R. Steele, "The cellular environment of lightweight hand-held portables," *IEEE Communications Magazine*, pp. 20–29, July 1989.

[159] J. G. Proakis, *Digital Communications.* McGraw-Hill Book Company, 1987.

[160] K.Bullington, "Radio propagation at frequencies above 30 mc/s," *Proc. IRE 35*, pp. 1122–1136, 1947.

[161] R. Edwards and J. Durkin, "Computer prediction of service area for VHF mobile radio networks," *Proc IRE 116 (9)*, pp. 1493–1500, 1969.

[162] W.T.Webb, "Sizing up the microcell for mobile radio communications," *IEE Electronics and communications Journal*, vol. 5, pp. 133–140, June 1993.

[163] M. Hata, "Empirical formula for propagation loss in land mobile radio," *IEEE Trans. on Vehicular Technology*, vol. 29, pp. 317–325, August 1980.

[164] Y. Okumura, E. Ohmori, T. Kawano, and K. Fukuda, "Field strength and its variability in VHF and UHF land mobile service," *Review of the Electrical Communication Laboratory*, vol. 16, pp. 825–873, September-October 1968.

[165] E.Green, "Radio link design for microcellular systems," *British Telecom Technology Journal*, vol. 8, pp. 85–96, January 1990.

[166] G. O. A. Rustako, N. Amitay and R. Roman, "Propagation measurements at microwave frequencies for microcellular mobile and personal communications," *Proc. of 39th IEEE VTC*, pp. 316–320, 1989.

[167] J.W.Kiebler, "The design and planning of feeder links to broadcasting satellites," *IEEE J-SAC*, vol. SAC-3, pp. 181–185, January 1985.

[168] C. Loo, "A statistical model for a land mobile radio satellite link," *IEEE Tr.on VT*, vol. VT-34, pp. 122–127, August 1985.

[169] C. Loo, "Digital transmission through a land mobile satellite channel," *IEEE Tr. on Comms.*, vol. 38, pp. 693–697, May 1990.

[170] E. Lutz, D. Cygan, M. Dippold, F. Dolainsky, and W. Papke, "The land mobile satellite communications channel - recording, statistics and channel model," *IEEE Tr. on VT.*, vol. 40, pp. 375–386, May 1991.

[171] J. Hagenauer, F. Dolainsky, E. Lutz, W. Papke, and R. Schweikert, "The maritime satellite communication channel – channel model, performance of modulation and coding," *IEEE J. on Selected Areas in Commum.*, vol. 5, pp. 701–713, May 1987.

[172] C.Loo, "Measurements and models of a land mobile satellite channel and their application to MSK signals," *IEEE Trans. Vehicular Tech.*, vol. VT-35, pp. 114–121, August 1987.

[173] H. Nyquist, "Certain factors affecting telegraph speed," *Bell System Tech Jrnl*, p. 617, April 1928.

[174] H. R. Raemer, *Statistical communication theory and applications*. Englewood Cliffs, New Jersey: Prentice Hall, Inc., 1969.

[175] Y. C. Chow, A. R. Nix, and J. P. McGeehan, "Analysis of 16-APSK modulation in AWGN and rayleigh fading channel," *Electronic Letters*, vol. 28, pp. 1608–1610, November 1992.

[176] K. Feher, ed., *Digital communications - satellite/earth station engineering.* Prentice Hall, 1983.

[177] N.G.Kingsbury, "Transmit and receive filters for QPSK signals to optimise the performance on linear and hard limited channels," *IEE Proc*, vol. 133, pp. 345–355, July 1986. Pt.F.

[178] B. Sklar, *Digital communications - Fundamentals and Applications.* Prentice Hall, 1988.

[179] M. Schwartz, *Information Transmission, Modulation and Noise.* McGraw-Hill, 1990.

[180] K. Feher, ed., *Advanced Digital Communications: Systems and Signal Processing.* Prentice-Hall, 1987.

[181] A. Saleh and D. Cox, "Improving the power-added efficiency of FET amplifiers operating with varying envelope signals," *IEEE Tr. on Microwave Theory Tech.*, vol. MTT-31, pp. 51–56, 1983.

[182] D. Green, "Characterisation and compensation of nonlinearities in microwave transmitters," *IEEE Tr. on Microwave Theory Tech.*, vol. MTT-30, pp. 213–217, 1982.

[183] F. Casadevall, "The LINC transmitter," *RF Design*, pp. 41–48, February 1990.

[184] Y. Akaiwa and Y. Nagata, "Highly efficient digital mobile communications with a linear modulation method," *IEEE JSAC*, vol. SAC-5, pp. 890–895, June 1987.

[185] D. H. A. Bateman and R. Wilkinson, "Linear transceiver architectures," in *Proc. IEEE Veh. Tech. Conf.*, pp. 478–484, 1988.

[186] A.S.Wright and W.G.Duntler, "Experimental performance of an adaptive digital linearised power amplifier," *IEEE VT*, vol. 41, pp. 395–400, November 1992.

[187] S. Stapleton and L. Quach, "Reduction of adjacent channel interference using postdistortion," in *Proceedings of IEEE VTC '92*, (Denver, Colorado, USA), pp. 915–918, IEEE, 10-13 May 1992.

[188] J.Namiki, "An automatically controlled predistorter for multilevel quadrature amplitude modulation," *IEEE Tr. Comm.*, vol. COM-31, pp. 707–712, May 1983.

[189] T. Nojima and T. Konno, "Cuber predistortion linearizer for relay equipment in the 800 MHz band land mobile telephone system," *IEEE Tr. on Veh. Tech.*, vol. VT-34, pp. 169–177, November 1985.

[190] P. M. M. Nannicini and F. Oggioni, "Temperature controlled predistortion circuits for 64 QAM microwave power amplifiers," *IEEE Microwave Theory Tech. Dig.*, pp. 99–102, 1985.

[191] Y. Nagata, "Linear amplification technique for digital mobile communications," in *Proceedings of IEEE Vehicular Technology Conference (VTC'89)*, (San Francisco, CA, USA), pp. 159–164, IEEE, 1–3 May 1989.

[192] A. Saleh and J. Salz, "Adaptive linearization of power amplifiers in digital radio systems," *Bell Systems Tech. Journal*, vol. 62, pp. 1019–1033, April 1983.

[193] B. Bunday, *Basic Optimisation Methods.* London: Edward Arnold, 1984.

[194] S.P.Stapleton and F.C.Costesu, "An adaptive pre-distortion system," in *Proceedings of IEEE VTC '92*, (Denver, Colorado, USA), pp. 690–693, IEEE, 10-13 May 1992.

[195] L. E. Franks, "Carrier and bit synchronization — a tutorial review," *IEEE Transactions on Communications*, vol. COM-28, pp. 1107–1121, August 1980.

[196] R. E. Ziemer and R. L. Peterson, *Digital Communications and Spread Spectrum System.* New York: Macmillan Publishing Company, 1985.

[197] L.E.Franks, "Synchronisation subsystems: Analysis and design," in Feher [176], ch. 7.

[198] A. B. Carlson, *Communication Systems.* McGraw-Hill, 1975.

[199] I.J.Wassell, *Digital mobile radio communication.* PhD thesis, University of Southampton, 1991.

[200] R.L.Cupo. and R.D.Gitlin, "Adaptive carrier recovery systems for digital data communications receivers," *IEEE J-SAC*, vol. 7, pp. 1328–1339, December 1989.

[201] W.C.Lindsey and M.K.Simon, "Carrier synchronisation and detection of polyphase signals," *IEEE Trans. Comms.*, pp. 441–454, June 1972.

[202] J.Smith, *Modern communications circuits.* McGraw Hill, 1986.

[203] M. Woodbury, "Inverting modified matrices," tech. rep., Statistical Research Group, Princeton University, Princeton, N.J., U.S.A. Mem.Rep. 42.

[204] B. Picinbono, "Adaptive signal processing for detection and communication," in *Communication Systems and Random Process Theory* (J. Skwirzinsky, ed.), Alphen aan den Rijn, The Netherlands: Sijthof and Noordhoff, 1978.

[205] K.Murota and K.Hirade, "GMSK modulation for digital mobile radio telephony," *IEEE Trans. Commun.*, vol. 29, pp. 1044–1050, July 1981.

[206] L. Lopes, "GSM radio link simulation," tech. rep., University research in Mobile Radio, 1990. IEE Colloquium.

[207] J. Cheung and R. Steele, "Modified viterbi equaliser for mobile radio channels having large multi-path delay," *Electronics Letters*, vol. 25, pp. 1309–1311, September = 1989.

[208] A. C. N.S. Hoult, C.A. Dace, "Implementation of an equaliser for the GSM system," in *Proc. of the 5th Int. Conf. on Radio Receivers Associated Systems*, (Cambridge, U.K.), 24-26 July 1990.

[209] M. S. R.D'Avella, L. Moreno, "An adaptive MLSE receiver for TDMA digital mobile radio," *IEEE Journal on Selected Areas in Communications*, vol. 7, pp. 122–129, January 1989.

[210] J. Anderson, T. Aulin, and C. Sundberg, *Digital phase modulation.* Plenum Press, 1986.

[211] J. Massey, "Coding and modulation in digital communications," in *Proc of International Zurich Seminar on Digital Communications 1994*, (Zurich, Switzerland), Mar 1974.

[212] H. Imai and S. Hirakawa, "A new multi-level coding method using error correcting codes," *IEEE Transactions on Information Theory*, vol. 23, pp. 371–377, May 1977.

[213] G. Ungerboeck, "Channel coding with multilevel/phase signals," *IEEE Transactions on Information Theory*, vol. IT-28, pp. 55–67, Jan 1982.

[214] G. Ungerboeck, "Treliis-coded modulation with redundant signal sets part 1: Introduction," *IEEE Communications Magazine*, vol. 25, pp. 5–11, Feb 1987.

[215] E. Biglieri and M. Luise, "Coded modulation and bandwidth-efficient transmission," in *Proc. of the Fifth Tirrenia Intern. Workshop*, (Elsevier, Netherlands), 8–12 Sept 1991.

[216] "Special issue on coded modulation," *IEEE Comms. Magazine*, vol. 29, December 1991.

[217] E.Biglieri, D.Divsalar, P.J.McLane, and M.K.Simon, *Introduction to trellis coded modulation with applications.* New York: MacMillan Publishing Co., 1991.

[218] G. D. Forney Jr, R. G. Gallager, G. R. Lang, F. M. Longstaff, and S. U. Qureshi, "Efficient modulation for band-limited channels," *IEEE Journal on Selected Areas in Communications*, vol. 2, pp. 632–647, Sept 1984.

[219] C. Shannon, *Mathematical Theory of Communication.* University of Illinois Press, 1963.

[220] J.M.Wozencraft and R.S.Kennedy, "Modulation and demodulation for probabilistic coding," *IEEE Trans. Inf. Theory*, vol. IT-12, pp. 291–297, 1966.

[221] J.M.Wozencraft and I.M.Jacobs, *Principles of communications engineering.* J.Wiley, 1965.

[222] R. Blahut, *Theory and practice of error control codes.* Addison-Wesley, 1983. ISBN 0-201-10102-5.

[223] E. Berlekamp, *Algebraic Coding Theory.* McGraw-Hill, New York, 1968.

[224] W. Peterson, *Error correcting codes.* Cambridge, Mass, USA: MIT. Press, 1st ed., 1961.

[225] A. Michelson and A. Levesque, *Error control techniques for digital communication.* J. Wiley and Sons, 1985.

[226] K. H. H. Wong and L. Hanzo, "Channel coding," in Steele [153], ch. 4, pp. 347–488.

[227] M.Oeder, "Rotationally invariant trellis codes for mPSK modulation," in *Proc. IEEE ICC'85*, (Chicago, USA), pp. 552–556, June 1985.

[228] L-F.Wei, "Trellis-coded modulation with multidimensional constellations," *IEEE Trans Inf.Theory*, vol. IT-33, pp. 483–501, July 1987.

[229] *International Consultative Committee for Telephone and Telegraph Recommendations.* Geneva. V.29 - V.33.

[230] L. Wei, "Rotationally-invariant convolutional channel coding with expanded signal space, part i and ii," *IEEE Tr. on Selected Areas in Comms*, vol. SAC-2, pp. 659–686, September 1984.

[231] K. S. Shanmugam, *Digital and Analog Communications Systems.* New York, USA: John Wiley, 1979.

[232] W. Lee, *Mobile communications engineering.* McGraw Hill Book Co., 1982.

[233] I.S.Gradshteyn and I.M.Ryzhik, *Table of integrals, series and products.* Academic Press, 1980.

[234] G.J.Saulnier and W.Raffety, "Pilot-aided modulation for narrowband satellite communications," in *Proc. Mobile Satellite Conf*, pp. 329–336, 1988.

[235] A. Bateman and J. McGeehan, "Feedforward transparent tone in band for rapid fading protection in multipath fading," in *IEE Int.Conf. Comms.*, vol. 68, pp. 9–13, 1986.

[236] A. Bateman and J. McGeehan, "The use of transparent tone in band for coherent data schemes," in *IEEE Int. Conf. Comms*, (Boston, Mass, USA), 1983.

[237] A. Bateman, G. Lightfoot, A. Lymer, and J. McGeehan, "Speech and data transmissions over a 942MHz TAB and TTIB single sideband mobile radio system," *IEEE Transactions on Vehicular Technology*, vol. VT-34, pp. 13–21, Feb 1985.

[238] A. Bateman and J. McGeehan, "Data transmissions over UHF fading mobile radio channels," *Proc IEE Pt.F*, vol. 131, pp. 364–374, 1984.

[239] J. McGeehan and A. Bateman, "A simple simultaneous carrier and bit synchronisation system for narrowband data transmissions," *Proc. IEE, Pt.F*, vol. 132, pp. 69–72, 1985.

[240] J. McGeehan and A. Bateman, "Theoretical and experimental investigation of feedforward signal regeneration," *IEEE Trans. Veh. Tech*, vol. VT-32, pp. 106–120, 1983.

[241] A. Bateman, "Feedforward transparent tone in band: Its implementation and applications," *IEEE Trans. Veh. Tech*, vol. 39, pp. 235–243, August 1990.

[242] M.K.Simon, "Dual pilot tone calibration technique," *IEEE Trans. Veh. Tech.*, vol. VT-35, pp. 63–70, May 1986.

[243] M.P.Fitz, "A dual-tone reference digital demodulator for mobile communications," *IEEE Tran. Veh. Tech.*, vol. VT-42, pp. 156–166, May 1993.

[244] S.Gamnathan and K.Feher, "Pilot tone aided QPRS systems for digital audio broadcasting," *IEEE Trans. on Broadcasting*, vol. 38, pp. 1–6, March 1992.

[245] F.Davarrin, "Mobile digital communications via tone calibration," *IEEE Trans. Veh. Tech.*, vol. VT-36, pp. 55–62, May 1987.

[246] J.K.Cavers, "Performance of tone calibration with frequency offset and imperfect pilot filter," *IEEE Tran. Veh. Tech.*, vol. 40, pp. 426–434, May 1991.

[247] D. Esteban and C. Galand, "Application of quadrature mirror filters to split band voice coding scheme," in *Proceedings of International Conference on Acoustics, Speech, and Signal Processing, ICASSP'77*, (Hartford, Conn, USA), pp. 191–195, IEEE, 9–11 May 1977.

[248] J. Johnston, "A filter family designed for use in quadrature mirror filter banks," in *Proceedings of International Conference on Acoustics, Speech, and Signal Processing, ICASSP'80*, (Denver, Colorado, USA), pp. 291–294, IEEE, 9–11 April 1980.

[249] J. Lodge and M. Moher, "Time diversity for mobile satellite channels using trellis coded modulations," in *IEEE Global Telecommun. Conf.*, (Tokyo, Japan), 1987.

[250] M. L. Moher and J. H. Lodge, "TCMP – a modulation and coding strategy for rician fading channels," *IEEE Journal on Selected Areas in Communications*, vol. 7, pp. 1347–1355, December 1989.

[251] S. Sampei and T. Sunaga, "Rayleigh fading compensation method for 16-QAM in digital land mobile radio channels," in *Proceedings of IEEE Vehicular Technology Conference (VTC'89)*, (San Francisco, CA, USA), pp. 640–646, IEEE, 1–3 May 1989.

[252] J. Cavers, "Pilot symbol assisted modulation in fading and delay spread," in *Proceedings of IEEE VTC '93*, (Secaucus, NJ, USA), pp. 13–16, IEEE, May 18-20 1993.

[253] M. F. J.P. Seymour, "Improved carrier synchronisation techniques for mobile communications," in *Proceedings of IEEE VTC '93*, (Secaucus, NJ, USA), pp. 901–904, IEEE, May 18-20 1993.

[254] AT&T Information Services, *A trellis coded modulation scheme that includes differential encoding for 9600 bit/sec full-duplex,two-wire modems*, August 1983. CCITT SG XVII.

[255] R. A. Salami, L. Hanzo, R. Steele, K. H. J. Wong, and I. Wassell, "Speech coding," in Steele [153], ch. 3, pp. 186–346.

[256] K. Larsen, "Short convolutional codes with maximal free distance for rate 1/2, 1/3 and 1/4," *IEEE Trans. Info. Theory*, vol. IT-19, pp. 371–372, May 1973.

[257] K. Wong, L. Hanzo, and R. Steele, "Channel coding for satellite mobile channels," *International Journal on Satellite Communications*, vol. 7, pp. 143–163, July–Sep 1989.

[258] P.Ho, J.Cavers, and J.Varaldi, "The effect of constellation density on trellis coded modulation in fading channels," in *Proceedings of IEEE VTC '92*, (Denver, Colorado, USA), pp. 463–467, IEEE, 10-13 May 1992.

[259] S.A.Fechtel and H.Meyr, "Combined equalisation, decoding and antenna diversity combining for mobile personal digital radiotransmission using feedforward synchronisation," in *Proceedings of IEEE VTC '93*, (Secaucus, NJ, USA), IEEE, May 18-20 1993.

[260] R.J.C.Bultitude and G.K.Bedal, "Propagation characteristics on microcellular urban mobile radio channels at 910MHz," *IEEE J-SAC*, vol. 7, pp. 31–39, January 1989.

[261] R.Steele, "Deploying personal communications networks," *IEEE Comms. Magazine*, pp. 12–15, September 1990.

[262] R.Bultitude, S.Mahmoud, and W.Sullivan, "A comparison of indoor radio propagation characteristics at 910MHz and 1.75GHz," *IEEE J-SAC*, vol. 7, pp. 20–30, January 1989.

[263] H. Harmuth, *Transmission of Information by Orthogonal Time Functions*. Berlin: Springer Verlag, 1969.

[264] H. Harmuth, "On the transmission of information by orthogonal time functions," *AIEE*, July 1960.

[265] H. Harmuth, "Die orthogonalteilung als verallgemeinerung der zeit- und frequenzteilung," *AEÜ*, vol. 18, pp. 43–50, 1964.

[266] D.Saha and T.G.Birdsall, "Quadrature-quadrature phase shift keying," *IEEE Trans. Comms.*, vol. 37, pp. 437–448, May 1989.

[267] H.J.Landau and H.O.Pollak, "Prolate spheroidal wave functions...," *BSTJ*, vol. 41, pp. 1295–1336, July 1962.

[268] W. C. Y. Lee, "Spectrum efficiency in cellular," *IEEE Tr. on Vech. Tech*, vol. 38, pp. 69–75, May 1989.

[269] J. Williams, L. Hanzo, R. Steele, and J. Cheung, "A comparative study of microcellular speech transmission schemes," *IEEE Tr. on Veh. Technology*, vol. 43, pp. 909–925, Nov 1994.

[270] R.Steele, J.E.B.Williams, and L.Hanzo, "Speech performance of adaptive transceivers for PCN," in *IEE Colloquium on Advanced channel coding and modulation*, (London), 16th November 1992.

[271] J.E.B.Williams, *Simulation of digital modulation and demodulation*. PhD thesis, University of Southampton, 1992. Ph.D. mini-thesis.

[272] R.Steele and J.E.B.Williams, "Third generation PCN and the intelligent multimode portable," *IEE Electronics and Comm. Journal*, vol. 5, pp. 147–156, June 1993.

[273] P. Vary and R. Sluyter, "MATS-D speech codec: Regular-pulse excitation LPC," in *Proc. of the Nordic Seminar on Digital Land Mobile Radio Communications (DMRII)*, (Stockholm, Sweden), pp. 257–261, October 1986.

[274] P. Vary and R. Hoffmann, "Sprachcodec für das europäische Funkfernsprechnetz," *Frequenz 42 (1988) 2/3*, pp. 85–93, 1988.

[275] J. Schur, "Über potenzreihen, die im innern des einheitskreises beschränkt sind," *Journal für die reine und angewandte Mathematik, Bd 14*, pp. 205–232, 1917.

[276] N. Kitawaki, M. Honda, and K. Itoh, "Speech-quality assessment methods for speech coding systems," *IEEE Communications Magazine*, vol. 22, pp. 26–33, October 1984.

[277] A. H. Gray and J. D. Markel, "Distance measures for speech processing," *IEEE Transactions on ASSP*, vol. 24, no. 5, pp. 380–391, 1976.

[278] N. Kitawaki, H. Nagabucki, and K. Itoh, "Objective quality evaluation for low-bit-rate speech coding systems," *IEEE Journal on Selected Areas in Communications*, vol. 6, pp. 242–249, Feb. 1988.

[279] E. Bacs and L. Hanzo, "A simple real-time adaptive speech detector for SCPC systems," in *Proc of ICC'85*, (Chicago, USA), pp. 1208–1212, May 1985.

[280] D. Freeman, G. Cosier, C. Southcott, and I. Boyd, "The voice activity detector for the pan-european digital cellular mobile telephone service," in *Proc. of ICASSP'89*, (Glasgow, UK), pp. 369–372, 23-26 May 1989.

[281] S. Hansen, "Voice activity detection (VAD) and the operation of discontinuous transmission (DTX) in the GSM system," in *Proc. of Digital Cellular Radio Conference*, (Hagen, Germany), pp. 2b/1–2b/14, October 12-14 1988.

[282] L. Hanzo, W. Webb, R. Salami, and R. Steele, "On speech transmission schemes for microcellular mobile PCNs," *European Transactions on Communications*, vol. 4, pp. 495–510, Sept./Oct 1993.

[283] W. Webb, L. Hanzo, R. A. Salami, and R. Steele, "Does 16-QAM provide an alternative to a half-rate GSM speech codec ?," in *Proceedings of IEEE Vehicular Technology Conference (VTC'91)*, (St. Louis, MO, USA), pp. 511–516, IEEE, 19–22 May 1991.

[284] O. Wasem, D. Goodman, C. Dvorak, and H. Page, "The effect of waveform substitution on the quality of PCM packet communications," *IEEE Tr. ASSP*, vol. 36, pp. 342–348, March 1988.

[285] S. Nanda, D. J. Goodman, and U. Timor, "Performance of PRMA: A packet voice protocol for cellular systems," *IEEE Tr. on VT*, vol. 40, pp. 584–598, August 1991.

[286] D.J.Goodman, "Cellular packet communications," *IEEE Trans Comms*, vol. 38, pp. 1272–1280, August 1990.

[287] L.Hanzo, J.C.S.Cheung, R.Steele, and W.T.Webb, "Performance of PRMA schemes via fading channels," in *Proceedings of IEEE VTC '93*, (Secaucus, NJ, USA), pp. 913–916, IEEE, May 18-20 1993.

[288] K. Wong, L. Hanzo, and R. Steele, "A sub-band codec with embedded reed-solomon coding for mobile radio speech communication," in *Proceedings of ICCS 1988, Singapore*, 31 October – 3 November 1988.

[289] H. J. Kolb Private Communications.

[290] J. Lindner Private Communications.

[291] D. Schnidman, "A generalized nyquist criterion and an optimum linear receiver for a pulse modulation system," *BSTJ*, pp. 2163–2177, November 1967.

[292] W. V. Etten, "An optimum linear receiver for multiple channel digital transmission systems," *IEEE Trans. Comm.*, vol. COM-23, pp. 828–834, August 1975.

[293] A. Kaye and D. George, "Transmission of multiplexed PAM signals over multiple channel and diversity systems," *IEEE Trans. Comm. Techn.*, vol. COM-18, pp. 520–525, October 1970.

[294] M. Aaron and D. Tufts, "Intersymbol interference and error probability," *IEEE Trans. Inform. Theory*, vol. IT-12, pp. 26–34, January 1966.

[295] D. Tufts, "Nyquist's problem: The joint optimization of transmitter and receiver in pulse amplitude modulation," *Proc. IEEE*, vol. 53, pp. 248–259, March 1965.

[296] H. Schüssler, *Digitale Systeme zur Signalverarbeitung.* Berlin, Heidelberg, and New York: Springer Verlag, 1974.

[297] W. T. Webb and L. Hanzo, *Modern Quadrature Amplitude Modulation: Principles and Applications for Wireless Communications.* IEEE Press-Pentech Press, 1994. ISBN 0-7273-1701-6.

[298] J. G. Proakis, *Digital Communications.* McGraw Hill, 3rd ed., 1995.

[299] R. O'Neill and L. B. Lopes, "Performance of amplitude limited multitone signals," in *Proceedings of IEEE VTC '94*, (Stockholm, Sweden), IEEE, June 8-10 1994.

[300] X. Li and L. J. Cimini, "Effects of clipping and filtering on the performance of OFDM," in *Proceedings of IEEE VTC '97*, (Phoenix, Arizona, USA), pp. 1634–1638, IEEE, 4–7 May 1997.

[301] A. Garcia and M. Calvo, "Phase noise and sub–carrier spacing effects on the performance of an OFDM communications system," *IEEE Communications Letters*, vol. 2, pp. 11–13, January 1998.

[302] W. Robins, *Phase Noise in signal sources*, vol. 9 of *IEE Telecommunication series.* Peter Peregrinus Ltd., 1982.

[303] C. Tellambura, Y. J. Guo, and S. K. Barton, "Equaliser performance for HIPERLAN in indoor channels," *Wireless Personal Communications*, vol. 3, no. 4, pp. 397–410, 1996.

[304] T. Ojanperä, M. Gudmundson, P. Jung, J. Sköld, R. Pirhonen, G. Kramer, and A. Toskala, "FRAMES: - hybrid multiple access technology," in *Proceedings of IEEE ISSSTA'96*, (Mainz, Germany), pp. 334–338, IEEE, Sept 1996.

[305] M. Failli, "Digital land mobile radio communications COST 207," tech. rep., European Commission, 1989.

[306] J. M. Torrance and L. Hanzo, "Comparative study of pilot symbol assisted modem schemes," in *Proceedings of IEE Conference on Radio Receivers and Associated Systems (RRAS'95)*, (Bath, UK), pp. 36–41, IEE, 26–28 September 1995.

[307] K. Fazel, S. Kaiser, P. Robertson, and M. J. Ruf, "A concept of digital terrestrial television broadcasting," *Wireless Personal Communications*, vol. 2, pp. 9–27, 1995.

[308] J. Kuronen, V.-P. Kaasila, and A. Mammela, "An all-digital symbol tracking algorithm in an OFDM system by using the cyclic prefix," in *Proc. ACTS Summit '96*, (Granada, Spain), pp. 340–345, 27–29 November 1996.

[309] M. Kiviranta and A. Mammela, "Coarse frame synchronization structures in OFDM," in *Proc. ACTS Summit '96*, (Granada, Spain), pp. 464–470, 27–29 November 1996.

[310] Z. Li and A. Mammela, "An all digital frequency synchronization scheme for OFDM systems," in *Proceedings of IEEE International Symposium on Personal, Indoor and Mobile Radio Communications, PIMRC'97*, (Marina Congress Centre, Helsinki, Finland), pp. 327–331, IEEE, 1–4 Sept 1997.

[311] J. A. C. Bingham, "Method and apparatus for correcting for clock and carrier frequency offset, and phase jitter in multicarrier modems." U.S. Patent No. 5206886, April 27 1993.

[312] T. de Couasnon, R. Monnier, and J. B. Rault, "Ofdm for digital tv broadcasting," *Signal Processing*, vol. 39, pp. 1–32, 1994.

[313] Paolo Mandarini and Alessandro Falaschi, "Sync proposals." MEDIAN Design Note, January 1996.

[314] T. Keller and L. Hanzo, "Orthogonal frequency division multiplex synchronisation techniques for wireless local area networks," in *Proc. of IEEE International Symposium on Personal, Indoor, and Mobile Radio Communications (PIMRC'96)*, vol. 3, (Taipei, Taiwan), pp. 963–967, IEEE, 15-18 October 1996.

[315] H. Matsuoka, S. Sampei, N. Morinaga, and Y. Kamio, "Adaptive modulation system with variable coding rate concatenated code for high quality multi-media communications systems," in *Proceedings of IEEE VTC '96*, (Atlanta, GA, USA), pp. 487–491, IEEE, 1996.

[316] S. Chua and A. Goldsmith, "Variable-rate variable-power mQAM for fading channels," in *Proceedings of IEEE VTC '96*, (Atlanta, GA, USA), pp. 815–819, IEEE, 1996.

[317] D. A. Pearce, A. G. Burr, and T. C. Tozer, "Comparison of counter-measures against slow Rayleigh fading for TDMA systems," in *IEE Colloquium on Advanced TDMA Techniques and Applications*, (London, UK), pp. 9/1–9/6, IEE, 28 October 1996. digest 1996/234.

[318] V. K. N. Lau and M. D. Macleod, "Variable rate adaptive trellis coded QAM for high bandwidth efficiency applications in rayleigh fading channels," in *Proceedings of IEEE Vehicular Technology Conference (VTC'98)*, (Ottawa, Canada), pp. 348–352, IEEE, May 1998.

[319] J. M. Torrance and L. Hanzo, "Latency and networking aspects of adaptive modems over slow indoors rayleigh fading channels," *IEEE Tr. on Veh. Techn.*, vol. 48, no. 4, pp. 1237–1251, 1998.

[320] J. M. Torrance, L. Hanzo, and T. Keller, "Interference aspects of adaptive modems over slow rayleigh fading channels," *IEEE Tr. on Veh. Techn.*, vol. 48, pp. 1527–1545, Sept 1999.

[321] A. Czylwik, "Adaptive OFDM for wideband radio channels," in *Proceeding of IEEE Global Telecommunications Conference, Globecom 96*, (London, UK), pp. 713–718, IEEE, 18–22 Nov 1996.

[322] P. S. Chow, J. M. Cioffi, and J. A. C. Bingham, "A practical discrete multitone transceiver loading algorithm for data transmission over spectrally shaped channels," *IEEE Trans. on Communications*, vol. 48, pp. 772–775, 1995.

[323] J. Torrance, *Adaptive Full Response Digital Modulation for Wireless Communications Systems*. PhD thesis, Dept. of Electronics and Computer Science, Univ. of Southampton, UK, 1997.

[324] K. Miya, O. Kato, K. Homma, T. Kitade, M. Hayashi, and T. Ue, "Wideband CDMA systems in TDD-mode operation for IMT-2000," *IEICE Trans. on Comms.*, vol. E81-B, pp. 1317–1326, July 1998.

[325] O. Kato, K. Miya, K. Homma, T. Kitade, M. Hayashi, and M. Watanabe, "Experimental performance results of coherent wideband DS-CDMA with TDD scheme," *IEICE Trans. on Comms.*, vol. E81-B, pp. 1337–1344, July 1998.

[326] T. Keller and L. Hanzo, "Blind-detection assisted sub-band adaptive turbo-coded OFDM schemes," in *Proceeding of VTC'99 (Spring)*, (Houston, Texas, USA), pp. 489–493, IEEE, 16–20 May 1999.

[327] J. M. Torrance and L. Hanzo, "Optimisation of switching levels for adaptive modulation in a slow Rayleigh fading channel," *Electronics Letters*, vol. 32, pp. 1167–1169, 20 June 1996.

[328] C. Berrou, A. Glavieux, and P. Thitimajshima, "Near shannon limit error-correcting coding and decoding: Turbo codes," in *Proceedings of the International Conference on Communications*, pp. 1064–1070, May 1993.

[329] L. Bahl, J. Cocke, F. Jelinek, and J. Raviv, "Optimal decoding of linear codes for minimising symbol error rate," *IEEE Transactions on Information Theory*, vol. 20, pp. 284–287, March 1974.

[330] T. Keller, M. Muenster, and L. Hanzo, "A burst–by–burst adaptive OFDM wideband speech transceiver." submitted to IEEE JSAC, 1999.

[331] T. Keller, J. Woodard, and L. Hanzo, "Turbo-coded parallel modem techniques for personal communications," in *Proceedings of IEEE VTC '97*, (Phoenix, Arizona, USA), pp. 2158–2162, IEEE, 4–7 May 1997.

[332] T. Keller and L. Hanzo, "Adaptive orthogonal frequency division multiplexing schemes," in *Proceeding of ACTS Mobile Communication Summit '98*, (Rhodes, Greece), pp. 794–799, ACTS, 8–11 June 1998.

[333] L. Piazzo, "A fast algorithm for near-optimum power and bit allocation in ofdm systems." submitted to Electronics Letters, November 1999.

[334] T. J. Willink and P. H. Wittke, "Optimization and performance evaluation of multicarrier transmission," *IEEE Transactions on Information Theory*, vol. 43, pp. 426–440, March 1997.

[335] R. F. H. Fischer and J. B. Huber, "A new loading algorithm for discrete multitone transmission," in *Proceeding of IEEE Global Telecommunications Conference, Globecom 96*, (London, UK), pp. 713–718, IEEE, 18–22 Nov 1996.

[336] S. K. Lai, R. S. Cheng, K. B. Letaief, and R. D. Murch, "Adaptive trellis coded mqam and power optimization for ofdm transmission," in *Proceeding of VTC'99 (Spring)*, (Houston, Texas, USA), IEEE, 16–20 May 1999.

[337] J. A. C. Bingham, "Multicarrier modulation for data transmission: an idea whose time has come," *IEEE Communications Magazine*, pp. 5–14, May 1990.

[338] Y. Li, "Pilot-symbol-aided channel estimation for OFDM in wireless systems," in *Proceeding of VTC'99 (Spring)*, (Houston, Texas, USA), IEEE, 16–20 May 1999.

[339] N. S. Szabo and R. I. Tanaka, *Residue Arithmetic and Its Applications to Computer Technology.* New York: McGraw-Hill Book Company, 1967.

[340] R. W. Watson and C. W. Hastings, "Self-checked computation using residue arithmetic," *Proceedings of the IEEE*, vol. 54, pp. 1920–1931, December 1966.

[341] R. Pyndiah, "Iterative decoding of product codes: Block turbo codes," in *Proceedings of the International Symposium on Turbo Codes & Related Topics*, (Brest, France), pp. 71–79, Sept 1997.

[342] P. Adde, R. Pyndiah, O. Raoul, and J.-R. Inisan, "Block turbo decoder design," in *Proceedings of the International Symposium on Turbo Codes & Related Topics*, (Brest, France), pp. 166–169, Sept 1997.

[343] W. K. Jenkins and B. J. Leon, "The use of residue number system in the design of finite impulse response filters," *IEEE Transactions on Circuits Systems*, vol. CAS-24, pp. 191–201, April 1977.

[344] M. A. Soderstrand, "A high-speed, low-cost, recursive digital filter using residue number arithmetic," *Proceeding IEEE*, vol. 65, pp. 1065–1067, July 1977.

[345] M. A. Soderstrand and E. L. Fields, "Multipliers for residue number arithmetic digital filters," *Electronic Letters*, vol. 13, pp. 164–166, March 1977.

[346] M. A. Soderstrand, W. K. Jenkins, and G. A. Jullien, *Residue Number System Arithmetic: Modern Applications in Digital Signal Processing.* New York, USA: IEEE Press, 1986.

[347] E. D. D. Claudio, G. Orlandi, and F. Piazza, "A Systolic Redundant Residue Arithmetic Error Correction Circuit," *IEEE Transactions on Computers*, vol. 42, pp. 427–432, April 1993.

[348] H. Krishna, K.-Y. Lin, and J.-D. Sun, "A coding theory approach to error control in redundant residue number systems - part I: Theory and single error correction," *IEEE Transactions on Circuits and Systems-II: Analog and Digital Signal Processing*, vol. 39, pp. 8–17, January 1992.

[349] J.-D. Sun and H. Krishna, "A coding theory approach to error control in redundant residue number systems - part II: Multiple error detection and correction," *IEEE Transactions on Circuits and Systems-II: Analog and Digital Signal Processing*, vol. 39, pp. 18–34, January 1992.

[350] T. Liew, L.-L. Yang, and L. Hanzo, "Soft-decision redundant residue number system based error correction coding," in *Proceeding of VTC'99 (Fall)*, (Amsterdam, Netherlands), pp. 2974–2978, IEEE, 19–22 September 1999.

[351] L.-L. Yang and L. Hanzo, "Residue number system arithmetic assisted m-ary modulation," *IEEE Communications Letters*, vol. 3, pp. 28–30, Feb. 1998.

[352] L.-L. Yang and L. Hanzo, "Performance of residue number system based DS-CDMA over multipath fading channels using orthogonal sequences," *ETT*, vol. 9, pp. 525–536, November - December 1998.

[353] H. Krishna, K.-Y. Lin, and J.-D. Sun, "A coding theory approach to error control in redundant residue number systems - part I: theory and single error correction," *IEEE Trans. Circuits Syst.*, vol. 39, pp. 8–17, January 1992.

[354] J.-D. Sun and H. Krishna, "A coding theory approach to error control in redundant residue number systems - part II: multiple error detection and correction," *IEEE Trans. Circuits Syst.*, vol. 39, pp. 18–34, January 1992.

[355] H. Krishna and J.-D. Sun, "On theory and fast algorithms for error correction in residue number system product codes," *IEEE Trans. Comput.*, vol. 42, pp. 840–852, July 1993.

[356] D. Chase, "A class of algorithms for decoding block codes with channel measurement information," *IEEE Trans. on Info. Theory*, vol. IT-18, pp. 170–182, January 1972.

[357] J. Hagenauer, E. Offer, and L. Papke, "Iterative decoding of binary block and convolutional codes," *IEEE Transactions on Information Theory*, vol. 42, pp. 429–445, March 1996.

[358] H. Nickl, J. Hagenauer, and F. Burkett, "Approaching shannon's capacity limit by 0.27 dB using simple hamming codes," *IEEE Communications Letters*, vol. 1, pp. 130–132, Sept 1997.

[359] T. Liew, C. Wong, and L. Hanzo, "Block turbo coded burst-by-burst adaptive modems," in *Proceeding of Microcoll'99, Budapest, Hungary*, pp. 59–62, 21-24 March 1999.

[360] B. L. Yeap, T. H. Liew, J. Hamorsky, and L. Hanzo, "Comparitive study of turbo equalisers using convolutional codes and block-based turbo-codes for GMSK modulation," in *Proceeding of VTC'99 (Fall)*, (Amsterdam, Netherlands), pp. 2974–2978, IEEE, 19–22 September 1999.

[361] M. S. Yee, T. H. Liew, and L. Hanzo, "Radial basis function decision feedback equalisation assisted block turbo burst-by-burst adaptive modems," in *Proceeding of VTC'99 (Fall)*, (Amsterdam, Netherlands), pp. 1600–1604, IEEE, 19–22 September 1999.

[362] C. H. Wong, T. H. Liew, and L. Hanzo, "Turbo coded burst by burst adaptive wideband modulation with blind modem mode detection," in *Proceeding of ACTS Mobile Communication Summit '99*, (Sorrento, Italy), pp. 303–308, ACTS, June 8–11 1999.

[363] ETSI, *Digital Video Broadcasting (DVB); Framing structure, channel coding and modulation for cable systems*, December 1997. EN 300 429 V1.2.1.

[364] ETSI, *Digital Video Broadcasting (DVB); Framing structure, channel coding and modulation for 11/12 GHz Satellite Services*, August 1997. EN 300 421 V1.1.2.

[365] S. O'Leary and D. Priestly, "Mobile broadcasting of DVB-T signals," *IEEE Transactions on Broadcasting*, vol. 44, pp. 346–352, September 1998.

[366] W.-C. Lee, H.-M. Park, K.-J. Kang, and K.-B. Kim, "Performance analysis of viterbi decoder using channel state information in COFDM system," *IEEE Transactions on Broadcasting*, vol. 44, pp. 488–496, December 1998.

[367] S. O'Leary, "Hierarchical transmission and COFDM systems," *IEEE Transactions on Broadcasting*, vol. 43, pp. 166–174, June 1997.

[368] L. Thibault and M. T. Le, "Performance evaluation of COFDM for digital audoo broadcasting Part I: parametric study," *IEEE Transactions on Broadcasting*, vol. 43, pp. 64–75, March 1997.

[369] B. G. Haskell, A. Puri, and A. N. Netravali, *Digital Video: An Introduction To MPEG-2*. Digital Multimedia Standards Series, Chapman & Hall, 1997.

[370] *ISO/IEC 13818-2: Information Technology - Generic Coding of Moving Pictures and Associated Audio Information - Part 2: Video*, March 1995.

[371] L. Hanzo and J. P. Woodard, "An intelligent multimode voice communications system for indoor communications," *IEEE Transactions on Vehicular Technology*, vol. 44, pp. 735–748, Nov 1995. ISSN 0018-9545.

[372] L. Hanzo and J. Streit, "Adaptive low-rate wireless videophone systems," *IEEE Tr. on CS for Video Technology*, vol. 5, pp. 305–319, Aug 1995.

[373] P. Shelswell, "The COFDM modulation system: the heart of digital audio broadcasting," *Electronics & Communication Engineering Journal*, vol. 7, pp. 127–136, June 1995.

[374] M. Failli, "Digital land mobile radio communications COST 207," tech. rep., European Commission, 1989.

[375] A. Aravind, M. R. Civanlar, and A. R. Reibman, "Packet loss resilience of MPEG-2 scalable video coding algorithms," *IEEE Transaction On Circuits And Systems For Video Technolo gy*, vol. 6, pp. 426–435, October 1996.

[376] M. Ghanbari and V. Seferidis, "Cell-loss concealment in ATM video codecs," *IEEE Tr. on Circuits and Systems for Video Technology*, vol. 3, pp. 238–247, June 1993.

[377] R. Steele and L. Hanzo, eds., *Mobile Radio Communications.* IEEE Press-John Wiley, 2 ed., 1999.

[378] G. Reali, G. Baruffa, S. Cacopardi, and F. Frescura, "Enhancing satellite broadcasting services using multiresolution modulations," *IEEE Transactions on Broadcasting*, vol. 44, pp. 497–506, December 1998.

[379] Y. Hsu, Y. Chen, C. Huang, and M. Sun, "MPEG-2 spatial scalable coding and transport stream error concealment for satellite TV broadcasting using Ka-band," *IEEE Transactions on Broadcasting*, vol. 44, pp. 77–86, March 1998.

[380] L. Atzori, F. D. Natale, M. D. Gregario, and D. Giusto, "Multimedia information broadcasting using digital TV channels," *IEEE Transactions on Broadcasting*, vol. 43, pp. 383–392, December 1997.

[381] W. Sohn, O. Kwon, and J. Chae, "Digital DBS system design and implementation for TV and data broadcasting using Koreasat," *IEEE Transactions on Broadcasting*, vol. 44, pp. 316–323, September 1998.

[382] C. Berrou and A. Glavieux, "Near optimum error correcting coding and decoding: turbo codes," *IEEE Transactions on Communications*, vol. 44, pp. 1261–1271, October 1996.

[383] J. Goldhirsh and W. J. Vogel, "Mobile satellite system fade statistics for shadowing and multipath from roadside trees at UHF and L-band," *IEEE Transactions on Antennas and Propagation*, vol. 37, pp. 489–498, April 1989.

[384] W. Vogel and J. Goldhirsh, "Multipath fading at L band for low elevation angle, land mobile satellite scenarios," *IEEE Journal on Selected Areas in Communications*, vol. 13, pp. 197–204, February 1995.

[385] W. Vogel and G. Torrence, "Propagation measurements for satellite radio reception inside buildings," *IEEE Transactions on Antennas and Propagation*, vol. 41, pp. 954–961, July 1993.

[386] W. Vogel and U. Hong, "Measurement and modelling of land mobile satellite propagation at UHF and L-band," *IEEE Transactions on Antennas and Propagation*, vol. 36, pp. 707–719, May 1988.

[387] K. Wesolowsky, "Analysis and properties of the modified constant modulus algorithm for blind equalization," *European Transactions on Telecommunication*, vol. 3, pp. 225–230, May–June 1992.

[388] M. Goursat and A. Benveniste, “Blind equalizers,” *IEEE Transactions on Communications*, vol. COM–28, pp. 871–883, August 1984.

[389] G. Picchi and G. Prati, “Blind equalization and carrier recovery using a “stop–and–go” decision–directed algorithm,” *IEEE Transactions on Communications*, vol. COM–35, pp. 877–887, September 1987.

[390] A. Polydoros, R. Raheli, and C. Tzou, “Per–survivor processing: a general approach to MLSE in uncertain environments,” *IEEE Transactions on Communications*, vol. COM–43, pp. 354–364, February–April 1995.

[391] D. N. Godard, “Self–recovering equalization and carrier tracking in two–dimensional data communication systems,” *IEEE Transactions on Communications*, vol. COM–28, pp. 1867–1875, November 1980.

[392] Y. Sato, “A method of self–recovering equalization for multilevel amplitude–modulation systems,” *IEEE Transactions on Communications*, vol. COM–23, pp. 679–682, June 1975.

[393] Z. Ding, R. A. Kennedy, B. D. O. Anderson, and R. C. Johnson, “Ill-convergence of Godard blind equalizers in data communications systems,” *IEEE Transactions on Communications*, vol. COM-39, pp. 1313–1327, September 1991.

[394] C.S.Lee, T. Keller, and L. Hanzo, “Turbo-coded hierarchical and non-hierarchical mobile digital video broadcasting,” *IEEE Transaction on Broadcasting*, 1999. Submitted for publication.

Index

N

O

R

S

Author Index

C

D

E

Q

R

S

T

U

V

W

Y

Z